Investigation of Fluid Inclusions in Marbles

Untersuchung von Flüssigkeits- und Gaseinschlüsse in Marmoren

Thesis submitted for the degree of Master of Science

Diplomarbeit zur Erlangung des akademischen Grades eines Diplomingenieurs
der Studienrichtung Angewandte Geowissenschaften

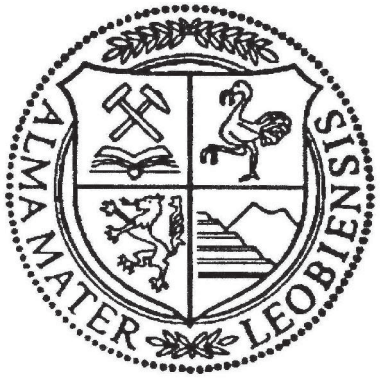

Angelika Reßler

Supervisor:

Ao.Univ.-Prof. Dr. Ronald J. Bakker

Department of Applied Geosciences and Geophysics
Chair of Mineralogy and Petrology
Montanuniversity Leoben

Leoben, November 2007

I declare herewith that this thesis is entirely my own work and that I have only consulted references quoted herein.

Angelika Reßler Leoben, November 2007

Danksagung

An dieser Stelle möchte ich allen danken die mich im Laufe dieser Arbeit begleitet haben.

Als erstes möchte ich mich herzlich bei meinem Betreuer seitens der Montanuniverstität Leoben, Herrn Ao. Univ.-Prof. Dr. Ronald J. Bakker und meinem Betreuer seitens OMYA GmbH, Herrn Dr. Bahman Tavakkoli, für die Anleitung und Geduld während dieser Zeit bedanken.

Natürlich möchte ich mich auch sehr herzlich bei meinen lieben Diplomarbeitszimmerkollegen, Christoph Piribauer, Philipp Hartlieb und Thomas Aiglsperger für zwischenzeitliche Zerstreuung und Unterhaltung bedanken.

Der größte Dank jedoch gilt meinen Eltern Gottfried und Getrude Reßler, die mir dieses Studium überhaupt ermöglicht haben und mich während dieser Zeit mit allen Mitteln liebevoll unterstützt haben, sowie meinem Lebensgefährten Lukas Ofner, der in den bisherigen 6 gemeinsamen Jahren mir stets motivierend und mit viel Liebe zur Seite stand.

Acknowledgment

This thesis is sponsored by OMYA GmbH (Gummern, Austria) under the supervision of Dr. Bahman Tavakkoli.

Prof. Dr. Ronald J. Bakker supervised this study at the Department of Applied Geological Sciences and Geophysics, Institute of Mineralogy and Petrology, Montanuniverstity of Leoben. The marble samples were collected during a field trip in western Turkey in April 2006, in Bayramic and Orhaneli. Sample preparation (thin and thick sections), optical microscopy (transmitted light) for petrography, Raman spectroscopy and microthermometry were performed at Mineralogy and Petrology Institute at Leoben. Crush-Leach analyses were performed at the Geology Institute in Leoben supervised by Prof. Prohaska. ICP-MS measurements were made under the guidance of Prof. Dr. Thomas Meisel. The RFA analysis was obtained in Graz at the Karl-Franzens-University, Department of Mineralogy and Petrology under guidance of Mag. Dr. Christoph A. Hauzenberger. The OMYA Standard measurements and the XRD analysis were made at the Technikum of G & M-Department of OMYA in Gummern.

Fig. 1: from the left to the right: Ronald Bakker (Montanuniverstiy Leoben), Mustafa Soylu (OMYA geologist in Turkey), “Turkish man” and Bahman Tavakkoli (OMYA)

Contents

1. Abstracts

1.1. Abstract

Selected Marbles from the West-Turkey and from Austria (Carinthia) were analysed with a variety of methods to determine minerlogical and fluid inclusions composition. In addition rocks directly adjacent to the marble formations were petrographically analysed. The objective of this study was to determine if the grey colour of selected marble samples is only caused by minerals or if fluid inclusions can affect a discolouration of marbles. Therefore a detailed fluid inclusion study was performed with Raman spectroscopy, microthermometry, and crush and leach tests.

The marbles mainly contain calcite with minor amounts of dolomite (up to 25 mass%). The marbles are characterized by dark and bright grey zones dependent on the amount of fluid inclusions. Two types of fluid inclusions are present in the marble samples: 1. Water-rich and 2. Gas-rich. Most inclusions have a diameter of around a few micrometers. The visual colour of the marbles is mainly dependent on the presence of gas-rich inclusions. The composition of the gases is characteristic for different marble regions: Region 1:CO_2-H_2S (96 - 4 mole%), Region 2:CO_2–H_2S–CH_4 (88 – 10 – 2 mole%), Region 3:CO_2–H_2S–CH_4–N_2 (75 – 14 – 5 – 6 mole %). The presence of H_2S causes a significant odour.

The marbles' rare earth element concentrations patterns and crush and leach analyses of the fluids illustrate a strong fingerprint of sea water interaction. Additional these signatures show an influence of diorite and granite intrusives.

1.2. Zusammenfassung

Ausgesuchte Marmore und ihre Flüssigkeitseinschlüsse (FE) aus der West-Türkei und Österreich (Kärnten) wurden mit unterschiedlichen mineralogischen Methoden auf ihre mineralogische und FE-Zusammensetzung untersucht. Zusätzlich wurden auch die angrenzenden Gesteine zu den Marmoren petrographisch analysiert. Ziel dieser Arbeit war herauszufinden, ob die Graufärbung von bestimmten Marmoren durch ihre mineralogische Zusammensetzung oder auch durch FE verursacht wird. Dazu wurden detaillierte FE Untersuchungen mit Hilfe der Raman Spektroskopie, Mikrothermometrie und Crush/Leach durchgeführt.

Die Marmore setzen sich hauptsächlich aus Kalzit und in kleineren Mengen Dolomit (bis zu 25 mass%) zusammen. Sie zeigen dunkel- und hellgraue Zonen abhängig von den

auftretenden FE Mengen. Es treten zwei unterschiedliche Typen von FE in den Marmoren auf: 1. Wasserreiche und 2. Gasreiche. Die meisten Einschlüsse haben einen Durchmesser von nur wenigen Mikrometern. Die Färbung der Marmore hängt hauptsächlich von der Anwesenheit gasreicher Einschlüsse ab. Die Zusammensetzung der Gase variiert zwischen den unterschiedlichen Regionen: Region 1: CO_2-H_2S (96-4 mol%); Region 2: CO_2–H_2S–CH_4 (88–10–2 mol%); Region 3: CO_2–H_2S–CH_4–N_2 (75–14–5–6 mol %). Die Anwesenheit von H_2S verursacht den intensiven Geruch.

Die SEE-Konzentrationen und die Crush/Leach Analysen der FE weisen auf eine Meerwasser Beeinflussung hin. Zusätzlich zeigen diese Signaturen eine Beeinflussung durch Diorit und Granit Intrusiva.

2. Objective

Calcite grains in marbles contain abundant fluid inclusions. The variable composition of these inclusions could have a positive or negative effect to the product feature of slurries such as brightness, opacity, viscosity and conductivity. The focus of this work is the investigation and analysis of fluid inclusions in selected carbonate rocks and their possible effect on the quality of filler and pigments produced out of these rocks. Additionally, the mineralogy of the marbles will be investigated with a variety of methods. Fluids trapped in inclusions in the marbles may be in part obtained from adjacent rock, of either igneous or sedimentary origin. Therefore, also the rocks around the marble complexes are analysed. The fluid may consist of water with or without dissolved salts or may consist of gas mixtures. The grains may include a variety of generations of different fluid types.

Within this thesis a basic research of the composition of the fluid inclusions of selected marbles deposits in the West Turkey (Bayramic, Orhaneli) and Austria (Merluzzi) will be made. This study will concentrate on the application of Raman spectroscopy to identify both mineral and fluid components in the marbles. Up to now, fluid inclusion studies on marbles only include the analyses of associated quartz veins, as calcite is regarded as an unreliable fluid container. Primary fluid inclusions in calcite are the main topic of this study, and an attempt is made to prove that calcite is able to conserve fluids that are trapped during metamorphic processes.

The results of this work should provide a basis for further technical investigations in regard to the influence of the inclusions to the product feature.

3. Geographical Overview

3.1. Turkey

Most of the investigated marble samples are from marble deposits in the NW of Turkey. We visited from the 18th to the 23th of April 2006 two regions south to the Marmara Sea (Fig. 3.1.):

- Bayramic, near the Aegean Sea
- Orhaneli, situated south of Bursa.

Fig 3.1.: Geographical overview of the N-W Turkey (Google Earth, http://earth.google.de)

Turkey is divided in 7 regions; Bayramic and Orhaneli are situated in the Marmara region. With an area of 67.000 km^2 is this region is the smallest but the most populous region. The Marmara Sea, with Dardanelles in the east and the Bosporus in the west separate the European from the Asian continent. The Marmara region is mainly hilly with bushes and forests (Fig. 3.2. and 3.3.) and in the western part of this region is the

Agrarian region (e.g. around Orhaneli is a large cherry producing area). In the region around Bursa are some of the last raw silk productions (Hoff, 2004).

Fig. 3.2.: Small village in Orhaneli

Fig. 3.3: A young shepherd in Sögüt near Orhaneli

3.2. Austria

Fig. 3.4: Geographical overview of region around Krastal-Valley (Google Earth, http://earth.google.de).

Some marble samples were collected in Krastal-Valley close to the marble deposit of Gummern/Carinthia. Carinthia is the most southern province of Austria. The Krastal-Valley is situated north of the river Drau close to the town of Villach, which lies a few kilometers away from the borders to Italia and Slovenia.

4. Geology of the western Turkey

Turkey was located at the boundary between the two megacontinents for 200 Ma: Gondwana to the south and Laurasia to the north (Göncüoglu et al.,1997). It is generally accepted that during its geological history, numerous continental fragments belonging to one of these megacontinents were rifted off from the main body and amalgamated to the next, so that the Anatolian realm is made of several oceanic and continental „terranes“ with different geological features. The last main orogenic event, the alpine orogeny, related to the closure of various Neotethyan branches directly controls the present distribution of these terranes.

There has been a long history of tectonic subdivision schemes of Turkey. However, the simplest and the most accepted one is by Ketin (1966), who, based on the age of orogenic development, divided Turkey into four major orogenic belts: Pontides, Anatolides, Taurides and the Border Folds (Fig. 4.1). With the advent of plate tectonic, the Pontides are regarded as being originally part of the Laurasia, whereas the Anatolides, the Taurides and the Border Folds are taken to belong to the Gondwana-Land realm; the collision of these two megacontinents, following the consumption of the intervening Tethys ocean, led to the Alpine orogeny in Turkey (Okay, 1987). The line of the present day contact of the Pontides and the Anatolides, thus that of the two former megacontinents, is accepted as the major Tethyan suture in Turkey and is given the name of the Izmir-Ankara suture.

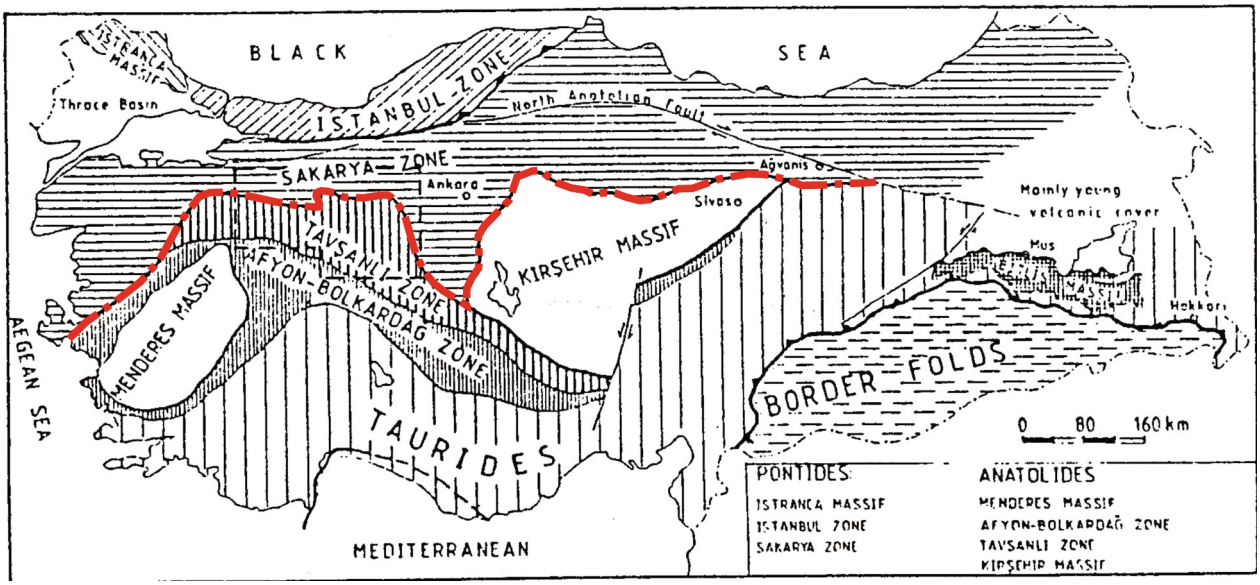

Fig 4.1: Tectonic map of Turkey showing the tectonic zones in the Pontides and Anatolides. Heavy red lines indicate major sutures (Okay, 1987).

The Orogenic belts of Turkey are further divided into zones based on common stratigraphic and tectonic features. Pontides comprise three zones: the Istranca Massif, the Istanbul Zone and the Sakarya Zone. The three zones of the Anatolides are the Tavsanli and Afyon zones and the Menderes Massif (Fig. 4.1). The studied marbles of Bayramic belongs to the Sakarya Zone (Pontides) and those of Orhaneli are part of the Tavsanli Zone (Anatolides).

SAKARYA ZONE (PONTIDES)

Istanbul Zone is separated from the Sakarya Zone by the Intra-Pontide Suture (Fig. 4.1, red line), whose age is disputed; it could be a Late Creataceous or older (Triassic) suture (Okay, 1987). The Sakarya Zone comprises a metamorphic basement, called the Karakaya Complex, and a Mesozoic cover with several major unconformities. Lower Paleozoic rocks are not recorded. Karakaya Complex is a metamorphosed and strongly deformed sequence of basic volcanic rocks, limestones and greywackes; it includes Permian limestone olistoliths, and is unconformably overlain by Liassic conglomerates, thus constraining the age of metamorphism and deformation to Triassic.

The Mesozoic cover of the Sakarya Zone comprises Liassic conglomerates and sandstones, Middle Jurassic to Early Cretaceous limestones and Late Cretaceous flysch and is rather different from the Mesozoic stratigraphy of the Istanbul Zone.

The base to the Karakaya Complex is observerd in the Uludag and Kazdag regions, where high-grade gneisses, amphibolites and marbles outcrop in tectonic window beneath the Karakaya Complex.

TAVSANLI ZONE (ANATOLIDES)

The Tavsanli Zone is seperated from the Sakarya Zone be the Izmir-Ankara suture of Late Cretaceous age (Fig. 4.1) (Okay, 1987). It is the other side of the ocean. Rocks of the Tavsanli Zone have undergone blueschist facies metamorphism and are tectonically overlain by an ophiolite.

Two units are differentiated within the Tavsanli Zone: the Ovacik and Orhaneli units. Orhaneli Unit consits of metaclastics overlain by marbles, which pass into a thick sequence of metabasites, metashales and metacherts. Ovacik Unit comprises only basic volcanic rocks, pelagic shales and radiolarian cherts, which, unlike the Orhaneli Unit, appear unmetamorphosed

in the field but reveal on petrographic examination HP/LT minerals such as lawsonite, aragonite and sodic pyroxene. The age of the blueschist facies metamorphism is mid-Cretaceous. Rocks of the Tavsanli Zone are overlain by an ophiolite, which consists mainly of peridotite and which has not undergone blueschist facies metamorphism.

The geological map of the areas Bayramic and Orhaneli are shown in the Figure 4.2.

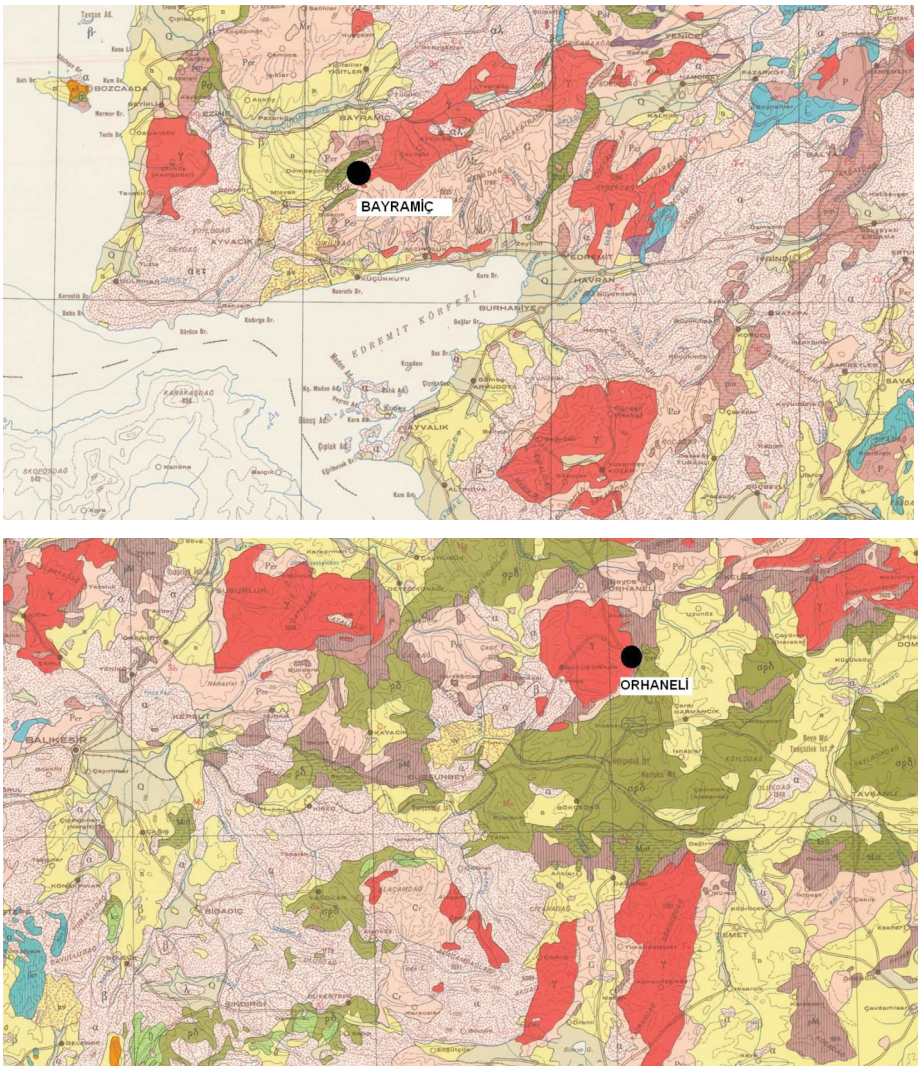

Color	Symbol	Formation
Red	γ	Granite, Granodiorite
Yellow		Neogene, Continental, Undifferentiated
Green	δ	Diorite, Gabbro
	ρ	Peridotite
	σ	Serpentine
	pof	Palaeozoic, Ophiolitic series
	mof	Mesozoic, Ophiolitc series
Rosa	Per	Palaeozoic, Metamorphic
	pm	Permian
	pM	Permian-Mesozoic
	α	Basalt
	β	Andesite

Fig. 4.2: Two sections of the „Geological Map of Turkey - IZMIR“, 1:500.000

5. The samples and their location

The sampling areas are marked with GPS (Global Positioning System) (Fig. 5.1, 5.10). GPS coordinates were determined with a GPS handheld *Garmin eTrex*.

5.1. Bayramic

Fig. 5.1: Geological map of Bayramic from Mustafa Soylu with the sample points.

5.1.1. The marble samples from Bayramic:

The samples of the quarry Sebastian (Bay 1 and Bay 4, Fig. 5.2 and 5.3) are coarse grained (grain size approximately 0.5 cm). The marbles of the deposit show large areas of greyish colour (some m^3) alternated with bright spots and strips along cracks. The grey zones represent the areas of marble exhibiting strong odours smelly areas.

Fig. 5.2: Marble of the quarry Sebastian (Bay 1)

Fig. 5.3: Marble of the quarry Sebastian (Bay 4)

The marbles from the quarry Charles (Bay 10, Fig. 5.4) are white and fine grained (grain size around 1 mm), hard and compact.

Fig. 5.4: Marble of the quarry Charles (Bay 10)

Fig. 5.5: Marble from Dereli (Bay 23)

From the quarry Dereli two different marble samples have been taken. Bay 23 (Fig. 5.5) is coarse grained (grain size 1-2 cm) with some fine red/orange veins and though it is grey it doesn't smell. Bay 24 is finer grained and a little bit more greyish then Bay 23 and the gray zone are smelly (like the samples Bay 1 and Bay 4).

Point	*Sample*	*GPS*
B 1	Bay 1	*© OMYA GmbH*
B 1	Bay 4	*© OMYA GmbH*
B 3	Bay 10	*© OMYA GmbH*
B 1	Bay 23	*© OMYA GmbH*
B 1	Bay 24	*© OMYA GmbH*

Tab. 5.1: GPS coordinates and quarries of the samples

5.1.2. The wall rock samples from Bayramic:

The sample Bay 9 (Fig. 5.6) is greenish coloured schist near the quarry Sebastian. It is fine grained and contains quartz veins, up to 0.5 cm thickness.

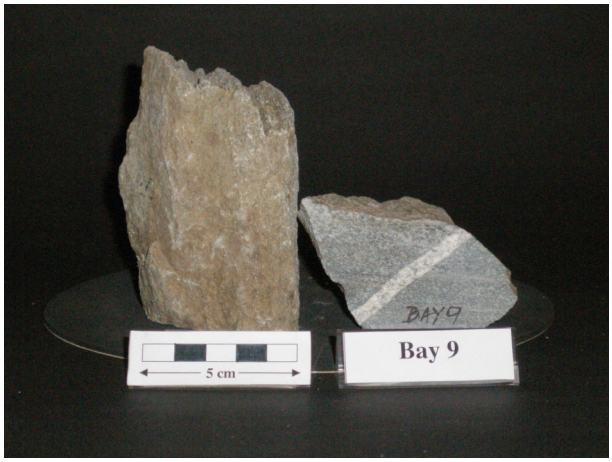

Fig. 5.6: Schist, with quartz vein (Bay 9)

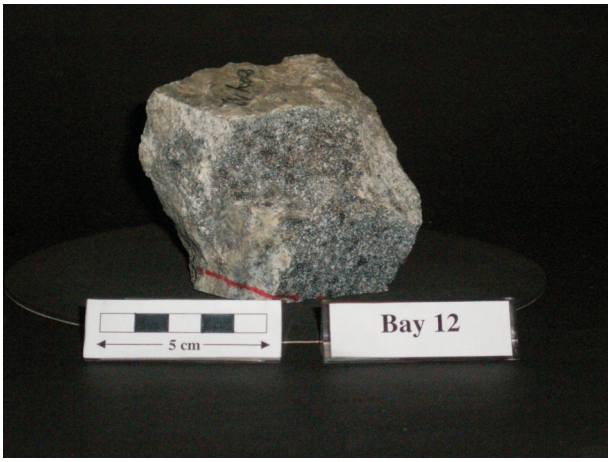

Fig. 5.7: Diorite (Bay 12)

The samples Bay 12 (Fig. 5.7) and Bay 13 (Fig. 5.8) were collected near the quarry Charles at the contact of the carbonates with the magmatic rock. Bay 12 is a fine to medium coarse grained Diorite. Bay 13 is a highly tectonized fine grained carbonate rock with many reddish coloured veins with a thickness from 1 mm up to 1 cm (around 40 vol%).

Fig. 5.8: Carbonate (Bay 13)

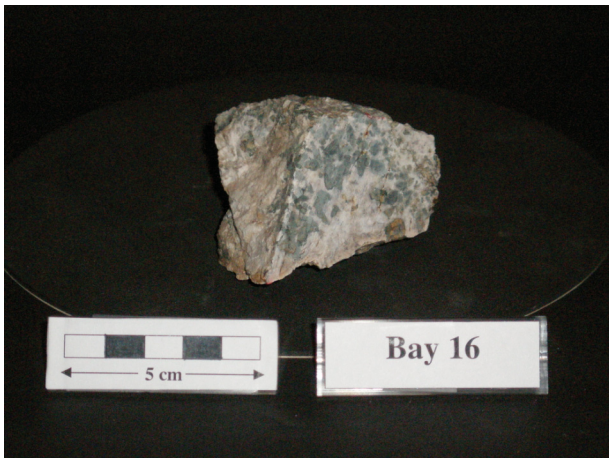

Fig. 5.9: Plagioclase-pyroxene bearing gabbro (Bay 16)

Bay 16 (Fig. 5.9) contains large pyroxene grains (grain size around 1 cm) and large feldspars (grain size around 0.5 cm). Plagioclase-pyroxene bearing Gabbro contain around 50 vol% plagioclase and around 50 vol% pyroxene. Other minerals are not visible in this sample.

Point	*Sample*	*GPS*
B 2	Bay 9	*© OMYA GmbH*
B 3	Bay 12	*© OMYA GmbH*
B 3	Bay 13	*© OMYA GmbH*
B 4	Bay 16	*© OMYA GmbH*

Tab. 5.2: GPS coordinates and the outcrop of the samples

5.2. Orhaneli

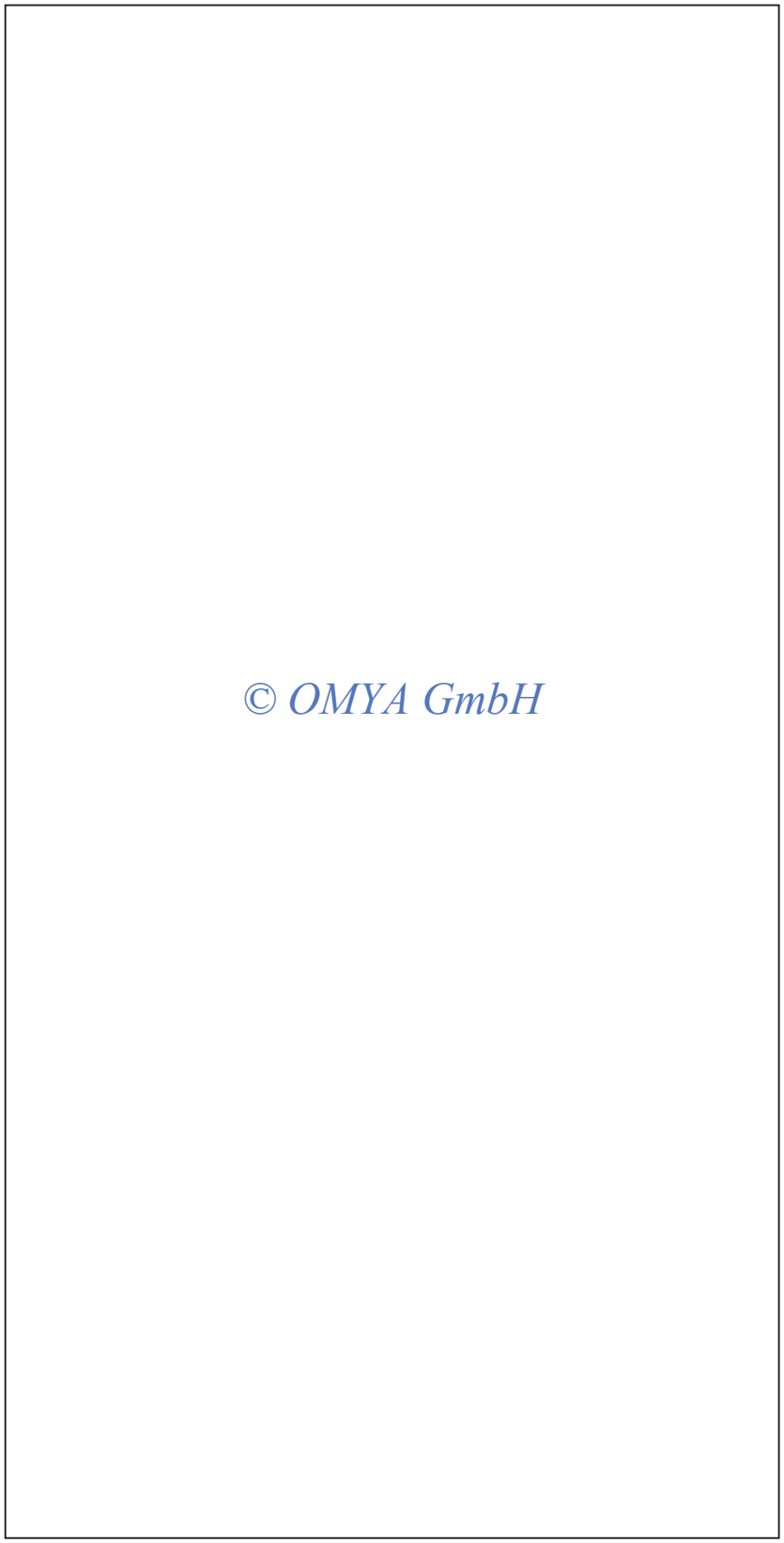

Fig. 5.10: Geological map of Orhaneli from Mustafa Soylu with the sample points.

5.2.1. The marble samples from Orhaneli:

The samples from the quarry Ceki 1 (Orh 1, see Fig. 5.11) are fine grained and laminated in greyish and bright colours. The layers have a maximum thickness of some dm. The bright zones contain some rose spots (Orh 2, see Fig. 5.12). The grey layers are the smelling zones.

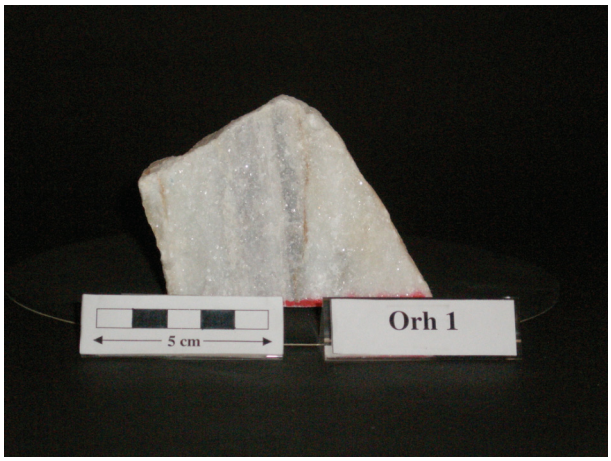

Fig. 5.11: Marble of the quarry Ceki 1 (Orh 1)

Fig. 5.12: Marble of the quarry Ceki 1 (Orh 2)

The sample from Ceki 2 (Orh 14, see Fig. 5.13) are finer layers (some cm thick) of alternating grey and brighter colours and these samples are coarse grained (around 1 mm) then the marble from Ceki 1 (Orh1 and Orh 2, see Fig. 5.11 and 5.12). The grey zones are again the smelling ones.

Fig. 5.13: Marble of the quarry Ceki 2 (Orh 14)

Fig. 5.14: Marble from Agachisar (Orh 26)

Orh 26 is from Agachisar (see Fig. 5.14). The marble has a grey-brownish colour and is fine grained. This marble has a less intensive smell than the others (Orh 1, 2 and 14).

The sample from Sögüt (Orh 37, see Fig. 5.15) was taken from the marble/granite contact. The marble is rich in silicate minerals. It is fine grained and the layers (1 to 3 cm thick) have a brownish colour.

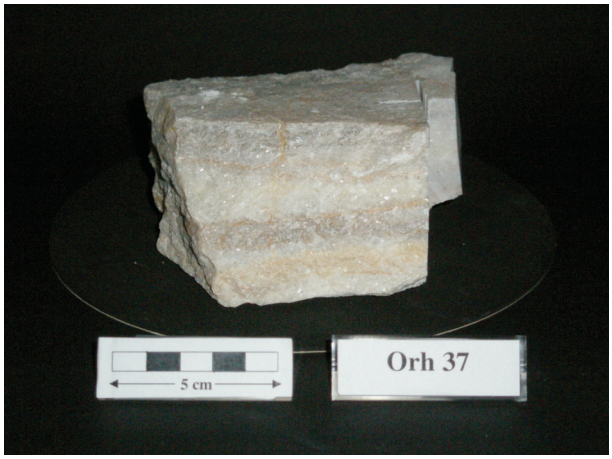

Fig. 5.15: Marble from Sögüt (Orh 37)

Point	*Sample*	*GPS*
O 1	Orh 1	*© OMYA GmbH*
O 1	Orh 2	*© OMYA GmbH*
O 3	Orh 14	*© OMYA GmbH*
O 5	Orh 26	*© OMYA GmbH*
O 6	Orh 37	*© OMYA GmbH*

Tab. 5.3: GPS coordinates and the quarries of the samples

5.2.2. The wall rock samples from Orhaneli:

Orh 8 (Fig. 5.16) is a quartz-sericite-schist sampled at quarry Ceki 1. Approximately 150 m far away along the street the sample Orh 12 (Fig. 5.17) was taken, which is a dark serpentinite.

Fig. 5.16: Quartz-serizite-schist (Orh 8)

Fig. 5.17: Serpentinite (Orh 12)

Fig. 5.18: Granite (Orh 24)

Fig. 5.19: Siliceous marble (Orh 41)

The sample Orh 24 (Fig. 5.18) is granite from the marble/granite contact zone. The grain size of this granite is from 1 to 5 mm and the recognizable minerals are quartz (~ 20 vol%), feldspar (~60 vol%) and dark minerals (~ 20 vol%).

Orh 41 (Siliceous marble, see Fig. 5.19) and Orh 44 (granite) are from the granite with the marble contact in Sögüt. The marble is rich of silicate and is fine grained. The granite (Orh 44, no photo) have a grain size from 1 mm up to 1 cm and the identifiable minerals are quartz (~ 25 vol%), feldspar (~ 35 vol%) and dark minerals (~ 40 vol%).

Point	*Sample*	*GPS*
O 2	Orh 8	*© OMYA GmbH*
O 2	Orh 12	*© OMYA GmbH*
O 4	Orh 24	*© OMYA GmbH*
O 6	Orh 41	*© OMYA GmbH*
O 6	Orh 44	*© OMYA GmbH*

Tab. 5.4: GPS coordinates and the outcrop of the samples

5.3. The marble samples from Merluzzi

The marbles from Merluzzi can be differentiated by color into three groups. The groups differ in respect to the intensity of their odour. The strongest odour is exhibited by the grey marble (Fig. 5.20). A decrease in the intensity of the odour corresponds to the progressive lightening of the marble's colour (see Fig. 5.21 and 5.22). All three types have a grain size around 1 mm to 4 mm.

Fig. 5.20: Merluzzi Grau (grey marble)

Fig. 5.21: Merluzzi Blau (blue marble)

Fig. 5.22: Merluzzi Hellbau (ligth blue marble)

6. Introduction to fluid inclusions

Fluid inclusions are a common feature of minerals. The main principle of fluid inclusion is to determine direct samples of pore fluid (mineral forming fluid), that remains conserved over million of years. In fact, it is much more common to find crystals with optically-resolvable fluid inclusions (bigger then 1 micrometer) than it is to find crystals with no visible inclusions (e.g. Fig 6.1a). Even gemstones, which are collected because of their beauty and apparent perfection, often contain large inclusions that are, in some cases, characteristic of the area or mine where they were found (Roedder 1986; Samson et al., 2003). Upper limit of the size of natural fluid inclusions is defined by the grain size, but those with dimensions greater than a few millimetres are uncommon. As noted by Roedder (1984), the number of inclusions in a given sample generally increases with decreasing inclusion size, and some milky quartz and calcite may contain as many as 10^9 fluid inclusions per cm^3 (Samson et al., 2003). Inclusions may contain a vapour bubble and one or more crystalline daughter phases in addition to an aqueous fluid (e.g. Fig. 6.1b).

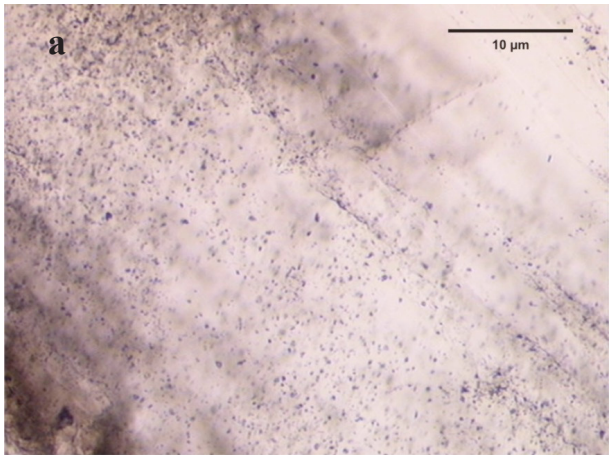

Fig 6.1a: A cloud of small inclusions in marble (Bay 1)

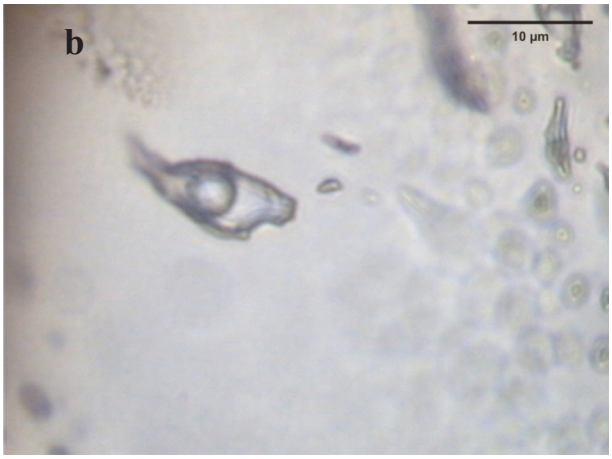

Fig 6.1b: An example of a 2 phase inclusion with a vapour bubble and a liquid in marble (Bay 22)

Such inclusions can help to understand metamorphic processes, diagenetic systems, subsurface fluid evolution and porosity evolution. It's also possible to interpret the petroleum migration history and to reconstruct the thermal and tectonic or stratigraphic history. Metamorphic minerals (like quartz and calcite) commonly contain many tiny fluid inclusions (sizes between 0,1 and 20 micrometer). Inclusions can provide important insights into pressure-temperature conditions of crystallisation or mineral precipitation and the composition of the fluid present when the host

mineral grain formed. Also the later history of the rock can be traced by the continuous entrapment of pure fluids in newly grown inclusions.

Fluid inclusions in general can be analysed with a variety of methods. This analysis can be divided into destructive and non destructive methods, such as microthermometry, Raman spectroscopy and crush-leach (see next chapters).

The inclusion shape definition model after Bakker & Diamond (2006) has been used (Fig. 6.2). The area, the perimeter and the major and minor axes of a best fit ellipse of the inclusions are measured with the program *ImageJ*. With these values the classification parameters have been calculated with Microsoft Excel and than plotted with the program IGOR PRO (wavemetrics).

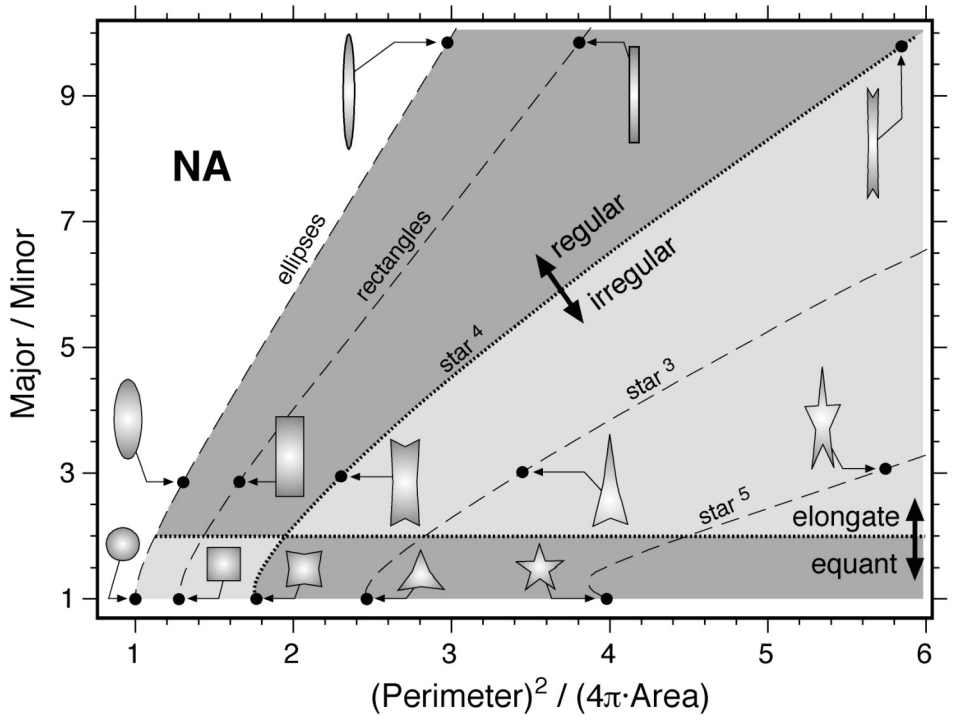

Fig. 6.2: Inclusion shape definition (from Bakker&Diamond, 2006).

7. Method description

7.1. Microthermometry

For microthermometry measurements the sample (i.e. a thick section which is removed from the glas plate) is put on a heating and cooling stage, (LINKAM MDS 600, see Fig. 7.1) and this stage is put on a polarisation microscope (Olympus BX 60 with adapted 40x and 100x LWD objective). The stage is cooled with liquid nitrogen and heated with electricity. The stage has a temperature range from -196°C to +600°C. The calibration is made with synthetic fluid inclusions in quartz (containing H_2O and CO_2-H_2O gas inclusion). These synthetic inclusions have well defined phase transitions at 0°C (melting of ice), -56.6°C (melting of solid CO_2) and +374°C (critical homogenisation of H_2O). The phase transitions of fluid components observed during heating and cooling provide information about pressure, temperature and composition/salinity of the inclusion. The phase transitions are expressed in melting and homogenisation temperatures of the inclusion.

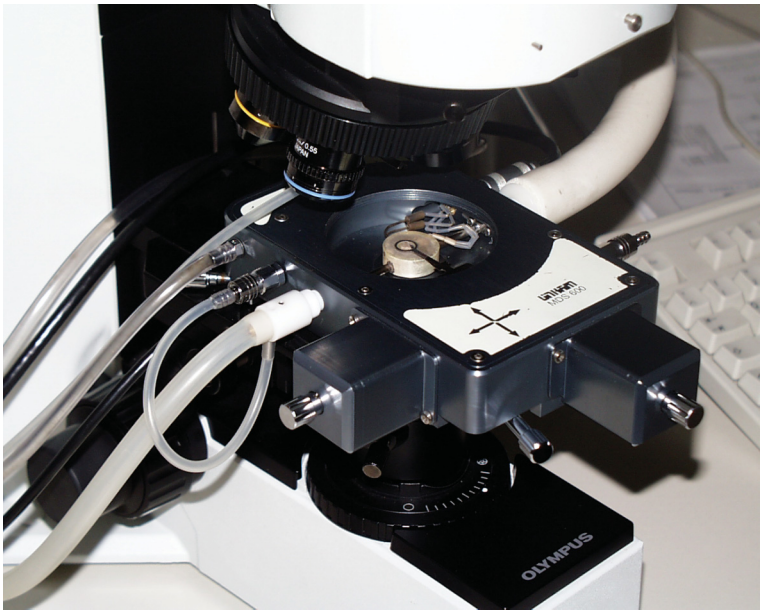

Fig.7.1: LINKAM MDS 600

7.2. Raman Spectroscopy

7.2.1. What is Raman spectroscopy about?

Raman spectroscopy and associated imaging techniques are generally non-destructive, and can be used to identify a wide range of materials, including minerals and gemstones (Hope et al, 2001). The Raman effect was discovered by the Indian physicist Chandrasekhara Venkata Raman in the year 1928. Raman is a sensitive technique which requires minimal sample preparation and can be used on massive specimens from lump ore to fine powders and liquids. Since glass and water are relatively weak Raman scatterers, spectra from minerals can be obtained from samples in air, through glass, and/or immersed in water. Examples of the application of Raman spectroscopy to mineral processing include:

1) detection of minerals containing light elements such as carbon and fluorine
2) distinguishing between polymorphs such as those of iron sulfides e.g. pyrite/markasite
3) characterizing sulfides containing minor elements such as iron in sphalerite and
4) the identification of silicates, oxides, and carbonate gangue minerals.

The Raman microprobe also permits Raman imaging and mapping of surfaces (Hope et al, 2001). In addition Raman can be used to identify fluids within inclusions. Most gases, e.g. CO_2, H_2S, CH_4, N_2 and fluids, e.g. H_2O, H_2S are Raman active (see Table, 7.1)

7.2.2. The Raman Effect

Wavelengths and intensities of inelastically scattered light are measured in Raman spectroscopy. The inelastic collision between a photon and a molecule is known as the Raman Effect. The energy difference between the inelastic scattered photons and the incident photons is exactly the difference between two energy levels of a molecular vibration (Dippel, 2002).

In other words Raman scattering means that the wavelength of monochromatic light is shifted by vibrations of molecules or crystal lattices. This vibration causes a change in the polarizability of a molecule. The spectral analysis of the scattered light shows an intense spectral line matching the wavelength of the light source (Fig. 7.2 - Rayleigh scatter). Due to the interaction between matter and monochromatic light, the vibrational energy of molecules changes. This is in contrast to infrared spectroscopy, where the vibrational energy of molecules changes by the absorption of infrared radiation.

Component	*Phase*		*Rel. Wavenumber in cm^{-1}*	*Rel. Intensity*
CO_2	Liquid	Fermi Double	1284	*56*
			1387	*100*
		$^{13}CO_2$	1370	*4*
		Hot Bands	1264	*7*
			1409	*9*
	Aqueous Sol.	Dissolved CO_2^0	1277	*42*
			1385	*100*
		HCO_3^-	1049	*18*
	Clathrate		1278	*40*
			1381	*100*
CH_4	Vapour		2917	
	Aqueous Sol.	Dissolved CH_4^0	2912	
	Clathrate		2904	*100*
			2914	*22*
N_2	Vapour		2331	
	Clathrate		2325	
H_2	Vapour	Bending	355	*23*
			588	*68*
			816	*14*
			1037	*10*
		Stretching	4107	*1*
			4129	*12*
			4146	*15*
			4158	*100*
			4163	*14*
H_2O	Liquid	Broad band	2900-3750	
		Gauss-Lorentz	3222	*80*
			3433	*100*
			3617	*14*
	Ice	-0 ˚C	3148	
		-190 ˚C	3102	
H_2S	Vapour		2611	
	Liquid		2607	
	Aqueous Sol.	Dissolved H_2S^0	2590	
		HS^-	2574	
Sulfate	Aqueous Sol.	HSO_4^-	1050	
		SO_4^{2-}	983	
O_2	Vapour		1555	
CO	Vapour		2143	
NH_3	Vapour		3334	
C_2H_6	Vapour		993	
			2954	
C_3H_8	Vapour		867	
			1451	
			2890	
SO_2	Vapour		519	
			1151	

Tab. 7.1: The different gases, which can be identify with Raman; from R.J.Bakker`s website: http://fluids.unileoben.ac.at

However, infrared and Raman spectroscopy are complementary regarding the molecular structural information. With selection rules, infrared and Raman active vibrations can be predicted. Typical applications of Raman spectroscopy are the chemical identification of substances, their quantitative analysis, and the determination of their molecular structure (Dippel, 2002).

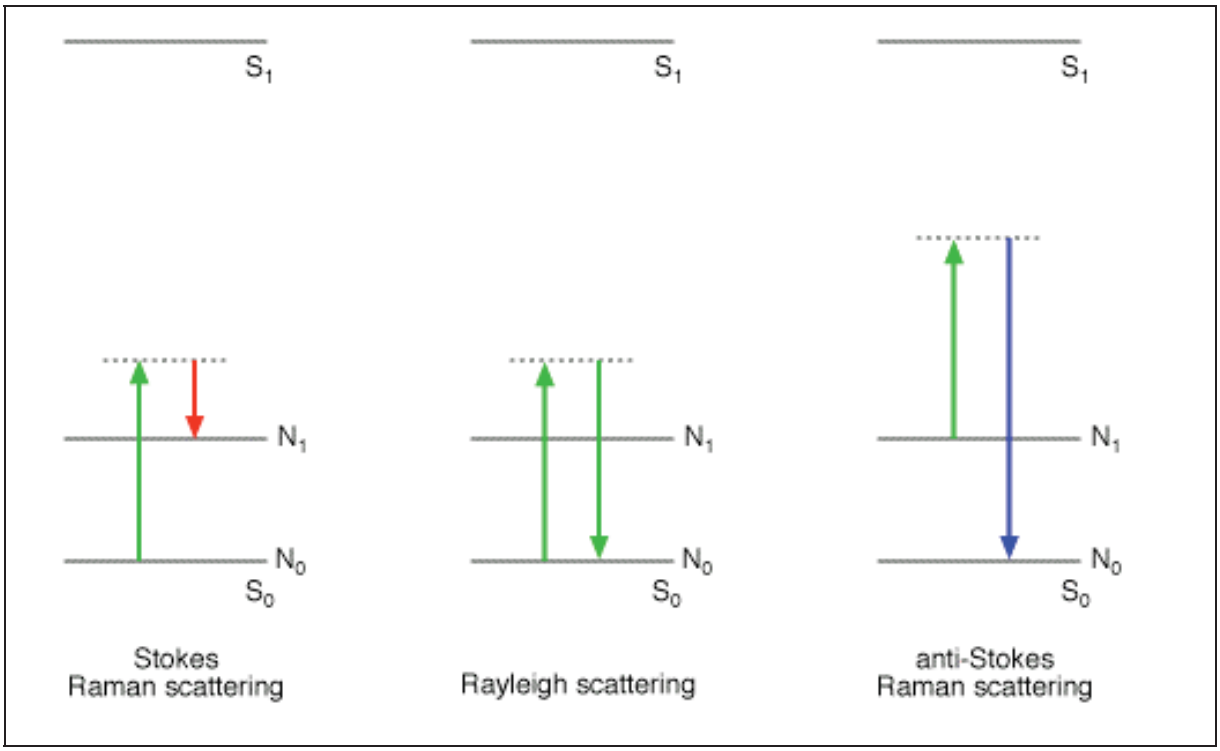

Fig. 7.2: R ,Schematic representation of the energy levels of Rayleigh and Raman scattering. With Raman scattering, the wavelength of the scattered light is shifted either towards longer wavelengths (Stokes Raman scattering, red arrow), or shorter wavelengths (anti Stokes Raman scattering, blue arrow). S0, N0: electronic or vibrational ground state; S1, N1: first excited electronic or vibrational state (Dippel, 2002).

The interaction between matter and light can be interpreted as a collision between a vibrating molecule and an incident photon. There are three possibilities (Fig. 7.2):

1. If the collision is elastic, the energy (green arrow) of the photon as well as the energy of the molecule do not change after the collision. The elastic scattering of the photon is called Rayleigh scattering.

2. If the vibrational energy of the molecule is increased after the collision, the energy of the scattered photons is decreased for the same amount and, therefore, can be detected at longer wavelengths (red arrow). The respective spectral lines are called Stokes-shifted.

3. If the vibrational energy of the molecule is decreased after the collision, the energy of the scattered photons is increased for the same amount and, therefore, can be detected at shorter wavelengths (blue arrow). The respective spectral lines are called anti-Stokes-shifted. This is only possible if the molecule is an excited vibrational state before the collision.

The energy-loss process of photons is the most probable because there will always be more molecules in lower than in higher energy states, and usually only the more intense Stokes side of the spectrum is analysed (Fig. 7.3) (Burke, 2001).

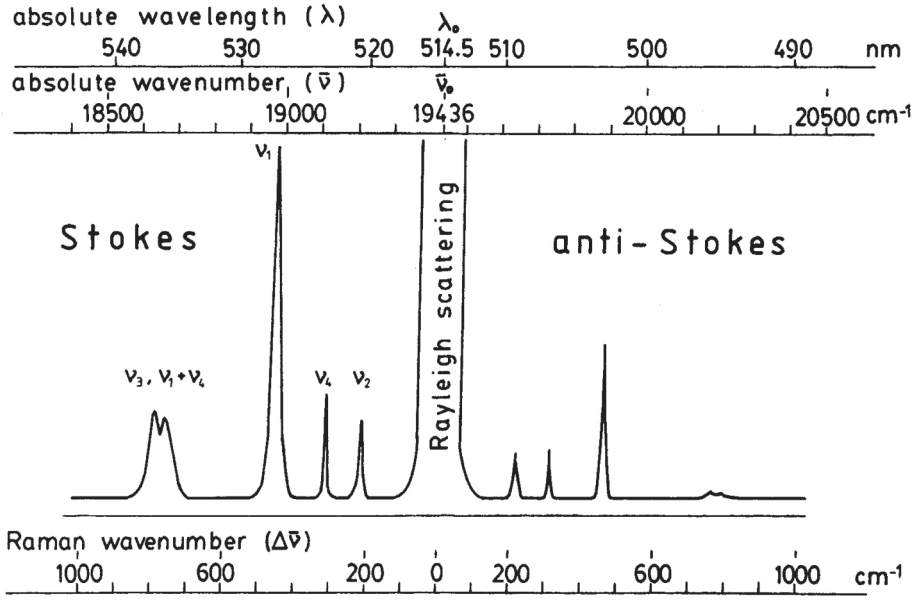

Fig 7.3: Spectrum with Stokes (higher intensity) and Anti-Stokes (lower intensity) illustrating the meaning of relative wavenumber.

7.2.3. Application of the Raman in this study

Raman spectroscopic measurements were performed with a LABRAM (ISA Jobin Yvon) instrument (Fig. 7.4). The laser beam is focussed through an Olympus BX 40 microscope onto the object of interest, either mineral or fluid, using 40x or 100x magnification combined with a confocal optical arrangement, enabling a spatial resolution in the order of one cubic micrometre. The apparatus has a 100 mW frequency-doubled Nd-YAG laser with 532 nm wavelength (green), which is reduced to 38 mW at the measured object. A portion of the scattered light is collected through the microscope and focussed onto a diffraction grating. The grating selects the desired region of the Raman spectrum and reflects this onto a Peltier-cooled, CCD matrix detector.

Fig. 7.4 : Raman LABRAM (ISA Jobin Yvon).

In this study spectra of minerals, fluids (including liquids and gases) have been measured. The spectrum in Fig. 7.5 illustrates a typical pattern as obtained from fluid inclusions in the studied marbles. Besides the spectrum of the calcite host (711, 1085, 1435 and 1748 cm^{-1}) several gases could be identified, e.g. CO_2 at 1288 and 1384 cm^{-1} and H_2S at 2611 cm^{-1}).

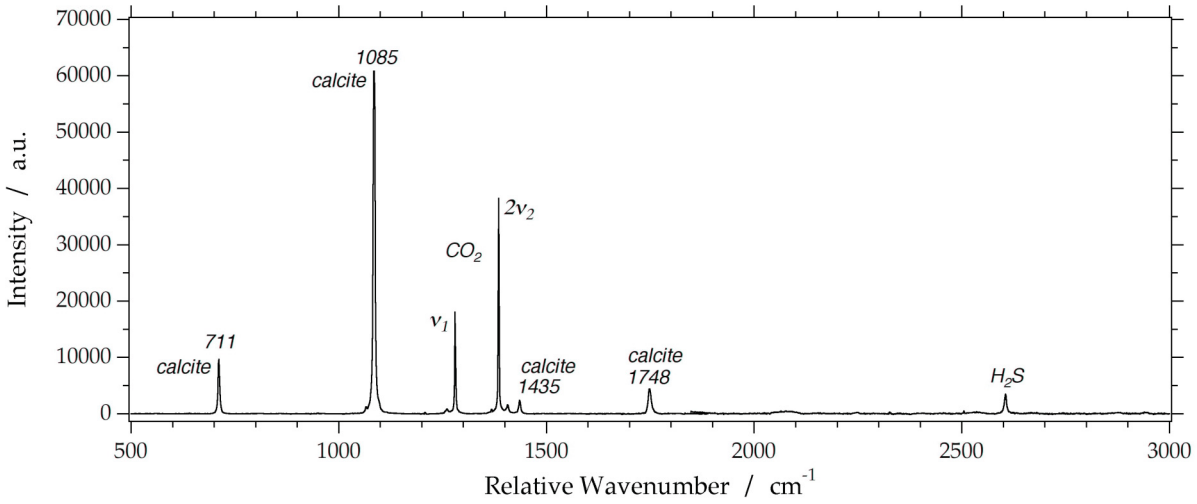

Fig. 7.5: Spectrum of calcite with CO_2 and H_2S.

The peak areas of gas spectra have been used for the calculation of relative mole fractions of CO_2, H_2S, CH_4 and N_2 (see Burke, 2001). A variety of gas composition was obtained for different types of marbles. Figure 7.6 and 7.7 illustrated the method of fluid composition calculations using peak areas of CO_2 and H_2S measured in a fluid inclusion. The mole fraction calculation is based on Placzek´s polarizability theory (eq. 7.1).

$$\chi_i = \frac{\left(\frac{a}{\sigma \cdot \zeta}\right)_i}{\sum_j \left(\frac{a}{\sigma \cdot \zeta}\right)_j} \qquad \text{eq. 7.1}$$

where χ_i is mole fraction, a is peak area, σ is Raman cross-section and ζ is instrumental efficiency. The areas under the peaks are calculated with the computer program *Labspec 2.09b2*.

7.2.4. Calculation example

The mole fraction calculation for the gases is obtained from the area's of individual peaks (eq. 7.2) according to eq. 7.1

$$\left(\frac{a}{\sigma\cdot\zeta}\right)_{CO_2} = \left(\frac{a_{\nu_1} + a_{2\nu_2}}{(1.0+1.5)\times 0.5}\right) \qquad \text{eq. 7.2a}$$

$$\left(\frac{a}{\sigma\cdot\zeta}\right)_{H_2S} = \left(\frac{a_{H_2S}}{6.4\times 1.0}\right) \qquad \text{eq. 7.2b}$$

$$\left(\frac{a}{\sigma\cdot\zeta}\right)_{CH_4} = \left(\frac{a_{CH_4}}{7.5\times 1.0}\right) \qquad \text{eq. 7.2c}$$

$$\left(\frac{a}{\sigma\cdot\zeta}\right)_{N_2} = \left(\frac{a_{N_2}}{1.0\times 1.0}\right) \qquad \text{eq. 7.2d}$$

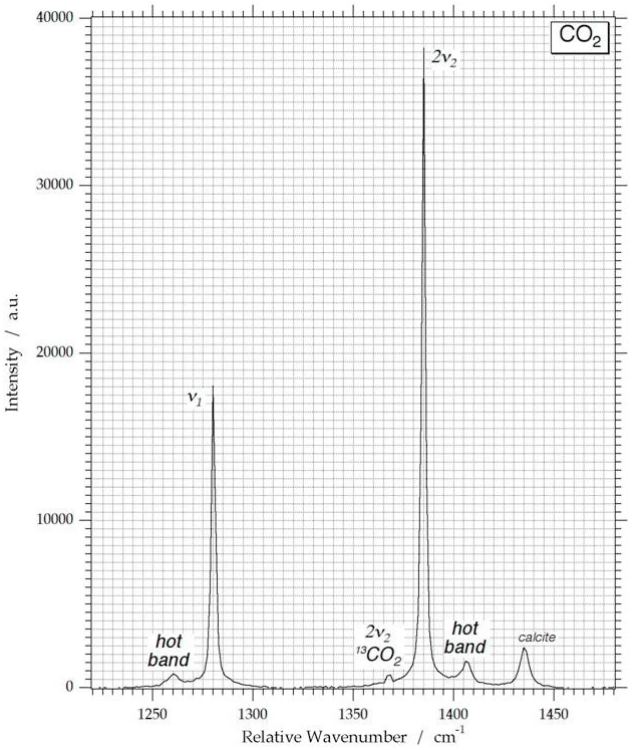

Fig. 7.6: CO_2 Peaks

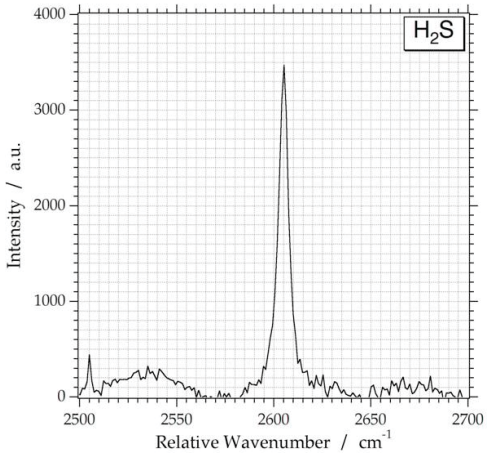

Fig. 7.7: H_2S Peaks

The example illustrated in Fig. 7.6 and Fig. 7.7 reveals a CO_2 mole fraction of 0.96 and a H_2S mole fraction of 0.04.

7.3. Crush and Leach

The “Crush and Leach” method includes the analyses of cations and anions in an aqueous fluid obtained from a large number of inclusions released from the samples by crushing (e.g. Gleesow, 2003). It is therefore a bulk fluid analysis. The method, as first described by Roedder (1958) and Roedder et al. (1963), involves crushing samples under vacuum, collection of the volatiles released, leaching the exposed inclusions with a known amount of solvent, which is then analyzed (e.g. Banks & Yardley, 1992). Once a leachate has been produced (see sample preparation), there are various methods by which it can be analysed. Ion chromatography (IC) has been used in this study (Fig. 7.8). IC is a form of liquid chromatography in which ions are separated by ion exchange resins in a chromatographic column. With the development of the IC it is today possible to measure the monovalent alkaliminerals Na and K, the halogenide F^-, Cl^-, Br^-, I^- as well as NO_3^-, PO_4^{3-} and SO_4^{2-} of a sample fluid (Prohaska, 1997). Quartz, carbonates, barite, and fluorite dominated by one population of fluid inclusions are suitable for this method. Gleeson (2003) has clearly emphasized that the validity of the results of this analytical technique is mainly dependent on the quality of petrographic and microthermometric work that precedes sample selection.

Fig. 7.8: Ionenchromatograph at Prof. Prohaskas office

7.3.1. Sample preparation

Sample material must be first cleaned with a brush and water. After drying the sample is crushed by a hammer and the grains with a size around 1 – 2 mm are screened out. These grains are several times cleaned with distilled water and dried again. One gram of this dried material is selected and put in an achat mortar. With 5 ml distilled water the sample is milled 2 min by hand. Through this operation the fluid inclusions are crushed and the entrapped fluids go in solution. Afterwards this solution is absorbed with an syringe which has a filter attachment on the head of the syringe. This solution is subsequently measured with the ionenchromatograph (Fig.7.8) among other onto Na, Br and Cl.

7.4. OMYA Standard Measurements

7.4.1. Brightness Measurement

The grain size distribution and brightness are important properties for filler industry. For brightness analyses a powder tablet must be pressed and then measured with a brightness analyser. The coarse marble samples are pre-crushed in a lab jaw crusher to a fineness of maximum 2 mm to prepare powder tablets. 30 g of this pre-crushed material is milled with an achat mill 10 minutes for the OMC 5 Product and 30 minutes for the OMC 2. The ground sample is pressed according to laboratory Test Method no. 008 and its brightness is measured according to LTM nos. 009, 010 or 035 (Laboratory Test Method OMYA, 2004).

This analyser measures the intensity of the reflection of the red, green and blue light with a clearly defined wavelength (Tegethoff, 2001). The result is proportional to a standard value (a so-called $BaSO_4$-normal) and is specified in percent. For the dry extender the green value R_y is selected, for the red value R_x and for the wet extender the blue value R_z or Tappivalue *R457* is specified,

$$W = \frac{(R_x = R_y)}{R_y} * 100\% \qquad \text{(eq. 7.3)}$$

where *W* is the brightness factor. The higher this value the more yellow is the material.

7.4.2. Acid insoluble residue - AIR

Part of the carbonate rock is insoluble in HCl (e.g. quartz, mica, etc.). This is measured with the acid insoluble residue test (AIR).

The sample is dissolved within a hot hydrochloric acid (HCl) and the acid insoluble minerals can be caught in a filter and after drying the insoluble parts could be calculated,

$$I_R = \left(\frac{(W_R - W_f)}{W_t} \right) * 100\% \qquad \text{(eq. 7.4)}$$

where I_R is the insoluble residue percentage of total mass, W_R is filter weight with residue, W_f is only filter weight and W_t is weight total (Laboratory Test Method OMYA, 2004).

7.4.3. Dolomite content

Similar to paragraph *7.4.2.* the samples were dissolved in hydrochloric acid (HCl) to analyse Ca/Mg ratios in the acid solution. This ratio is expressed in percentage calcite ($CaCO_3$) and magnesite ($MgCO_3$) although Mg is only present in the form of dolomite.

7.5. X-ray fluorescence analysis – XRF

7.5.1. Analytical characteristics

X-ray fluorescence spectrometry is a technique to analyse bulk specimens (Potts, 1987). Samples are prepared as compressed powder pellets or fused glass discs and excited with x-ray radiation, normally generated by an x-ray tube operated at a potential of between 10 and 100 kV. Interaction of this primary radiation with atoms of the sample causes ionisation of discrete orbital electrons. During the subsequent electronic rearrangement by which the atom then de-excites back to the ground state, fluorescence x-ray of energy characteristics of that element are emitted. The emission intensity of this characteristic radiation is measured with a suitable x-ray spectrometer and compared with that from a standard sample. The technique is one of the most widely used routine instrumental methods of analysing rock samples both for the major elements Na, Mg, Al, Si, P, K, Ca, Ti, Mn, Fe and selected trace elements, including Rb, Sr, Y, Nb, Zr, Cr, Ni, Cu, Zn, Ga, Ba, Pb, Th and U. Detection limits for many of these trace elements lie in the range 1 to 10 ppm rock under routine operation conditions.

Modern instrumentation is capable of achieving such a high degree of precision that it is generally accepted that analytical statistics in silicate rock analysis are principally limited by sample inhomogeneity effects (Potts, 1987). The very high order of statistical precision that can be obtained from modern instrumentation has tended to mask the fact that analytical accuracy depends both on the reliability of the matrix correction program and the procedures used for calibration. This touches on one of the limitations of x-ray spectrometry: the fact that it is a comparative technique in which calibrations must generally be carried out relative to assumed compositions in silicate rock reference materials. Accuracy is therefore critically affected both by the selection of samples to be included in the calibration set and the confidence that may be placed in compiled compositions of these materials. There have been serious shortcomings in compilations of some elements (particularly trace elements) in some reference rocks. If x-ray fluorescence spectrometry has one shortcoming, it is the confusion that can arise between

accuracy and instrumental precision and the complacency that can the result when critically assessing analytical data.

Conventional instrumentation for x-ray fluorescence analysis is based in wavelength dispersive spectrometers (Potts, 1987). In consequence, the origin of x-ray spectra are normally considered in terms of the wavelength (in Ångstrom or nm) of the corresponding emission lines.

7.5.2. Construction of the XRF

X-ray Fluorescence Analysis (XRF) uses x-rays generated by an X-ray tube to excite analytical X-rays from the sample (Fig. 7.9). The tube consists of a cathode running a current of 40 to 60 milliamps (mA) producing electrons that are accelerated by a voltage of 5 to 100 keV and fired at a target anode. The target generates broadband continuum X-rays and lots of heat (about 99% of the energy output). Both the cathode and target are put in vacuum to avoid oxidization and to minimize absorption of X-rays by air. The resulting X-rays are directed at the sample, causing it to emit X-rays characteristic of its constituent Schematic cross-section of x-ray fluorescence unitelements. The X-rays emitted by the sample are collimated and diffracted by an analyzing crystal in the spectrometer and their intensities measured using detectors mounted on a goniometer. The bulk chemistry of the sample is determined by comparing the intensities of the X-rays to those from standards.

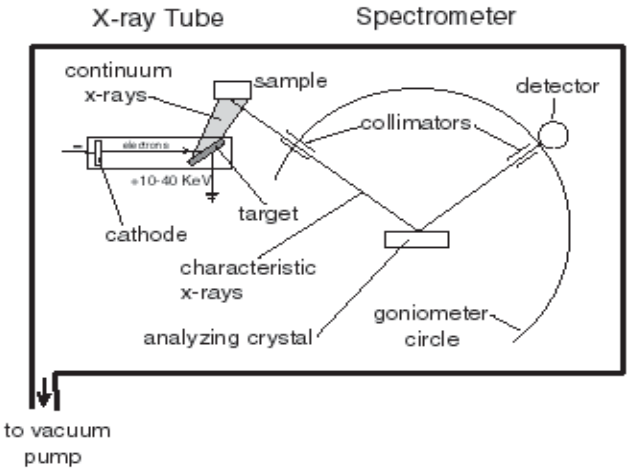

Fig. 7.9: Schematic diagram of the components of a typical wavelength-dispersive X-ray fluorescence (XRF) spectrograph from (Wittke, 2003).

The tube consists of a cathode running a current of 40 to 60 milliamps (mA) producing electrons that are accelerated by a voltage of 5 to 100 keV and fired at a target anode. The target generates broadband continuum X-rays and lots of heat (about 99% of the energy output). Both the cathode and target are put in vacuum to avoid oxidization and to minimize absorption of X-rays by air. The resulting X-rays are directed at the sample, causing it to emit X-rays characteristic of its constituent Schematic cross-section of x-ray fluorescence unitelements. The X-rays emitted by the sample are collimated and diffracted by an analyzing crystal in the spectrometer and their intensities measured using detectors mounted on a goniometer. The bulk chemistry of the sample is determined by comparing the intensities of the X-rays to those from standards. The measurements were done at Department of Earth Science at the Karl-Franzens University under the supervision of Dr. Hauzenberger. The used apparatus is a S4 PIONEER WDXRF produced by Bruker AXS (Fig. 7.10).

Fig.7.10: RFA - S4 PIONEER WDXRF produced by Bruker AXS

7.6. Inductively coupled plasma-mass spectrometry (ICP-MS)

This analytical technique is used to determine rare earth elements (REE). The mass spectrum (MS) of this ion source is measured using a quadrupole mass spectrometer (Potts, 1987) (Fig. 7.11). This was made possible by the development of an interface whereby plasma gases can be physically sampled through an orifice, via a differential pumping unit and into the quadrupole mass filter.

Fig. 7.11: ICP-mass spectrometer

The technique, therefore, combines the freedom from matrix interferences characteristic of the inductively coupled argon plasma with the very favourable signal-to-background ratios obtainable by mass spectrometry. Samples must first take up into solution (description next page) and are then aspirated into the argon plasma in the conventional manner. Detection limits for applications in multi-element silicate rock analysis have not, at the time of writing, been fully characterized. ICP-MS has a clear application in the analysis of waters and is likely to have a significant impact on routine trace geochemical analysis. This is so, in view of the potential of this technique to determine simultaneously a wide range of heavier trace elements, often down to ppm whole-rock levels, using a simple sample dissolution technique with no preconcentration stage. Of particular interest in this respect is the application of ICP-MS in the determination of the rare-earth elements and a wide range of trace elements important in economic geology studies including As, Sb, Se, Te, Bi, Hg, Au, Ag, and the platinum group elements.

As a mass spectrometry technique, ICP-MS is capable of determining individual isotope ratios (Potts, 1987). There is, therefore, considerable potential in applying isotope ratios can be measured (about 1-3% two sigma) is not adequate to permit reliable determination of radiogenic isotope ratios (e.g. Rb-Sr, Nd-Sm, U-Th-Pb). The technique does not, therefore, rival conventional thermal ionization mass spectrometry in geochronological studies, although ICP-MS does show some potential in the specialized determination of osmium isotope ratios required for the Re-Os geochronometer.

7.6.1. Sample preparation of marble samples for ICP-MS measurement

For the sinter disintegration the sample must be pulverised, dried and mixed with Na_2O_2 in a proportion of 1:6 (100mg sample + 600 mg Na_2O_2). After sintering in the oven (480 C, 30 minutes) water is added to the mixed powder. The fluid sample is centrifuged and after separating the solid residuum has to be dissolved with HCl (Piribauer, 2007).

7.7. X-Ray Diffraction

X-ray diffraction analysis (XRD) was used as a non-destructive method and as a destructive method (powder diffraction) – this method was used for the study - for the structure analysis of crystals and to analyse the mineral content of a rock and special in this work the acetic acid insoluble part of the marbles (Cullity, 1987). X-ray diffraction analysis is based on the possibility of crystal lattices to diffract monochromatic X-ray light. Diffraction is due essentially to the existence of certain phases relations between two or more waves. The interferences of the waves are described by Bragg's equation

$$n\lambda = 2d\sin\theta \qquad (n = 1, 2, 3,\ldots) \qquad \text{(eq. 7.5)}$$

where λ is the wavelength, d is the lattice plane distance and θ is half the diffraction angle. This relation is used for the structure analysis of crystals.

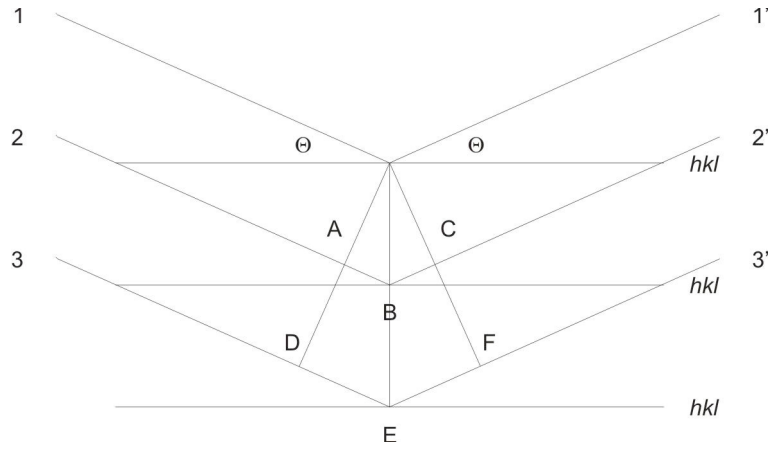

Fig. 7.12: Diffraction of X-rays from the planes in a crystal (Lifshin, 1999) and hkl are the Miller Indices. The length *AB* + *BC* must correspond to the wavelength of the X-ray.

Fig. 7.13: XRD Siemens D5000

The XRD measurements have been conducted at the lab of OMYA-TBG in Gummern with a powder diffractometer of Siemens D5000 (Fig. 7.13). The data was interpreted with the analysis program *EVA*.

8. Results of Investigations

8.1. Petrographic of marbles, fluid inclusions and wall rock

8.1.1. Mineral composition of marbles:

Thick sections (100 µm thickness) with polished surface were made from the marble samples. The marbles consist mainly of calcite, coarse grained and minor amounts of dolomite. Dolomite occurs in layers or as relicts within calcite grains (e.g. sample Bay 10, see Fig. 8.1). Graphite, hematite and magnetite are accessory minerals, up to 2 vol.% in respectively Merluzzi samples, Bayramic and Orhaneli. The Mer-Grau (grey marble) sample contains more graphite than the Mer-Blau (blue marble) samples (Fig. 8.2). Hematite and magnetite occur up to 2 vol.% in Bayramic samples (Bay 22, 23) and in much smaller amounts in Orhaneli samples (Orh 1, 2, 14 and 26) (Fig. 8.3). Silicates can be found in the darker layers of Orh 37 and Orh 2.

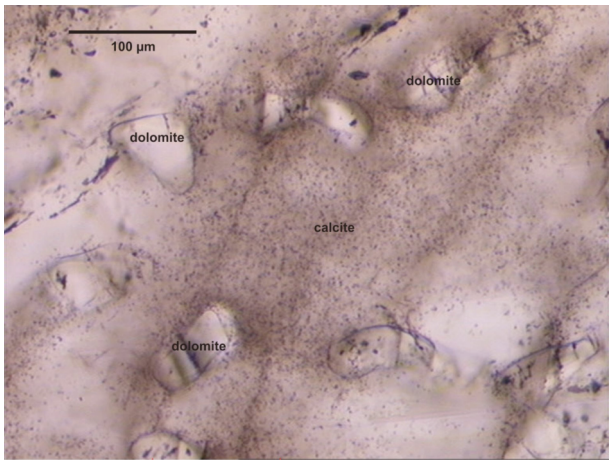

Fig. 8.1: Relicts of dolomite in calcite (Bay 10)

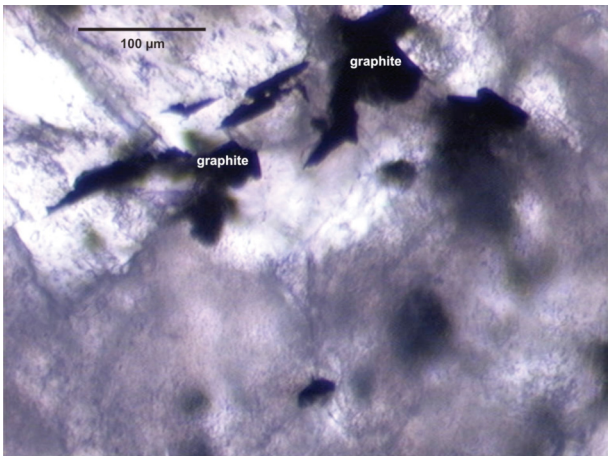

Fig. 8.2: Graphite in the sample Merluzzi Grau.

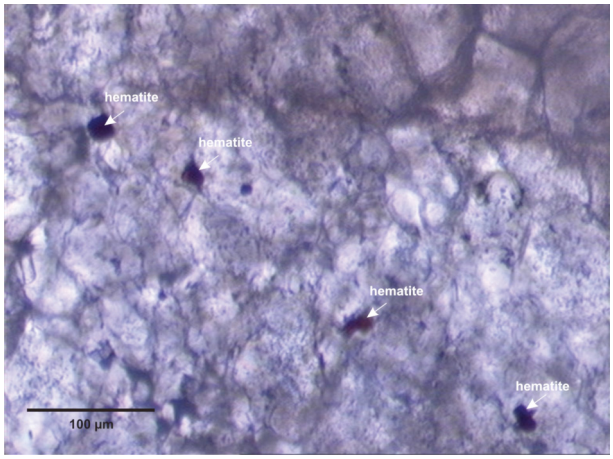

Fig. 8.3: Hematite in Orh 14

All marble samples have similar inclusion aspects and similar inclusion arrangements. Most of the inclusions appear in cloudy zones. These clouds are not restricted to single grains. Mostly they are covering various grains (Fig. 8.4 and 8.5).

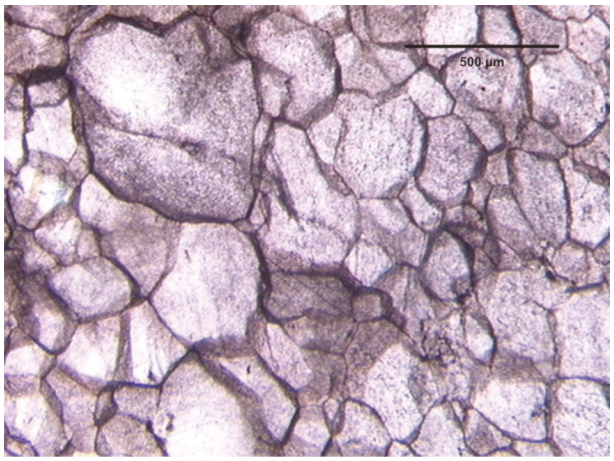

Fig 8.4: An overview of small calcite grains (from 100 to 500 μm diameter) with clouds of fluid inclusions (Orh 14)

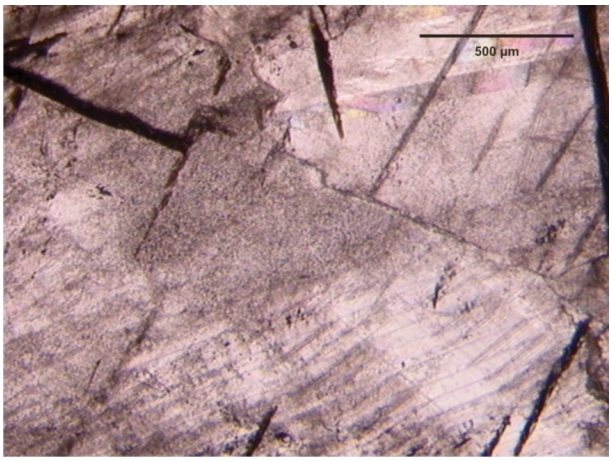

Fig 8.5: Clouds in large grains (2 mm) defined by the occurrence of many small fluid inclusions (Bay 1)

8.1.2. Fluid inclusions in marbles

The marbles from Bayramic, Orhanelli and Merluzzi contain two types of fluid inclusions:

1. Water-rich inclusions
2. Gas-rich inclusions

In greyish samples like those from Bayramic and Merluzzi, the inclusions are present over the whole section. Grains cannot be divided in cloudy and clear zones because the fluid inclusions are distributed evenly. The shape of the inclusions is similar in all marble samples from Bayramic, Orhaneli and Merluzzi. Mostly they are round or oval (Fig. 8.6), especially for gas-rich inclusions. Others (mainly water-rich inclusions) are elongated (Fig. 8.7) or irregular.

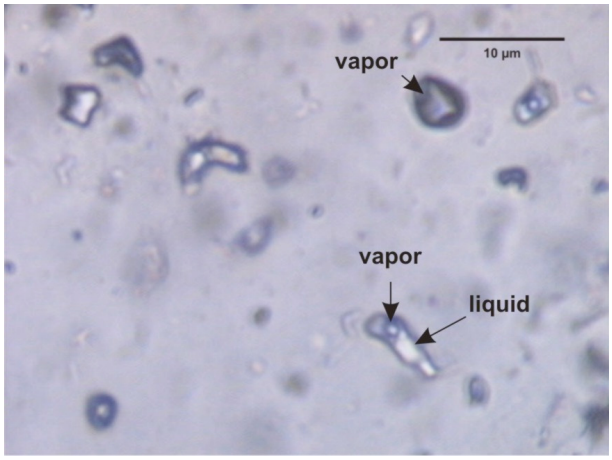

Fig.8.6: Gas-rich and water-rich inclusions (Bay 1)

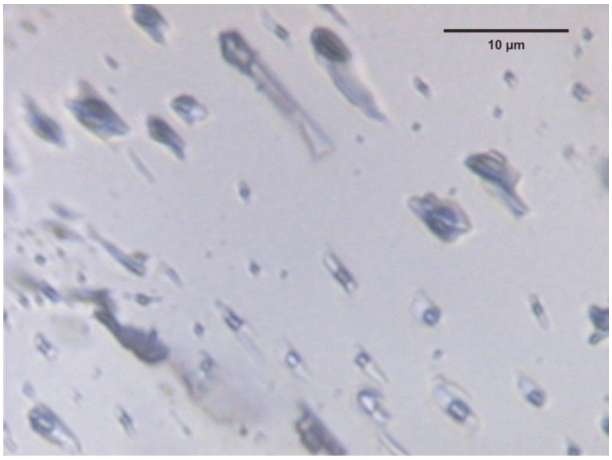

Fig.8.7: Typical elongated water rich inclusions (Bay 4)

Fifteen inclusions were analysed from the gas rich samples Bay 1 and Bay 4 on shape definition (Fig. 8.8). These measurements are representative for all inclusions which are occurring in the other marble samples. The inclusions have regular shapes, most of them are equant and some are elongate.

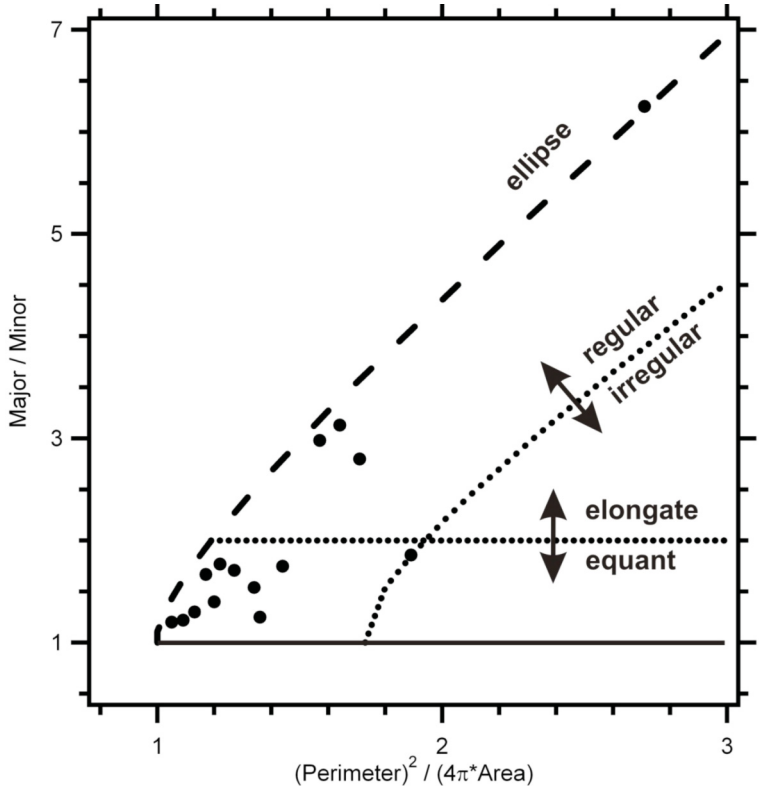

Fig. 8.8: Measured shapes of the inclusions from Bay 1 and Bay 4

In the samples from Bayramic, Orhaneli and Merluzzi the "clear" zones appear bright in transmitted light (Fig. 8.9) and contain only few inclusions (water-rich). These inclusions occur in small groups in small parts of the grain (Fig. 8.10) or along trails (Fig. 8.11).

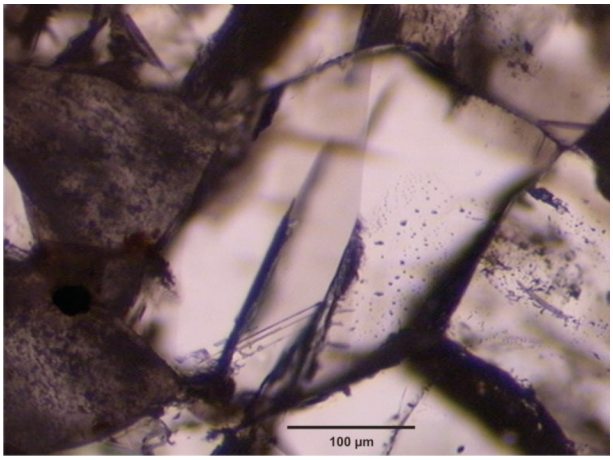

Fig.8.9: A clear grain in Bay 1

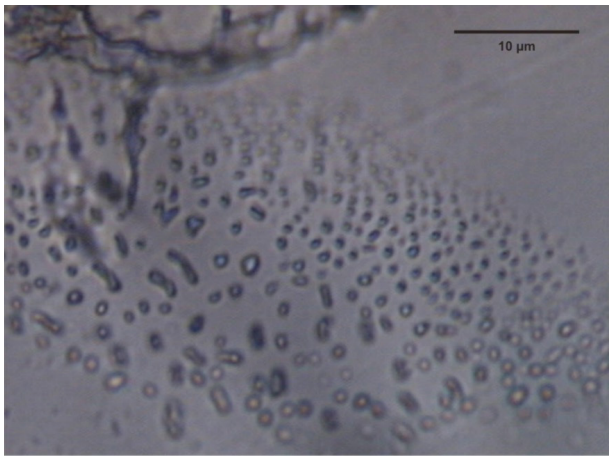

Fig.8.10: Water rich inclusions in the clear zone (Bay 22)

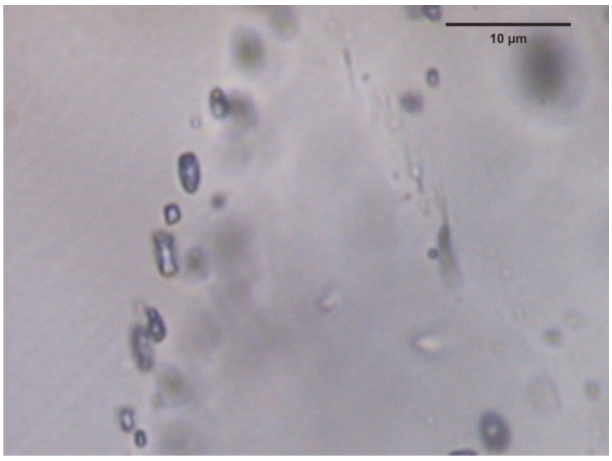

Fig.8.11: An inclusion trail in the clear zone (Orh 1)

Water rich inclusions occur in the entire section – in both clear and in cloudy zones. The analysed gas rich inclusions occur only in the "cloudy" zones and are not homogeneous distributed but rather disseminated in the "cloudy" zones (Fig. 8.12 and 8.13). The sizes of the inclusions range from lesser than one µm up to around 15µm in diameter. The larger inclusions (>10µm) are only water-rich, whereas the smaller fluid inclusions are gas-rich and water-rich. The water-rich inclusions contain a liquid phase (H_2O) and a vapour bubble (H_2O or gas). Gas-rich inclusions contain in general one-phase, occasionally with a rim of water.

The samples from Orhaneli show some darker zones. These zones contain most of the inclusions. In the lighter parts of the samples clearer zones can be found but they show some inclusions whereas only very few inclusions are found in the clear zones.

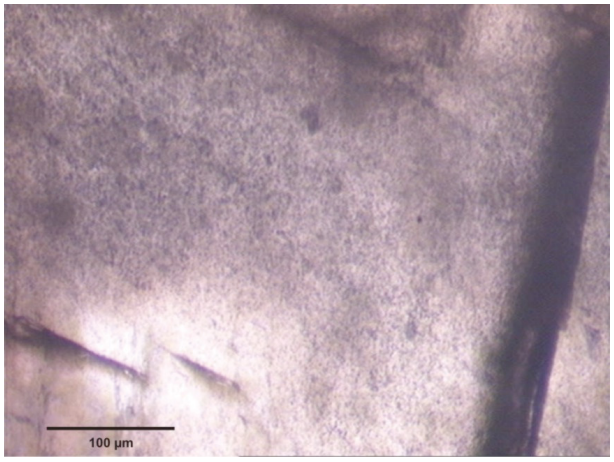

Fig.8.12: A dark zone, containing a cloud of fluid inclusions (Mer-Blau)

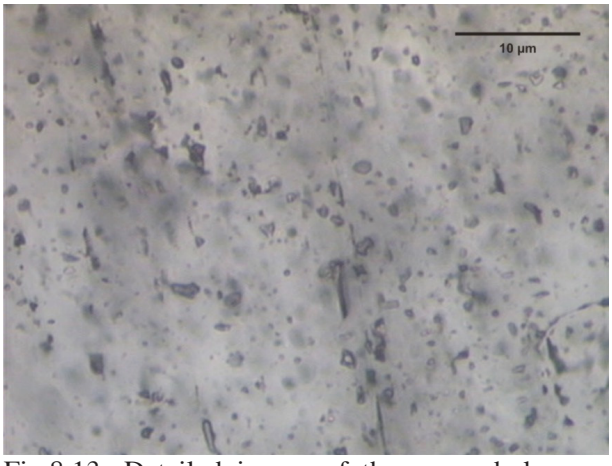

Fig.8.13: Detailed image of the same dark zone (see Fig. 8.12), illustrating the presences of many fluid inclusions.

The number of fluid inclusions and the total fluid in a calcite grain in the marble is estimated with a two-dimensional projection, as seen through the optical microscope. In "clear" zones,

the maximum number of inclusions (only water-rich) is about 50 in an area of 1750 µm^2. The average size (area in projection) of inclusions is about 2.25 µm^2. Consequently, a calcite grain contains about 6 vol.% H_2O. In cloudy zones, up to 80 inclusions were counted in the same area. These inclusions are both water-rich (around 25-30%) and gas-rich (around 70-75%). Consequently, 10 vol.% of these calcite grains consist of fluid inclusions, of which 3 vol.% are water-rich and 7 vol.% gas-rich.

8.1.3. Mineral composition of wall rocks:

Sample Bay 9, Schist

Schists are found near the quarry "Sebastian" in direct contact with the marble (Fig. 8.14). The mineral composition of the schist is quartz, biotite, chlorite, muscovite, feldspar (plagioclase), aktinolite/tremolite, zircon, and tourmaline. The percentage of the minerals outside of the vein is estimated as follows: Quartz (~50 %); biotite, chloride and muscovite (together also ~50%); zircon, tourmaline and aktinolite/tremolite are only accessories. The schist is fine grained (50 µm to 100µm) and elongated minerals (i.e. biotite, chlorite, aktinolite/tremolite and tourmaline) are aligned parallel to the foliation. The sample is penetrated with 0.5 cm thick vein containing bright minerals such as quartz (70 %), muscovite (15 %) and feldspar (15 %) – feldspar (plagioclase) only occurs in the vein (Fig. 8.15). The grain size in the vein varies from 0.1 mm to 0.5 mm. Foliation or other deformation phenomenons are not observed in the vein (Fig. 8.14).

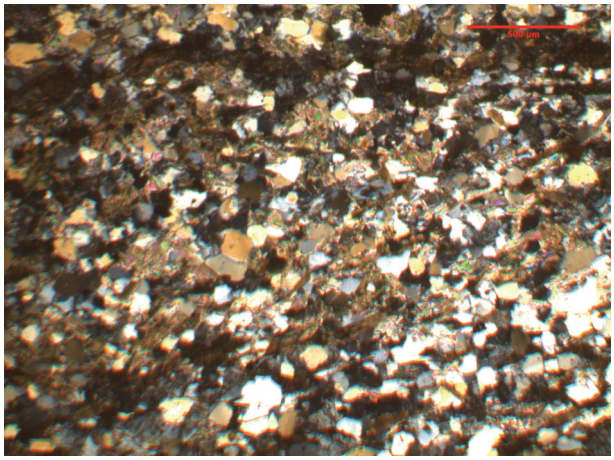

Fig. 8.14: Schist containing quartz and muscovite

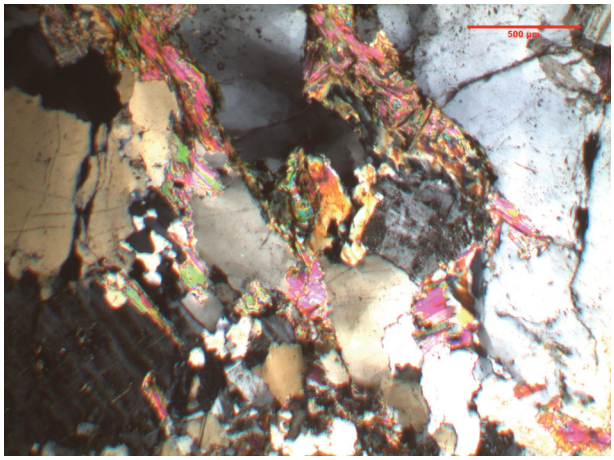

Fig. 8.15: Vein in schist, with quartz and muscovite

Sample Bay 12, Diorite

Diorite is located near the "Charles" quarry in contact with carbonate rock. It contains feldspar (plagioclase) (~80 %), biotite (max. 5 %), pyroxene (orthopyroxene) and amphibole (together ~15 %). The diorite is relativly undeformed and no foliation can be observed (Fig. 8.16). Plagioclase is hypidiomorphe with a zonar structure and twins. Pyroxene is partly altered into amphibole, which appears in spots (Fig. 8.17).

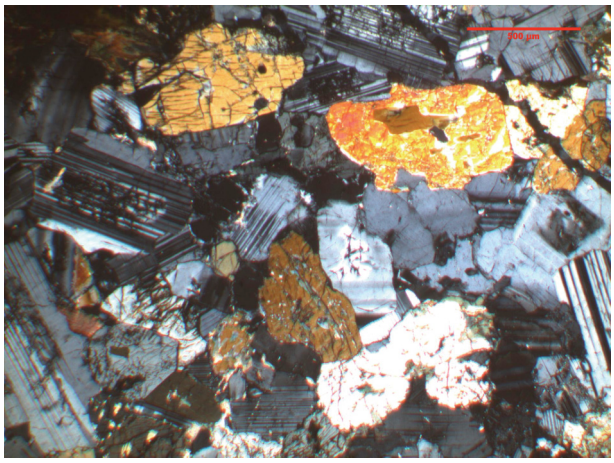

Fig. 8.16: Diorite with plagioclase, biotite, pyroxene and amphibole crystals

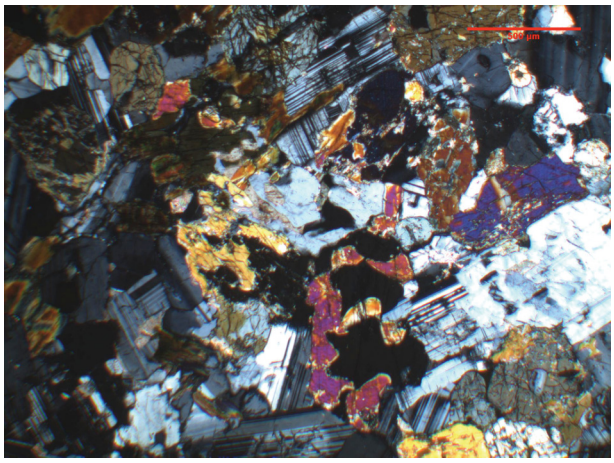

Fig. 8.17: Alteration of pyroxene into amphibole

Sample Bay 13, Marble (deformed)

The sample consists of highly deformed and altered marble in contact with the diorite. This rock is highly fractured and hosts many small veins. The veins (1 mm to 100 µm thick) cross other veins and lager calcite grains (Fig. 8.18 and 8.19). In the veins show much smaller grain sizes than the host rock.

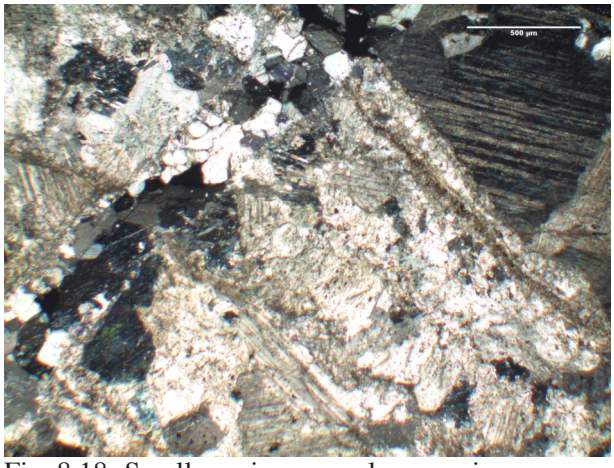

Fig. 8.18: Smaller vein cross a larger vein

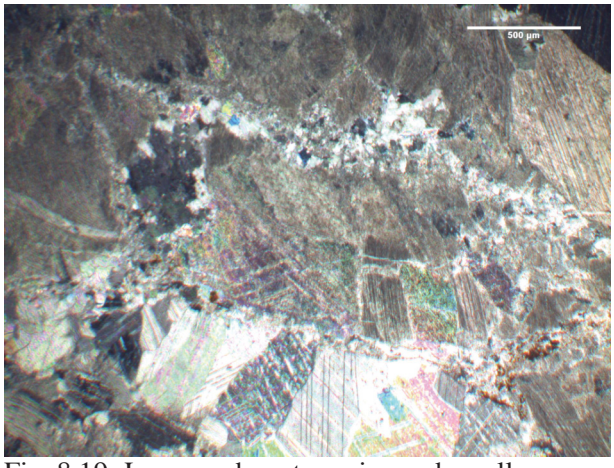

Fig. 8.19: Large carbonate grains and small carbonate grains in a vein.

Sample Bay 16, Gabbro

A plagioclase-pyroxenes bearing Gabbro was found in outcrops in the forest below around 100 m the quarry "Charles". It contains feldspar (~ 50 %), pyroxene and amphibole (~ 50 %), apatite, and accessorily titanite, and hematite. Small hematite needles can be found along the cleavage within the pyroxene crystals (Fig. 8.20). The pyroxene is highly altered and often hardly to differ from amphiboles. The core is pyroxene and the rim is amphibole (Fig. 8.21 and 8.22). Maximum grain sizes are about 0.5 cm. The amphibole is an aktinolite with inclusions of small epidote grains and tremolite needles (Fig. 8.23). The feldspar (plagioclase) is also altered. The grains show hypidiomorphe forms and they have a zonar structure (Fig. 8.24). The apatite show hexagonal idiomorphic shapes (Fig. 8.25).

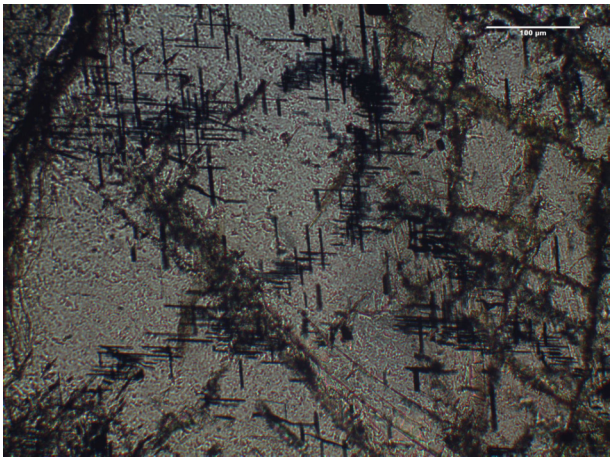

Fig. 8.20: Hematite needles in pyroxene, // Nichols

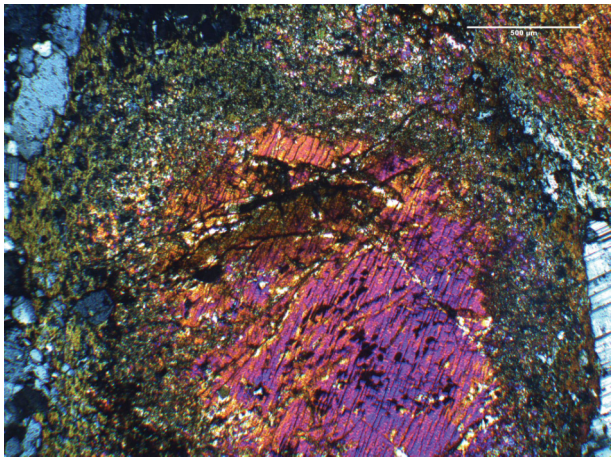

Fig. 8.21: Alternated pyroxene under X Nichols

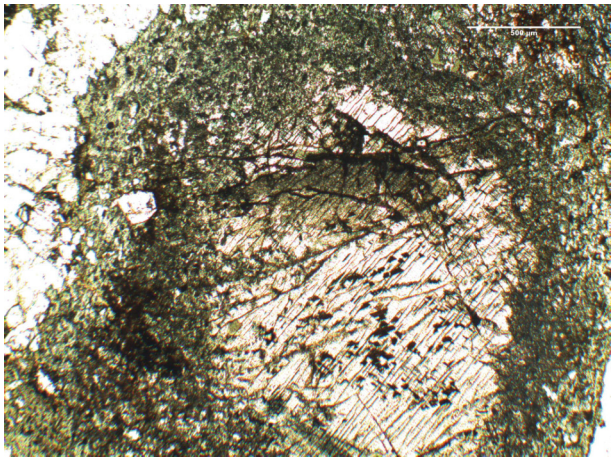

Fig. 8.22: Alternated pyroxene under II Nichols

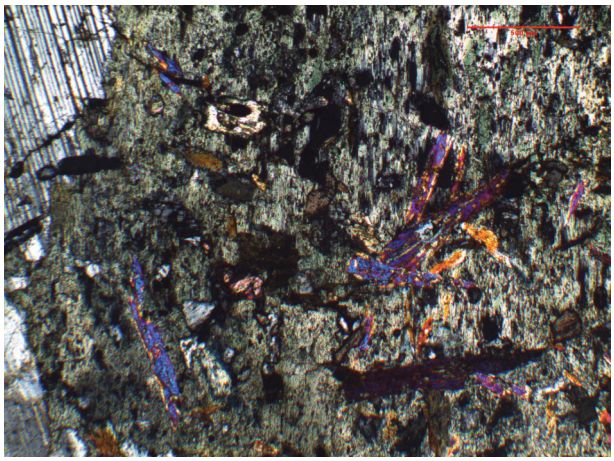

Fig. 8.23: Tremolite and epidote in aktinolite, crossed Nichols

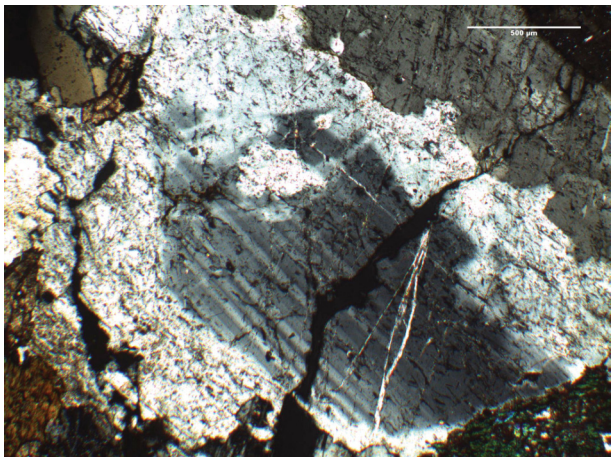

Fig. 8.24: Zonar structure of plagioclase

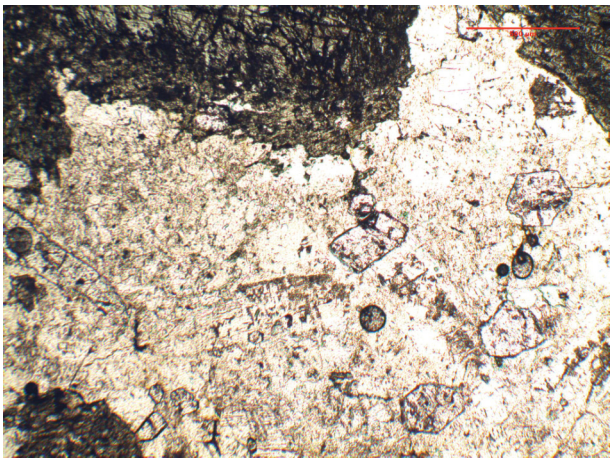

Fig. 8.25: Apatite

Sample Orh 8, Schist

A quartz-serizite-schist was collected near "Ceki 1". It consists of approximately 80 % estimation of quartz and 20 % serizite/muscovite. The muscovite occurs in short lamellas (100 µm). The quartz shows grain sizes up to 250 µm, an undulatory extinction and a polycrystalline network (Fig. 8.26). A 1 cm to 2 cm thick fine grained quartz and muscovite vein crosses the section (Fig. 8.27).

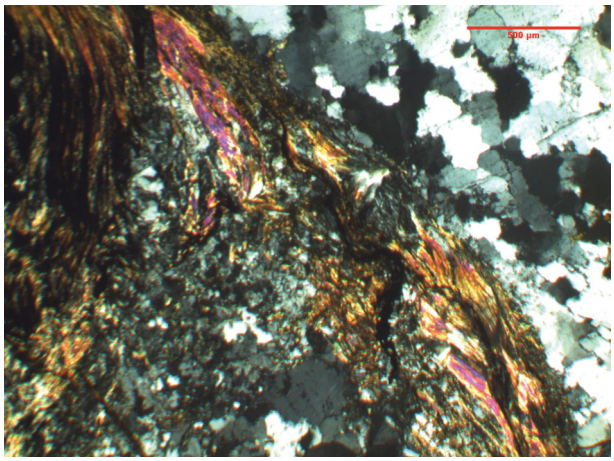

Fig. 8.26: Quartz and muscovite

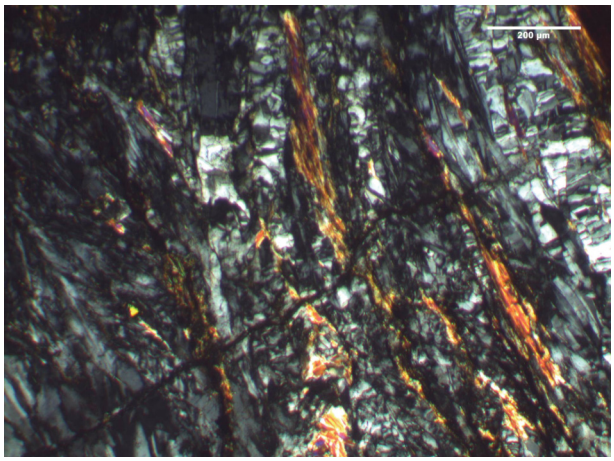

Fig.8.27: Fine grained muscovite and quartz in the vein with preferred orientation

Sample Orh 12, Serpentinite

A serpentinite with mainly serpentine can be found close to "Ceki 1" (similar locality as Orh 8). Serpentine shows the typical "Maschenstruktur" (Fig. 8.28). It contains relicts of olivine (~ 10 %) and pyroxene (~ 10 %) crystals which derived from the earlier magmatic rock (ophiolite). Opake minerals are identified as chromite with small veins of magnetite (~10 µm thick) (Fig. 8.29)

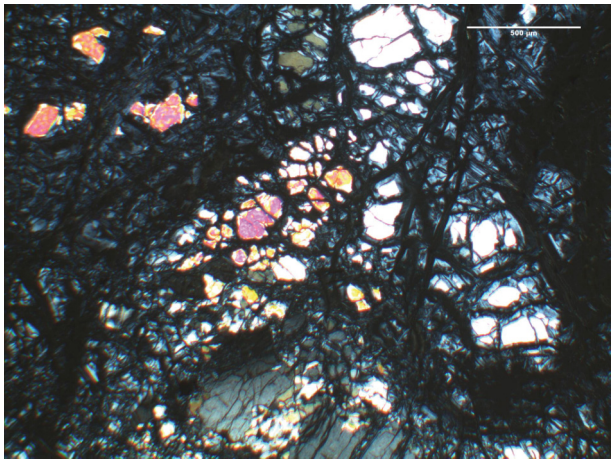

Fig. 8.28: Pyroxene- and olivine relicts in serpentine (Maschenstruktur), crossed nichols

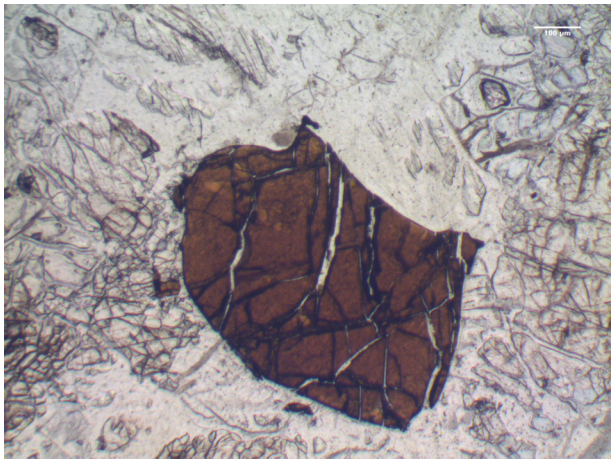

Fig. 8.29: Reflective light image of chromite with magnetite veins

Sample Orh 24, Granite

Granite occurs at the contact with the marble near Ceki 2. It consists of quartz (~ 20 %), hornblende (~ 10 %), feldspar (plagioclase) (~ 60 %), biotite (~ 10 %) and titanite (accessory). The quartz shows no undulatory extinction and the grains have similar dimension (size ~ 0.5 mm to 1 mm). The titanite is formed in the typically wedge shape (Fig. 8.30). The feldspar grains (plagioclase) have a zonar texture (Fig. 8.31) and twins. Biotite occurs in large sheets and is often included in the other minerals.

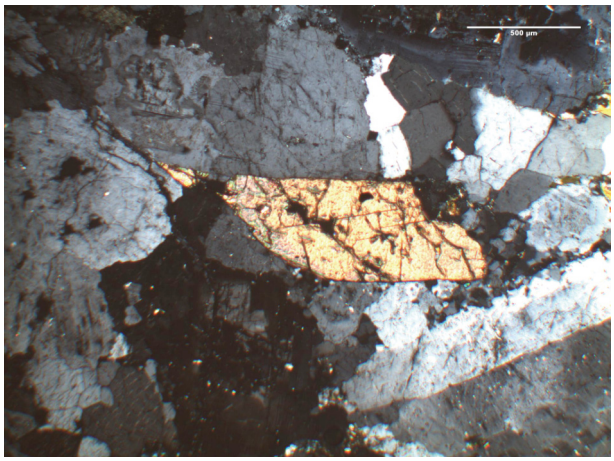

Fig. 8.30: Titanite surrounded by plagioclase and quartz

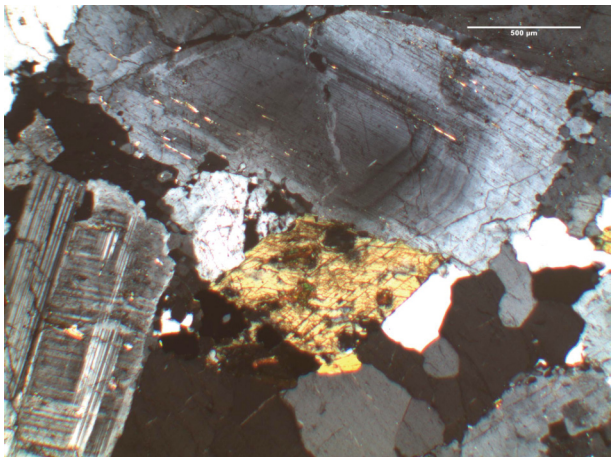

Fig. 8.31: Pyroxene with biotite surrounded by plagioclase and quartz.

Sample Orh 41, Siliceous Marble

A siliceous marble with garnet (~ 50 %), quartz (~ 25 %) and carbonate (~ 25 %) occurs between the marble and granite in Sögüt. The garnet grains are large (~ 1 cm diameter) with an euhedral form and interspersed with carbonate and quarts veins (~ 0.5 mm thick) (Fig 8.32). The calcite occurs in large grains (~ 500 µm) (Fig. 8.33) and in fine-grained (~50 µm) in veins. The veins through the garnet also contain grains of calcite and cherts (Fig. 8.34, 8.35)

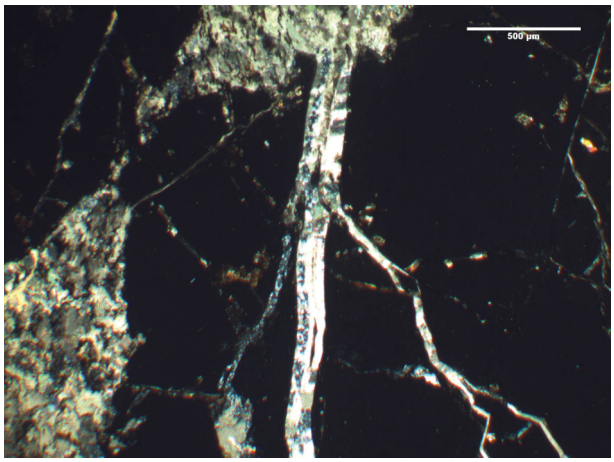

Fig. 8.32: Garnet with quartz vein (+cherts)

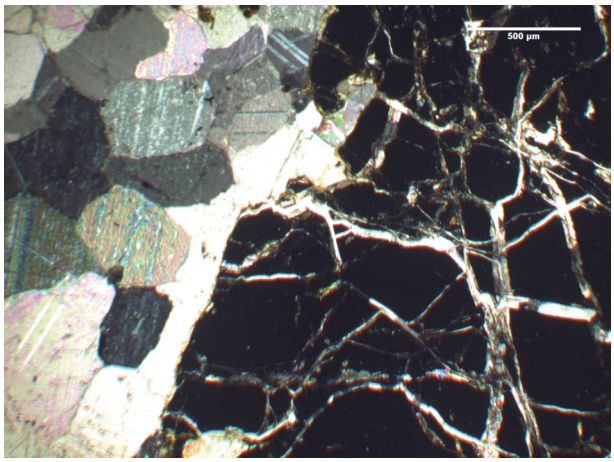

Fig. 8.33: Euhedral carbonate crystals in a granoblastic texture and a garnet crystal

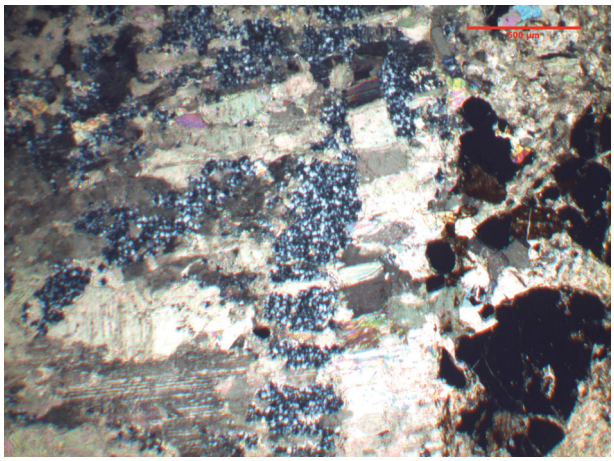

Fig. 8.34: Carbonate gangue with cherts

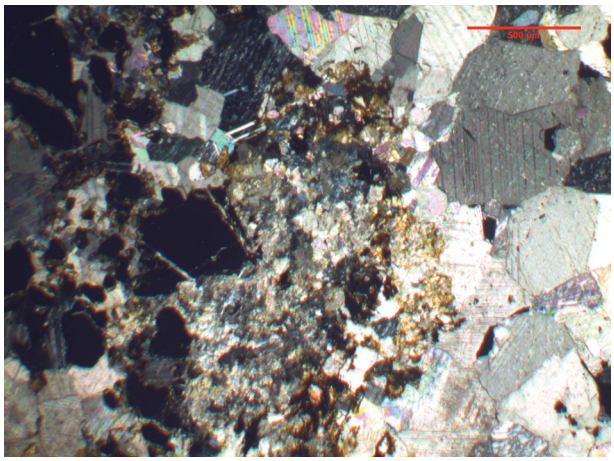

Fig. 8.35: Coarse- u. fine grained carbonate

Sample Orh 44, Granite

This sample shows granite with the mineral composition of quartz (~ 25 %), feldspar (plagioclase) (~ 35 %), hornblende (~ 15 %) and biotite (~ 25 %) from Sögüt. The sample Orh 44 is very similar to the sample Orh 24. The feldspar has a clear zoned texture (Fig. 8.36) with twins. Hornblende also shows twins (Fig. 8.37 and 8.38). The quartz has no undulatory extinction and shows also polycrystalline form. The biotite occurs in large sheets (Fig. 8.39)

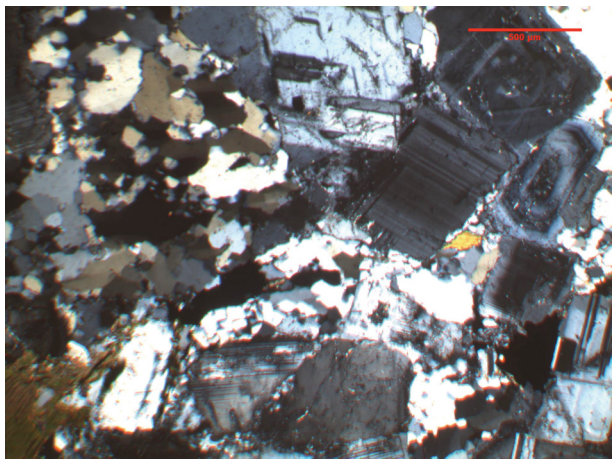

Fig. 8.36: Quartz, biotite and feldspar with zonar structure

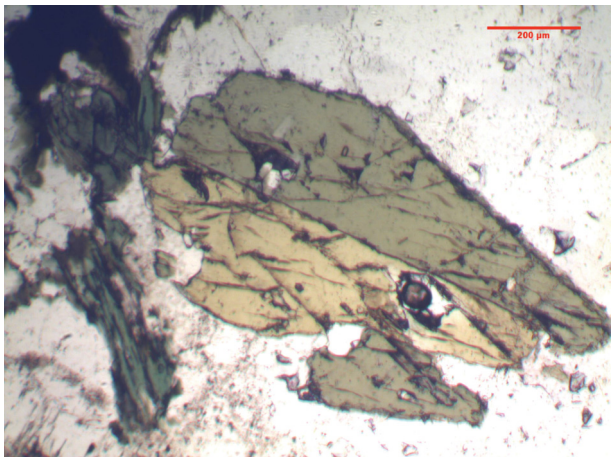

Fig. 8.37: Hornblende twins, // nichols

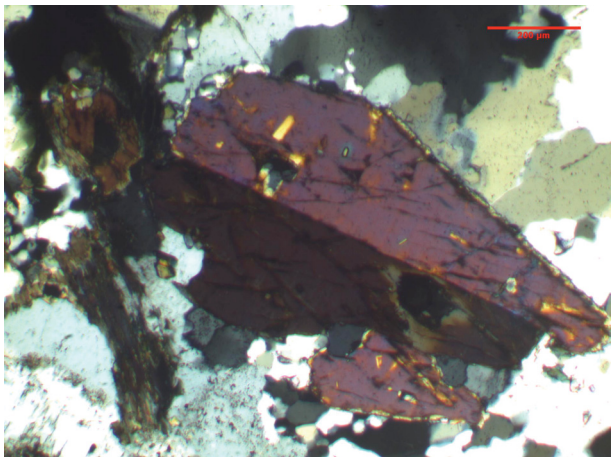

Fig. 8.38: Hornblende twins, crossed nichols

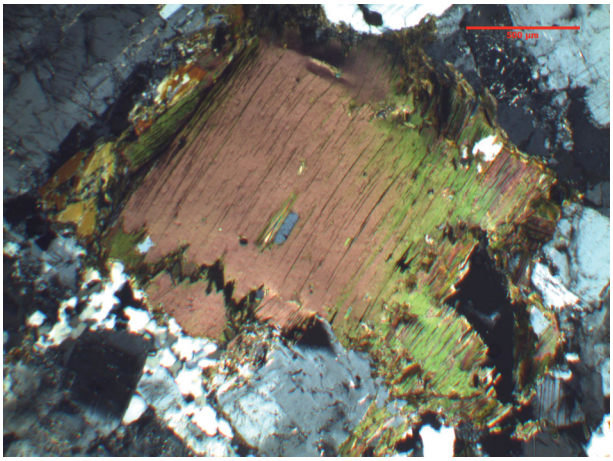

Fig. 8.39: Biotite surrounded by feldspar and quartz

8.2. Raman summary

8.2.1. Raman spectroscopy of the fluid and gas inclusions

Raman spectroscopy is an important analytical technique to characterize and distinguish the different types of fluid inclusions in the sample, and to qualify mineral phases.

Around 20 gas-rich fluid inclusions were measured in the samples (Bay 1, Bay 7, Orh 1, Orh 2, Orh 14, Mer-grau and Mer-blau). The vapour phase in the gas-rich fluid inclusions consist of different mixtures of CO_2-H_2S-CH_4-N_2 (see Tab. 8.1 and Fig. 8.41) and also within one sample the compositions of the gases are not equal. The variation in composition increases with the presence of more gases of different types. The different quarries show distinctive gas compositions (Tab. 8.1, Fig. 8.40).

Sample	Mole fraction of CO_2 (%)		Mole fraction of H_2S (%)		Mole fraction of CH4 (%)		Mole fraction of N_2 (%)		Quarry
	average	*Range*	*average*	*range*	*average*	*range*	*average*	*range*	
Bay 1	96.3	93.6 - 97.9	3.7	2.1 - 4.0	-	-	-	-	Bayramic
Bay 7	95.8	91.5 - 99.6	4.2	0.3 - 8.5	-	-	-	-	Bayramic
Orh 1	89.5	0.0 - 93.2	6.7	4.5 - 72.1	3.7	2.1 - 27.9	-	-	Orhaneli
Orh 2	90.8	83.8 - 97.9	6.4	1.3 - 14.4	2.8	0.6 - 5.5	-	-	Orhaneli
Orh 14	84.5	77.3 - 94.4	13.8	4.3 - 21.7	1.6	0.0 - 5.3	-	-	Orhaneli
Mer-grau	77.2	69.6 - 87.5	14.6	7.2 - 28.6	5.6	2.5 - 9.0	2.7	0.0 - 11.7	Krastal
Mer-blau	72.3	44.9 - 87.1	13.3	4.3 - 21.2	5.2	2.5 - 10.7	9.2	0.0 - 33.5	Krastal

Tab. 8.1: Molefraction and margin of CO_2, H_2S, CH_4 and N_2 of the samples from Bayramic, Orhaneli and Gummern.

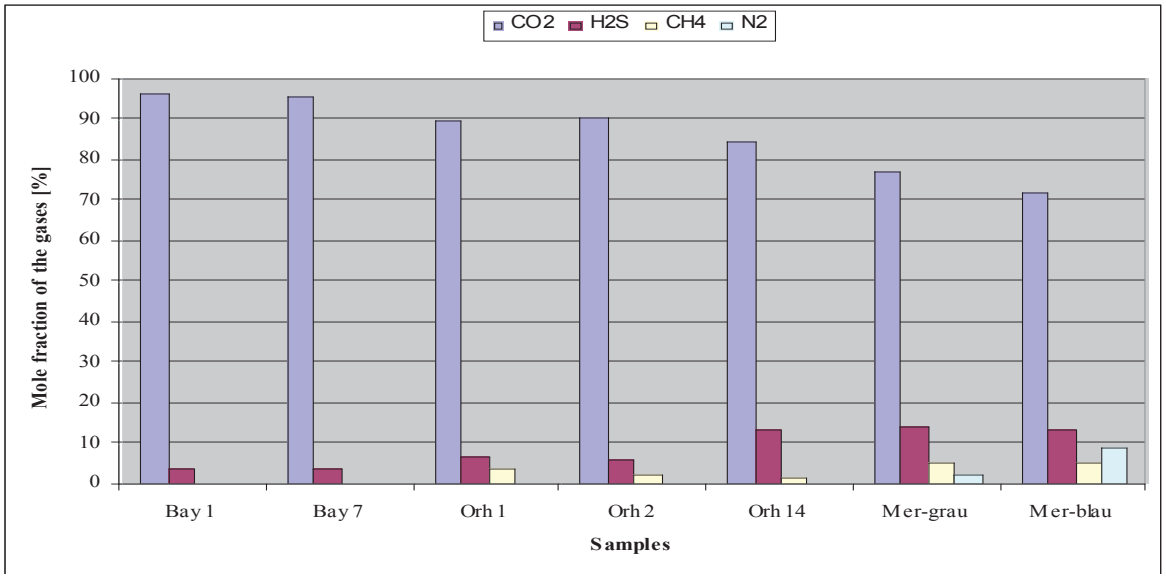

Fig. 8.40: Different gas compositions of the samples.

The samples from Bayramic contain mainly CO_2, with minor amounts of H_2S and no other gases. The samples from Orhaneli also contain CH_4 in the vapour phase. Ceki 1 (Orh 1 and Orh 2) contains relatively less H_2S than Ceki 2 (Orh 14). The samples from Merluzzi show considerable amounts of N_2 in addition to H_2S and CH_4 whereas CO_2 makes up only 72-77 mole %. The samples of Merluzzi have the greatest variation and Bayramic the least. For diagrams and charts of all results see appendix.

The CO_2 spectrum (Fig. 8.41) has in all samples a similar peak position (1285 and 1390 cm^{-1}). However, the intensity of the peaks depends on the depth of the inclusion beneath the calcite surface and the CO_2 density. Those who are close to the surface give the highest intensity.

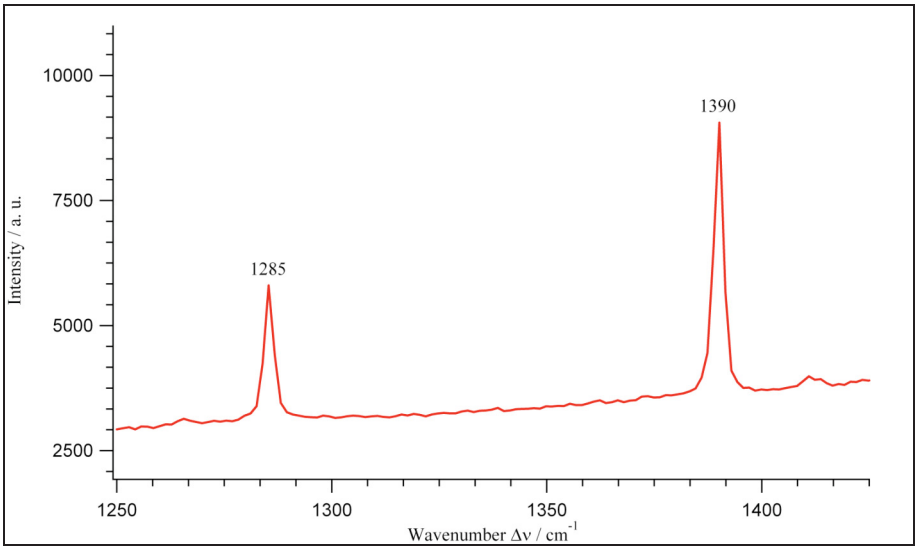

Fig. 8.41: CO_2 spectrum with two main peaks (Bay 1)

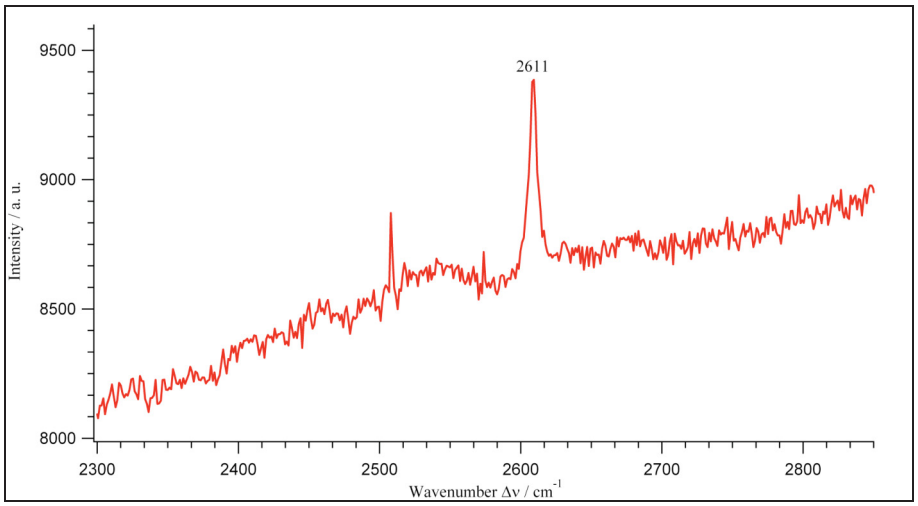

Fig. 8.42: H_2S spectrum with a peak of the calcite (Bay 7)

Figure 8.42 shows a typical H_2S spectrum of Bayramic. The high irregular background signal is caused by fluorescence of the calcite.

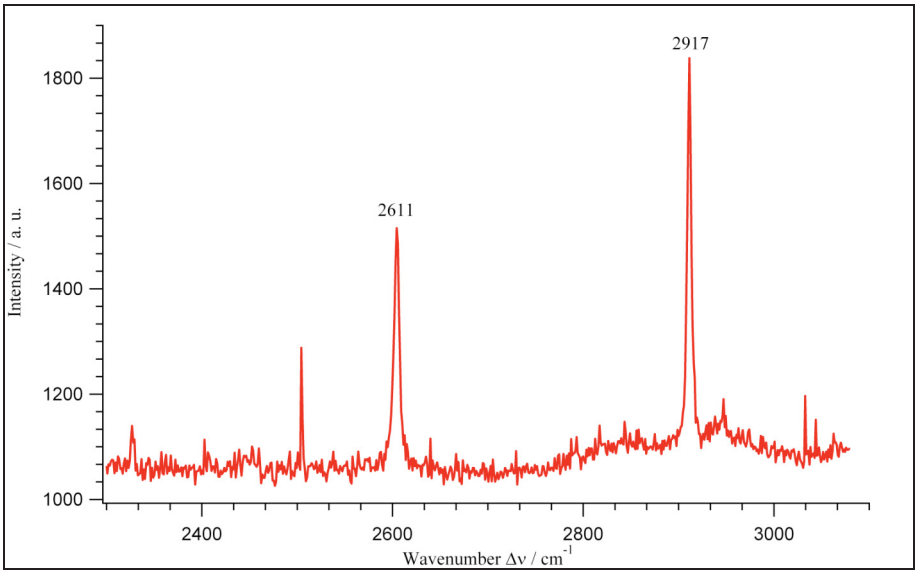

Fig. 8.43: H_2S and CH_4 spectra with peaks at 2611 cm^{-1} and 2917 cm^{-1} (Orh 2)

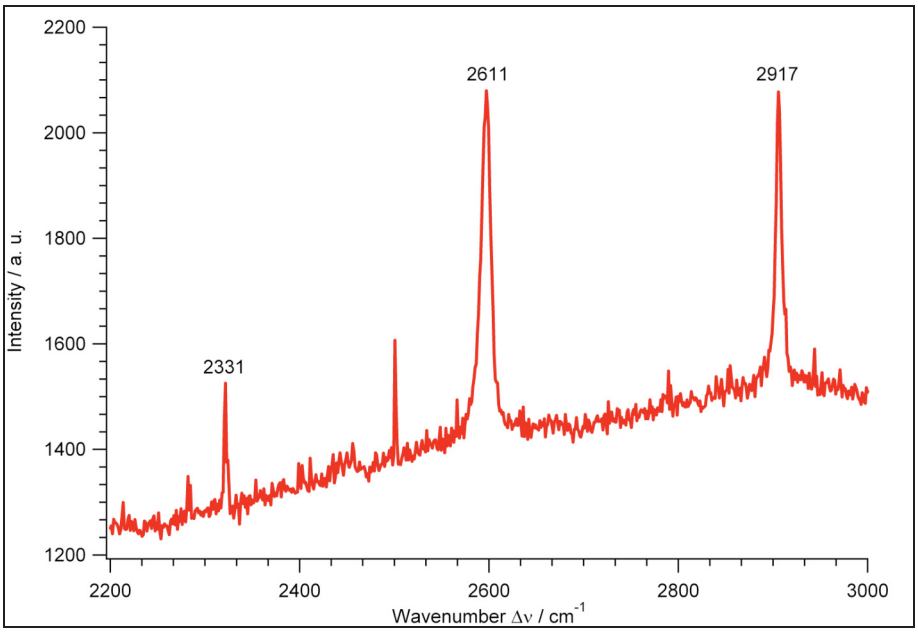

Fig. 8.44: N_2, H_2S and CH_4 spectra with 2331 cm^{-1}, 2611 cm^{-1} and 2917 cm^{-1} (Mer-grau)

All the spectra from the Orhaneli samples are similar to those illustrated in Figure 8.43, whereas the Merluzzi samples are characterised by the spectrum Figure 8.44.

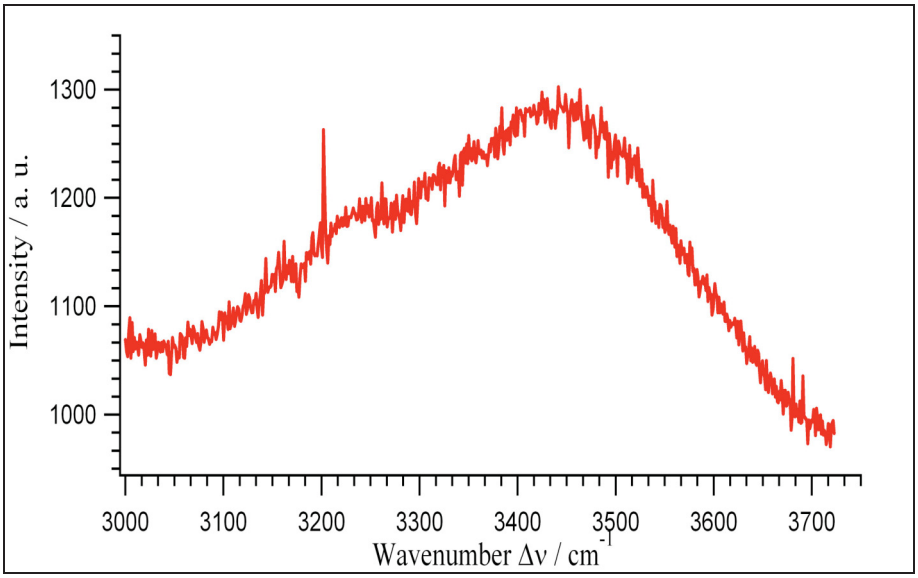

Fig. 8.45: A spectrum of an aqueous solution from inclusions in Bay 1

The water-rich fluid inclusions reveal a spectrum typical of H_2O with minor amounts of dissolved salts in the range 3000 to 3700 cm^{-1} (Fig. 8.45, see also Bakker, 2004).

8.2.2. Raman spectroscopy of carbonates

In addition Raman spectroscopy is used to identify solid inclusions within calcite grains in the marbles and to make a distinction between calcite and dolomite (Fig. 8.46 and 8.47)

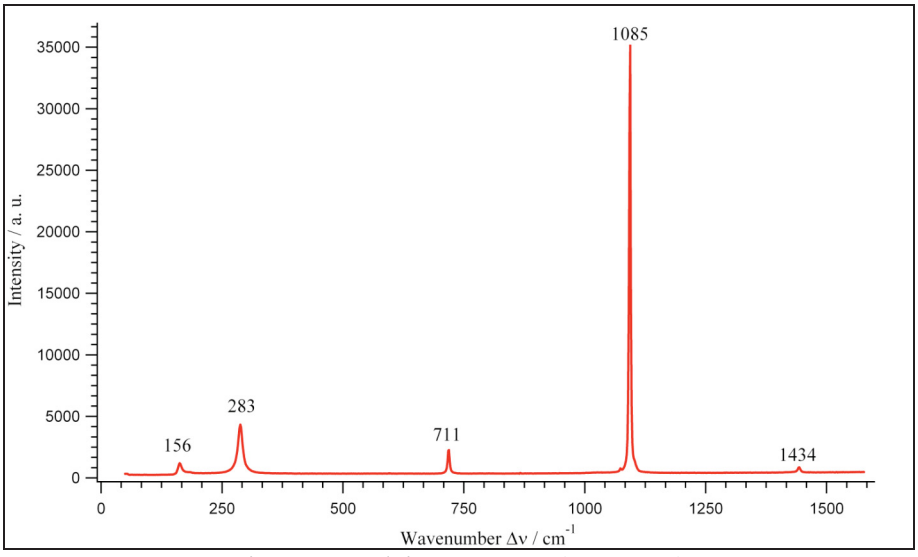

Fig. 8.46: Calcite spectrum (Mer-grau)

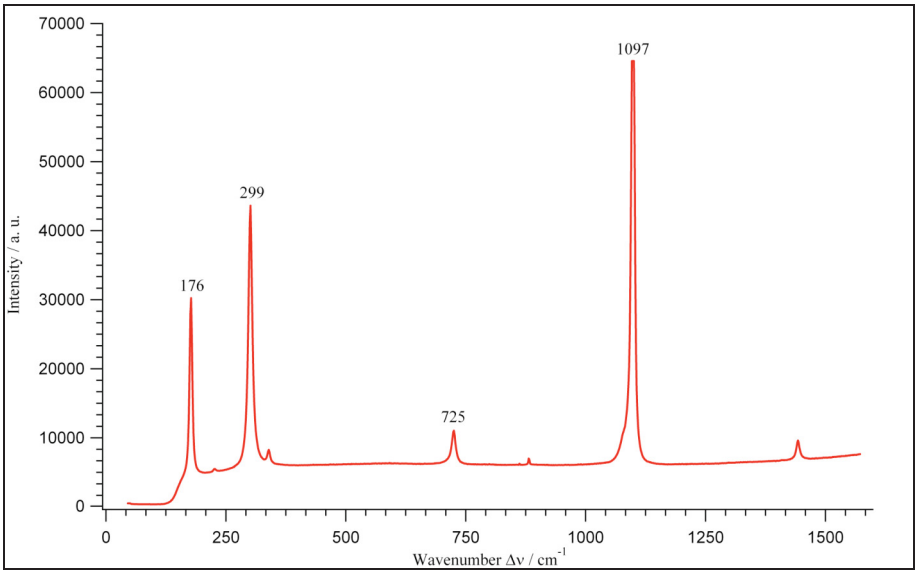

Fig. 8.47: Dolomite spectrum (Bay 4)

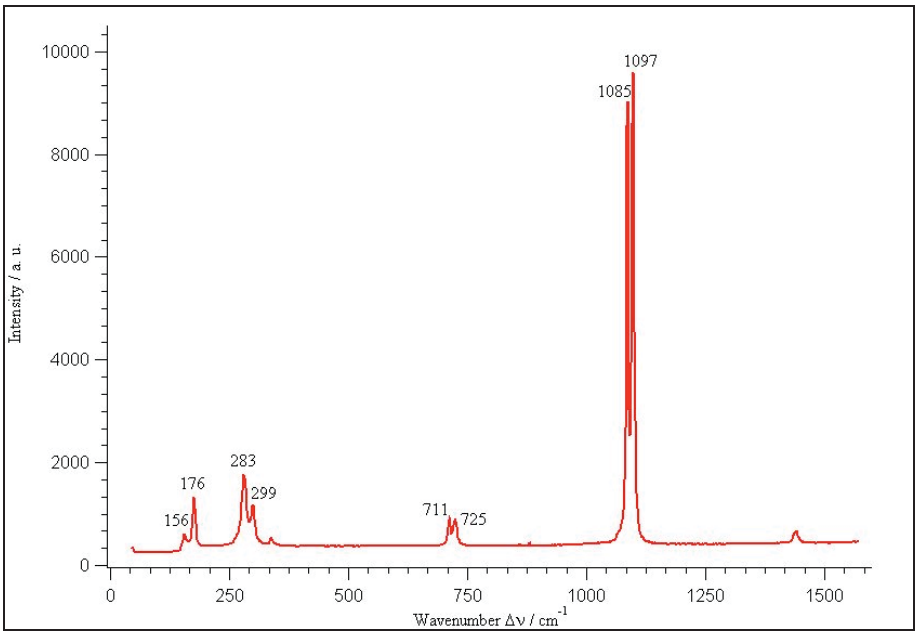

Fig. 8.48: Mechanical mixture of calcite and dolomite (Mer-grau)

The spectra of the calcite (Fig. 8.46) and the dolomite (Fig 8.47) are similar in appearance. However, the dolomite peaks have a higher wavenumber (main peak at 1097 cm^{-1}) than calcite (main peak at 1085 cm^{-1}). The presence of both carbonates within the laserspot of detection (6 µm diameter) is noticed by the occurrence of both spectra simultaneously (Fig. 8.48).

8.3. Crush and Leach results

Na/Br and Cl/Br ion ratios are used to interpret the data from crush-leach tests. It should be noted that these results represents bulk fluid analyses which does not allow an identification of separate generations of fluids in one grain. The existence of different generations has already been illustrated in the previous sections (petrography). The results are illustrated in Table 8.2.

The measurement of inclusion-free calcite was used to evaluate the accuracy and precision of this method. Table 8.2 indicates small total amounts of Na, Cl and Br in this sample, whereas Na/Br and Cl/Br ratios are similar to some samples from Bayramic (Bay 1), Orhaneli (Orh 2, dark) and Merluzzi (Mer-Grau). These ratio numbers are artefacts from this analytical technique because the calcite is pure and inclusion-free.

The highest total amount of Na, Cl, and Br are found in the Merluzzi samples, followed by Bayramic samples, and the lowest contents are detected in Orhaneli samples (Tab. 8.2). For example, sample Orh 37 light does not contain any detectable Na, Cl and Br (c.f. calcite standard).

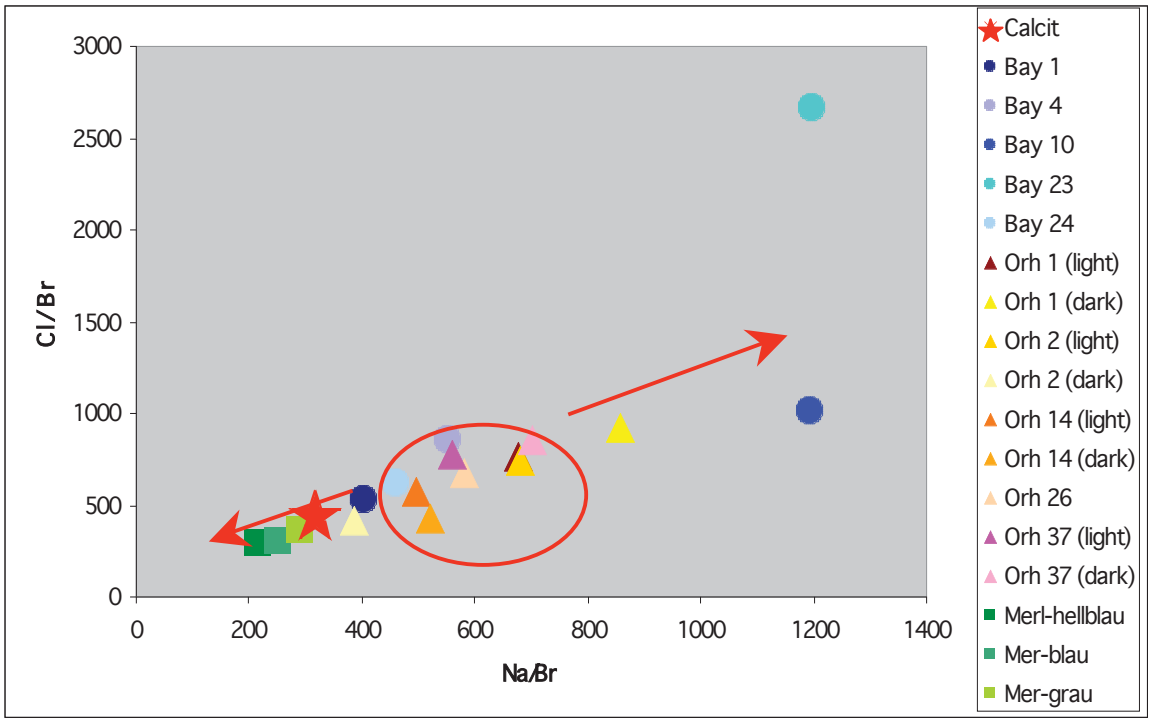

Fig.8.49: Cl/Br – Na/Br diagram

The ratio of Cl/Br and Na/Br are plotted in Figure 8.49. The circle in this diagram indicates the values for present-day seawater (Bottrel et al., 1988). Most of the data from Orhaneli are plotted in this area. Alteration due to evaporation or mixing with meteoric water is illustrated with the arrows in Figure 8.50 (evaporation is lower Cl/Br and Na/Br ratios; meteoric water is higher Cl/Br and Na/Br ratios). The samples from Bayramic are spread over a wide range of Cl/Br and Na/Br ratios. The influence of evaporation is evident for the samples from Merluzzi.

The samples from Orhaneli are split up in dark and light rock parts which were separately analysed (see Tab. 8.2). The dark samples have consequently higher Na/Br and Cl/Br ratios than the light samples.

The measurement of the standard inclusion free calcite indicates that the ratio-numbers should be taken with care. In addition to the previous mentioned restrictions of this bulk analytical technique, it must be concluded that this method is insufficient for the characterisation of fluids. Moreover, gases like CO_2, CH_4, N_2 and H_2S cannot be analysed with this method.

Probe	Na mol	Cl mol	Br mol	Na/Br	Cl/Br
Bay 1	98,87	130,13	0,24474	403,99	531,69
Bay 4	43,66	67,11	0,07889	553,40	850,61
Bay 10	92,13	77,79	0,07707	1195,44	1009,34
Bay 23	42,46	94,50	0,03547	1196,97	2663,93
Bay 24	63,19	85,15	0,13674	462,15	622,73
Orh 1 *light*	32,87	36,92	0,04856	676,91	760,19
Orh 1 *dark*	67,33	71,86	0,07836	859,19	917,09
Orh 2 *light*	39,36	42,93	0,05784	680,49	742,17
Orh 2 *dark*	54,49	59,04	0,14062	387,46	419,85
Orh 14 *light*	38,57	44,22	0,07770	496,36	569,19
Orh 14 *dark*	46,21	38,19	0,08844	522,45	431,85
Orh 26	31,52	36,68	0,05421	581,46	676,59
Orh 37 *light*	23,33	32,29	0,04170	559,50	774,34
Orh 37 *dark*	27,96	34,17	0,03978	702,80	858,96
Calcit	23,37	30,56	0,07474	312,60	408,88
Merl-hellblau	166,54	225,00	0,76688	217,17	293,40
Merl-blau	510,63	606,80	2,03780	250,58	297,77
Merl-grau	616,17	756,81	2,11644	291,14	357,59

Tab. 8.2: Na, Cl and Br fluid data from specific samples

8.4. OMYA standard measurement results

8.4.1. Brightness

The brightness of the samples was measured with the OMYA standard. Orh 14 is cut in two rock parts (the lighter and the darker) and measured separately. Additionally Bay 1 was milled with the zirkonia mill for 12 min to demonstrate that the brightness is getting higher with mill grad. The results are given in Table 8.3.

	d 50 4.5-5.5µm			d 50 <2µm			Zirkonia mill, 12 minutes		
	Tappi	**Ry**	**Index**	**Tappi**	**Ry**	**Index**	**Tappi**	**Ry**	**Index**
Bay 1	91.72	91.88	0.24	91.86	92.18	0.47	93.56	93.55	0.00
Bay 4	91.85	93.60	2.44	90.78	92.77	2.77			
Bay 10	96.10	96.87	1.06	95.36	96.21	1.17			
Bay 23	80.54	83.44	4.60	80.99	84.40	5.30			
Bay 24	92.24	92.78	0.79	93.00	93.54	0.65			
Orh 1	91.52	93.33	2.50	92.69	94.42	2.36			
Orh 2	87.39	91.85	6.39	89.17	92.43	4.66			
Orh 14 dark	88.91	89.07	0.19	88.52	88.42	-0.18			
Orh 14 light	93.09	93.69	0.83	93.56	93.99	0.58			
Orh 15	79.45	80.23	1.37	85.86	86.15	0.46			
Orh 26	93.49	93.79	0.45	94.05	94.36	0.37			
Orh 37	88.26	92.59	6.00	88.98	92.89	5.41			
Mer-Grau	78.74	78.15	-1.03	69.95	68.57	-2.75			
Mer-Blau	86.80	87.06	0.42	87.98	88.16	0.27			
Mer-Hellblau	91.14	91.86	0.83	91.63	92.30	0.89			

Tab. 8.3: Results of the brightness measurement; Tappi (R_z) is the blue value, R_y is the green value, Index is the yellow value

The brightness of Bay 1 is raised a little bit when it was milled longer. The samples don't show a significant rise of brightness from d 50 (4.5-5.5 µm) to d 50 (<2 µm) but most of them become whiter. Most small fluid inclusions are not crushed with the d 50 (4.5-5.5 µm), but are effected by the d 50 (<2 µm). The loss of these inclusions with d 50 (<2 µm) causes an increasing in brightness. For example, the degrade from d 50 (4.5-5.5 µm) to d 50 (<2 µm) at Mer-grau is because of the small (< 5µm) graphite sheets which begin to get milled at the finer grade.

8.4.2. Acid insoluble residue and Determination of Ca/Mg

The highest content of HCl insoluble materials is present in the samples Bay 4, Bay 10, Bay 23, Orh 2, Orh 37 and Mer-Grau. These high contents are caused by the iron oxides like in the samples from Bay 23 or from silicates which are shown in different quantities in all samples. This result is mostly confirmed by the petrography (§ 8.1.). In the samples Orh 1 and Orh 14 with Raman also hematite and magnetite were determined but nevertheless the insoluble part is not very high. However, the Raman analyses are not quantitative measurements.

	Measured values			*Calculated values*	
	HCl insoluble	**$CaCO_3$**	**$MgCO_3$**	**Dolomite**	**Calcite**
Bay 1	0.09	98.3	1.3	2.7	97.2
Bay 4	0.20	97.4	2.0	4.4	95.4
Bay 10	0.20	87.9	11.8	25.8	74.0
Bay 23	0.26	97.7	1.4	3.1	96.6
Bay 24	0.14	98.6	0.9	1.9	97.9
Orh 1	0.10	94.2	5.2	11.3	88.6
Orh 2	0.50	98.9	0.1	0.2	99.3
Orh 14 dark	0.04	96.5	3.0	6.7	93.3
Orh 14 bright	0.03	99.1	0.9	1.9	98.1
Orh 15	0.04	98.9	0.7	1.6	98.4
Orh 26	0.08	98.0	1.4	3.0	97.0
Orh 37	0.58	96.6	1.8	4.0	95.4
Mer-Grau	0.20	92.3	6.9	15.0	84.8
Mer-Blau	0.02	96.0	3.7	8.0	92.0
Mer-Hellblau	0.05	96.1	3.1	6.7	93.2

Tab. 8.4: Results of the acid insoluble residue and determination of Ca/Mg in mass%

The real dolomite and calcite content was calculated from the measured $CaCO_3$, $MgCO_3$ and HCl insoluble.

$$Dolomite = MgCO_3 * 2{,}187$$

$$Calcite = 100 - Dolomite - HCl\ insoluble \qquad \text{eq. 8.1}$$

8.5. RFA Results

The RFA measurement shows that the marble samples contain mainly CaO (50 to 56 mass%) (Tab.1). The MgO is present up to 5 mass% and Fe_2O_3, SiO_2, Al_2O_3, MnO are only occur in traces. The elements Cr, La, Ni, Rb, Sr and Zn whereas Ni, Rb and Zn are also detected in traces close to the diction limits of the instrument. The higher Sr values are supposable an instrumental error. The other elements and oxides (Ba, Ce, Cd, Co, Cu, Ga, Hf, Mo, Nb, Pb, Sc, Th, U, V, Y, Zr, P_2O_5, TiO_2, K_2O, Na_2O –values see appendix) are too minor to give a proper statement (pers. comm. Prof. Meisel). The higher Fe_2O_3 and MnO content of Bay 23 is caused by the presence of hematite (also detected with Raman spectroscopy) and magnetite (detected with Raman spectroscopy and XRD) and biotite (detected only with XRD). Orh 2 contains minor amounts of silicates (muscovite, anorthite, kaolinte – measured with XRD) which cause the higher Fe_2O_3, SiO2 and Al_2O_3 content.

mass %	CaO	MgO	Fe_2O_3	SiO_2	Al_2O_3	MnO
Bay 1	55.00	0.94	0.04	<0.02	0.01	0.009
Bay 4	53.22	2.27	0.07	<0.02	0.03	0.020
Bay 10	50.00	5.13	0.03	<0.02	0.01	0.014
Bay 23	54.60	0.53	0.51	0.05	0.13	0.043
Bay 24	55.17	0.80	0.04	<0.02	0.02	0.006
Orh 1 light	55.80	0.28	0.03	<0.02	0.01	0.005
Orh 1 dark	51.65	3.67	0.04	<0.02	0.05	0.005
Orh 14 light	55.17	0.56	0.03	<0.02	0.01	0.005
Orh 14 dark	54.09	1.62	0.04	<0.02	0.06	0.005
Orh 2 light	55.15	0.28	0.10	0.35	0.30	0.005
Orh 2 dark	51.88	3.36	0.05	0.05	0.11	0.005
Orh 26	55.08	0.97	0.04	<0.02	0.01	0.006
Orh 26-2	55.11	0.98	0.04	<0.02	0.02	0.005
Orh 37 light	54.77	0.80	0.08	0.15	0.04	0.011
Orh 37 dark	55.20	0.49	0.09	0.29	0.09	0.011

Tab.8.5: Mass % of the main elements (as oxides), CaO, MgO, Fe_2O_3, SiO_2, Al_2O_3 and MnO as obtained from RFA measurement.

The Calcite and Dolomite content was calculated with eq. 8.2 using the results given in Table 8.5. The results of the calcite/dolomite calculation of RFA measurement are in the Table 8.6.

$$MgO(\%) * 4{,}57 = Dol(\%)$$
$$\left[CaO(\%) - Dol(\%) * 0{,}304\right] * 1{,}784 = Cal(\%) \qquad \text{eq. 8.2}$$

Mole %	Bay 1	Bay 4	Bay 10	Bay 23	Bay 24	Orh 1		Orh 2		Orh 14		Orh 26	Orh 37	
						light	dark	light	dark	light	dark		light	dark
Calcite	95.8	89.3	76.5	96.1	96.4	98.9	83.0	97.7	84.2	97.0	92.5	95.9	95.7	97.3
Dolomite	4.3	10.4	23.4	2.4	3.7	1.3	16.8	1.3	15.4	2.6	7.4	4.4	3.7	2.2

Tab. 8.6: Calcite and dolomite content calculated of the RFA measurement.

The highest dolomite contents occur in the samples Bay 4 and Bay 10. The light and the darker zones in the sample from Orhaneli differ in calcite/dolomite ratio. The darker zones always contain more dolomite than the bright zones. Orh 37 is the only exception to this trend, where the dark zone contains less dolomite. This sample is the only one with brownish layers (sheet silicates) and it was collected in Sögüt at the marble/granite contact.

Figure 8.50 illustrates the comparison of the dolomite/calcite ratios from the two different analytical techniques (OMYA and RFA).

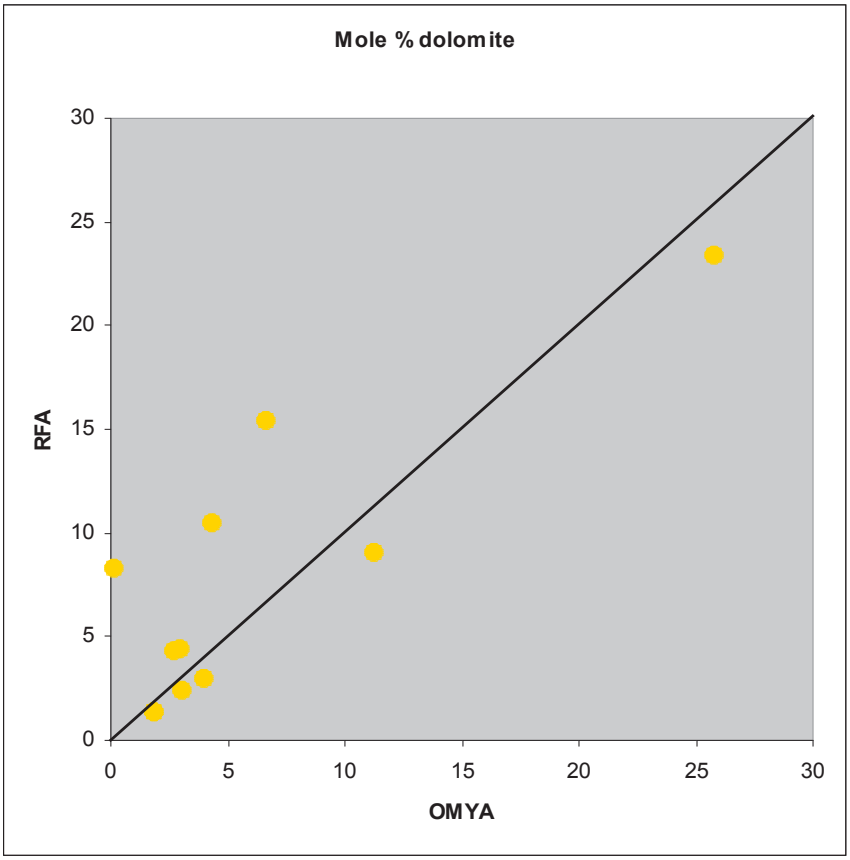

Fig. 8.50: Values from the OMYA calcite/dolomite determination and the RFA measurement

Most of the data is consistent according to both analytical techniques. However, Bay 4, Orh 2 and Orh 14 (dark) deviate, with the RFA method always giving higher dolomite values. First,

heterogeneous samples may give different values in different techniques because the analysed material can only be used in one technique. Second, Ca and Mg can be present in other minerals than carbonates. The calculation calcite/dolomite ratios do not represent true carbonate contents.

8.6. ICP-MS Result

The Rare-Earth-Elements REE data are chondrite normalized. To eliminate analytical errors and to estimate concentration variation each sample is measured twice (1 = first measurement, 2 = second measurement). Most of the samples from Orhaneli are divided in the light part (a) and the dark part (b or c). The REE concentration pattern (Fig. 8.51 and 8.52) of the sample 1, 4, and 23 from Bayramic represent seawater (Nothdurft et al, 2003). This pattern illustrates negative Eu anomaly, whereas a positive anomaly is observed in Bay 10 which represent fresh water (pers. comm. Prof. Meisel). The negative Ce anomaly of samples 1, 4 and 23 illustrates the effect of oxidation in seawater. The patterns of Bay 10 correspond to typical basalts or diorites (Nothdurft et al, 2003; pers. comm. Prof. Meisel). Patterns results from an interaction between marble and diorite intrusive (see chapter "Samples and their location") (see Fig. 8.51)

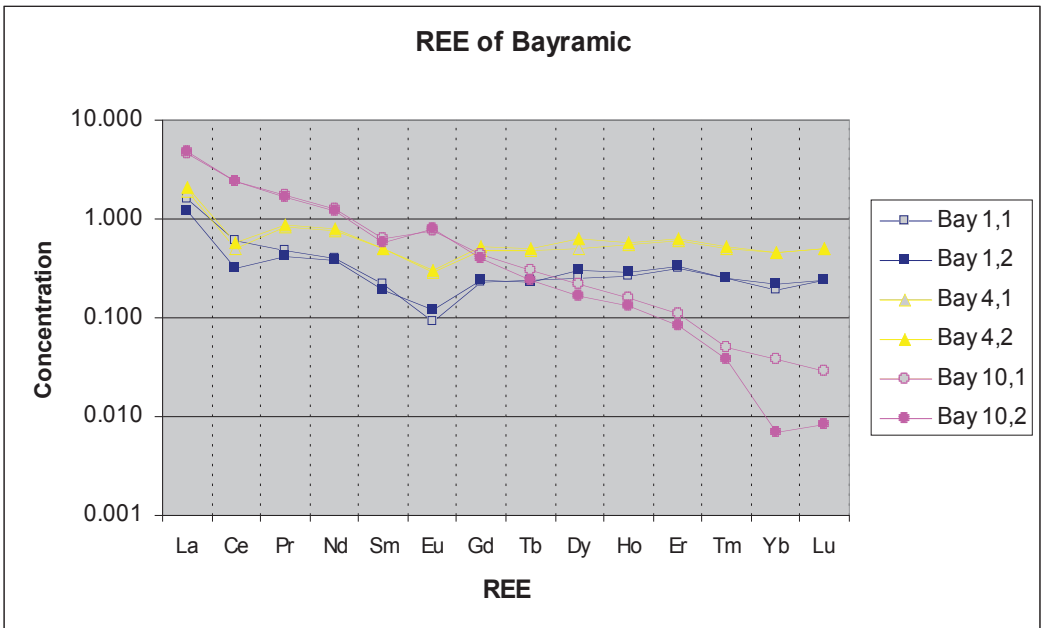

Fig. 8.51: REE of Bayramic (Bay 1, 4, and 10), Chondrite standardized

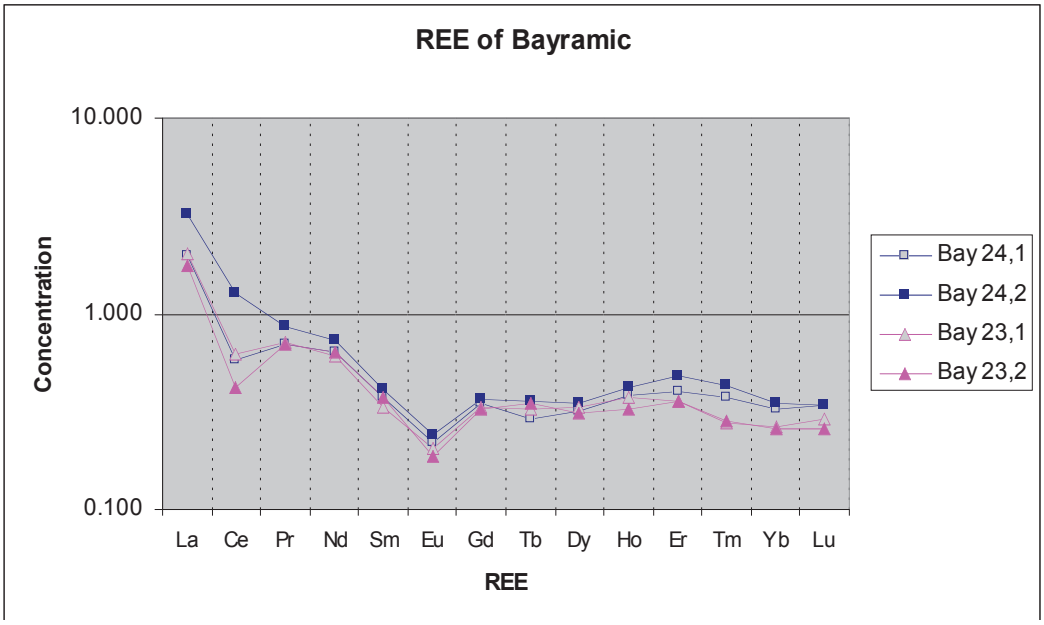

Fig. 8.52: REE of Bayramic (Bay 24 and 23), Chondrite standardized

The REE concentration patterns from samples of Orhaneli also represent a primary seawater-carbonate interaction (Fig. 8.52 and 8.53). Orh 37 shows higher values than the others but this could be caused by lesser dilution or it is affected by the crust (granite) (Fig. 8.55). The sample Orh 37 is from the contact zone of the marble with the granite in Sögüt. The negative Eu anomaly with values below 0.080 is too low and can be neglected therefore. Within the sample Orh 1a the value of Eu was not measured, due to measurement fault.

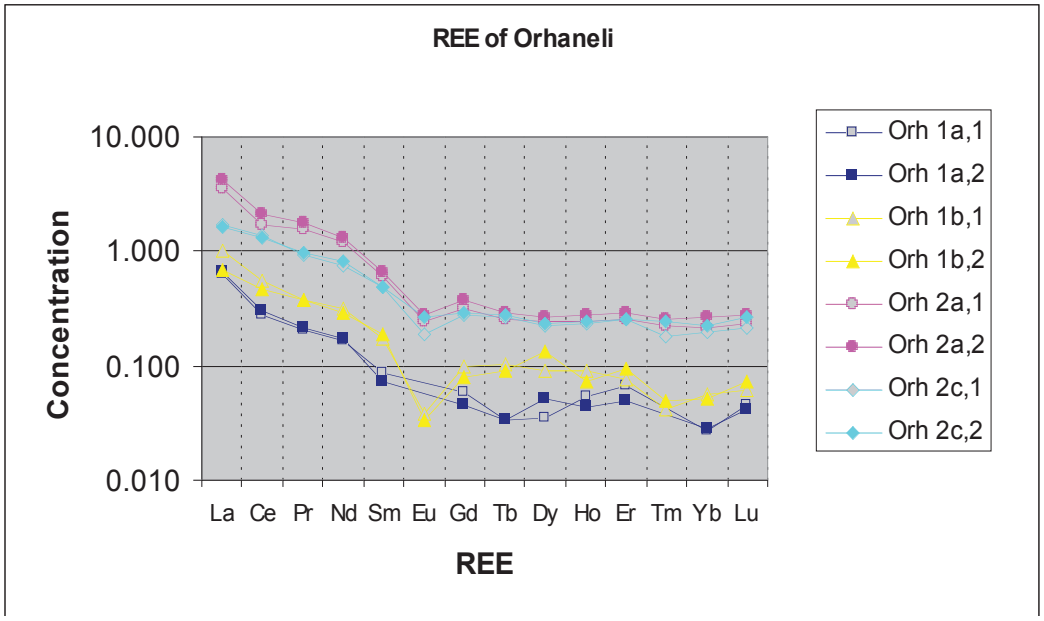

Fig. 8.53: REE of Orhaneli (Orh 1a, 1b, 2a and 2c), Chondrite standardized

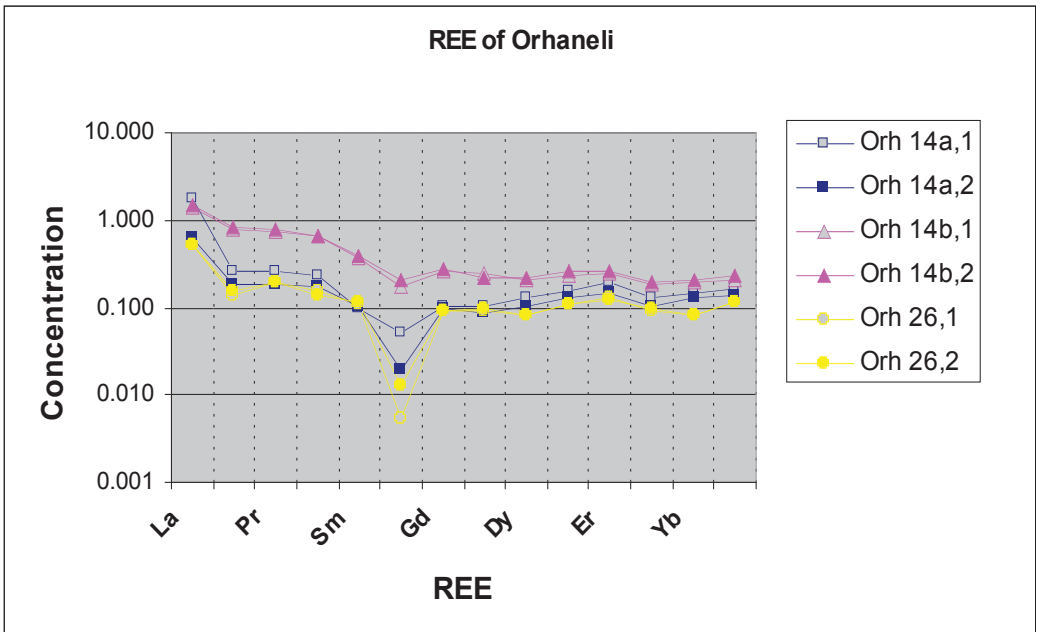

Fig. 8.54: REE of Orhaneli (Orh 14a, 14b and 26), Chondrite standardized

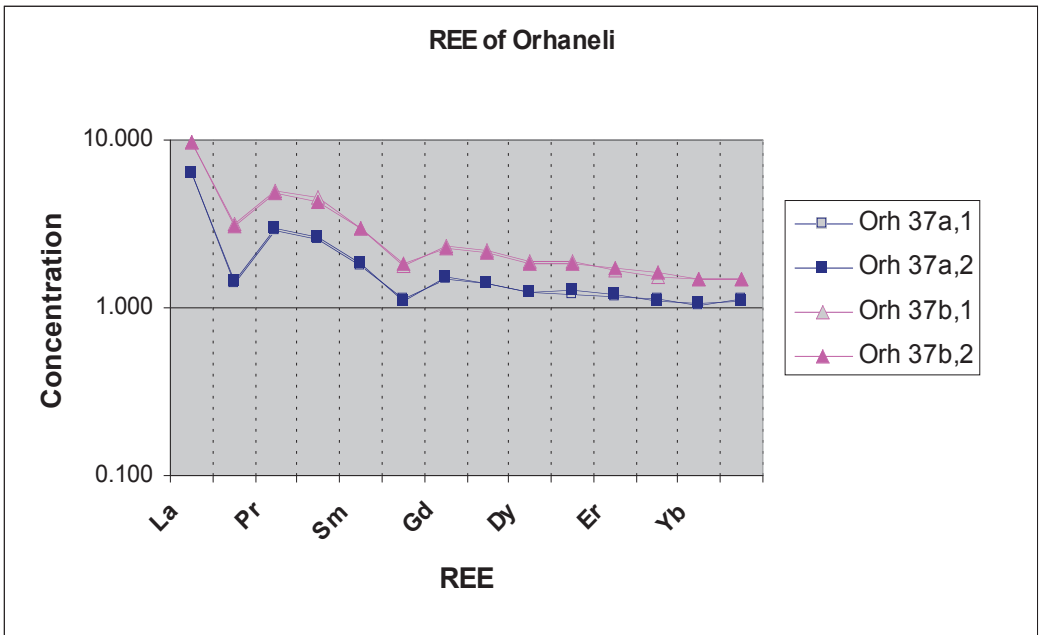

Fig. 8.55: REE of Orhaneli (Orh 37a and b), Chondrite standardized

In conclusion, the marbles from Bayramic and Orhaneli are mainly influenced by primary interaction with seawater and they correspond well with the local geology.

8.7. XRD-Results

The acetic acid insoluble residues (same process then with hydrochloric acid insoluble residues) of the marble samples were analysed with XRD (Tab. 8.7). The highest content of acetic acid insoluble material occurs in Bay 10 because of the high dolomite/magnesite content (see XRD and RFA results). The same can be observed in Orh 1 – it shows only lower dolomite content as Bay 10 (see RFA results).

Bay 1	*Bay 4*	*Bay 10*	*Bay 23*	*Bay 24*	*Orh 1*	*Orh 2*	*Orh 14 (dark)*	*Orh 14 (bright)*	*Orh 15*	*Orh 26*	*Orh 37*	*Mer-Grau*	*Mer-Blau*	*Mer-Hellblau*
0.16	0.78	12.06	0.51	0.14	4.71	0.63	2.40	0.46	0.12	0.07	0.58	4.58	0.71	0.52

Tab. 8.7: Acetic acid insoluble part of the marble samples in mass% of the original samples

Most of the detected minerals are conform to the results of other measurements. For example the insoluble test of Bay 10 show a high rate of insoluble minerals, the RFA gave a high $MgCO_3$ rate and the XRD detected dolomite and magnesite. Raman spectroscopy did not reveal the presence of magnesite but only dolomite was measured. The RFA data of Bay 23 have a higher rate of SiO_2 and Fe_2O_3 and that matches the content of quartz and the iron minerals pyrite and magnetite. The XRD measurements of Orh 1, Orh 2 and Orh 37 achieve almost the same results as the other methods. Orh 15 and the samples from Merluzzi cannot be compared with other methods. As for Orh 15 only OMYA standard measurements were conducted whereas the Merluzzi samples were measured with the OMYA standard measurements and with Raman.

Graphite was measured with Raman spectroscopy and identified in thick sections in the sample Mer-Grau. But XRD measurements did not reveal any graphite. A lot of hematite was measured in Bay 23 with Raman spectroscopy but XRD did not detect it. On the other hand no pyrite was measured with Raman spectroscopy but with XRD. Bay 4 contains a low amount of pyrite (Raman) but XRD showed none at all. With XRD quartz and other silicates were determined in the samples Bay 1, Bay 4, Bay 23, Bay 24, Orh 2, Orh 15, Orh 26, Orh 37, Mer-Grau, Mer-Blau and Mer-Hellblau. RFA determined a higher content of SiO_2 only in Orh 2 and Orh 37 and in all the other samples the SiO2 content is under the detection limit (except for the samples from Merluzzi and Orh 15 because they were not measured with RFA).

Also no calcite should have been measured in the samples Bay 1, Orh 14 and Bay 24 because of the acetic acid insoluble parts of the samples were used and normally, calcite should be dissolved in acetic acid.

	quartz	carbonate	sheet silicates	rest
Bay 1	x	dolomite calcite	muscovite	hornblende
Bay 4		dolomite	phlogopite montmorillonite clinochlor	
Bay 10		dolomite magnesite		
Bay 23	x		biotite clinochlor stilpnomelane	pyrite magnetite
Bay 24	x	dolomite calcite	biotite clinochlor	hornblende
Orh 1		dolomite		
Orh 2		dolomite	muscovite kaolinite	anorthite
Orh 14 (light)		dolomite calcite		
Orh 14 (dark)		dolomite calcite		
Orh 15	x	dolomite	biotite	
Orh 26	x	dolomite	kaolinite	anorthite illite
Orh 37	x	dolomite	kaolinite	anorthite illite
Mer-grau	x	dolomite	polylithionite biotite	
Mer-blau	x	dolomite	biotite	fluorite
Mer-hellblau	x	dolomite	clinochlor	illite

Tab. 8.8: With XRD measured mineral content of the samples from Bayramic, Orhaneli and Merluzzi.

The spectres of the XRD are shown in the appendix.

8.8. Microthermometry result

Two samples (Bay 1 and Orh 1) were taken for microthermometrie measurement. In both samples 19 fluid inclusions were selected and inspected on temperature dependent phase changes which characterize the enclosed fluids. These two samples show different homogenisations temperatures (T_h) of the vapour and liquid phases.

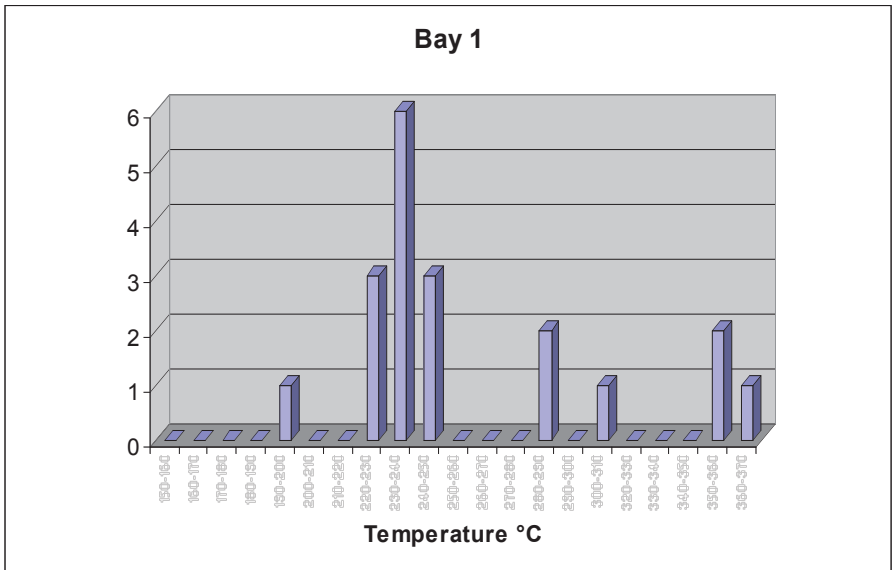

Fig. 8.56: Homogenisations temperatures of the inclusions of Bay 1

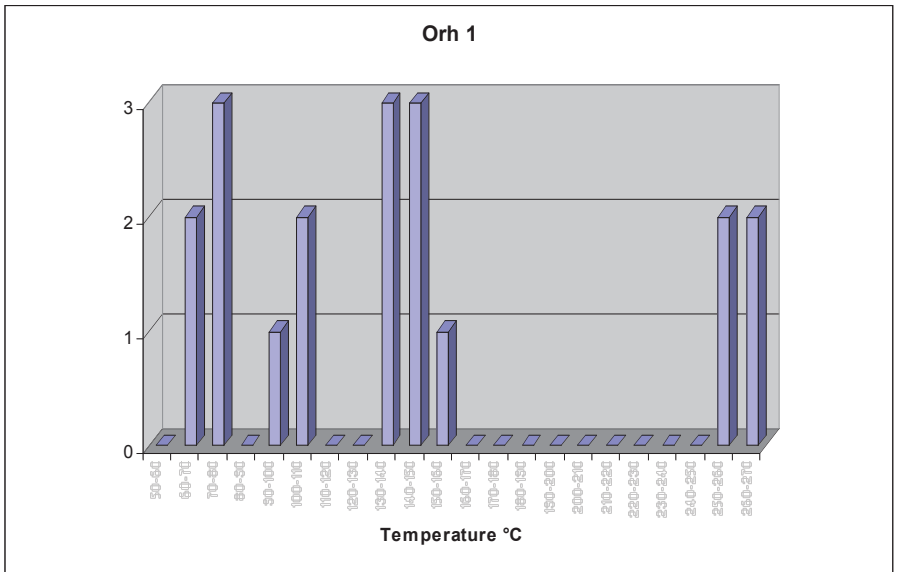

Fig. 8.57: Homogenisations temperatures of the inclusions of Orh 1

Bay 1 has a well defined mode around 230 – 240°C and maximum temperatures up to 370°C have been measured (Fig. 8.56). The measurements at high temperatures are believed to

represent stretched fluid inclusions, due to either sample preparation or mircrothermometrical caused overpressures. Inclusions from Orhaneli have a broader range of T_h at clearly lower temperatures than Bay 1. One group appears around 130 to 160°C, whereas other appear at 90 – 110°C and 60 – 80°C (Fig. 8.57). In conclusion, the inclusions formation temperatures in Bayramic are higher than those in Orhaneli. This may correspond to higher metamorphic conditions of marble formation in Bayramic. The presence of CH_4 in Orhaneli also corresponds to lower formation temperature conditions, because methane is usually stable at shallower depths than CO_2 (Touret, 1977).

9. Interpretation and Conclusion

9.1. Mineralogy

The petrography of the marbles was optically made with thin/thick sections and individual mineral grains were identified by Raman spectroscopy. In addition, the mineralogy was determined with RFA, XRD and OMYA standard measurements.

The analyses showed that the marbles are mainly consists of calcite and marginal dolomite except to the samples from Merluzzi, one samples from Bayramic (Bay 10) and two samples from Orhaneli (Orh 1 and 14). These samples have a higher content of dolomite (up to 25 %). It also shows that the darker parts of the samples have higher dolomite content. In the samples from Merluzzi the dolomite content increases with darkness (from Merl-hellblau to Merl-grau). The accessory minerals include mainly silicates and oxides (magnetite and hematite).

The XRD analyses of the insoluble minerals from the marbles are not always corresponding to petrographical observations. For example, magnetite and hematite were detected in the samples Bay 23 and 24 with the Raman spectroscopy but XRD analyses shows only magnetite in the sample Bay 23. Similar observations were obtained from Merluzzi samples. Raman spectroscopy detected graphite in all samples, whereas XRD analyses do not reveal its presence. These examples illustrate that the combination of Raman spectroscopy and petrography on thin/thick sections is the most important tool for the description of the mineralogy of the rock samples.

9.2. Fluid Inclusions

The darker parts of the samples, which are usually richer in dolomite (see § 9.1) also contain gas-rich and water-rich fluid inclusions. However, the brighter parts contain only water-rich fluid inclusions. The presence of the gas-rich inclusions may have an effect on the brightness of the samples, similar as dolomite. The inclusion are small, most of them have a diameter less than 1 μm. (see Fig. 8.6 and 8.7). Gas-rich inclusions are in general even smaller than water-rich inclusions. Raman spectroscopy has revealed the composition of the gas mixtures in the inclusions. The samples from Bayramic contain CO_2 and H_2S, the samples from Orhaneli contain as well CH_4 and the samples from Merluzzi contain additionally CH_4 and N_2.The variation in gas composition may depend on a variation in the originally enclosed amount and type of organic matter and/or on a variation in metamorphic conditions of the

marbles. At higher temperatures and pressures it is expected that CH_4 will react to CO_2. It is known from literature (e.g. Touret & Dietvorst, 1983) that pore fluid compositions vary with depth (Fig. 9.1).

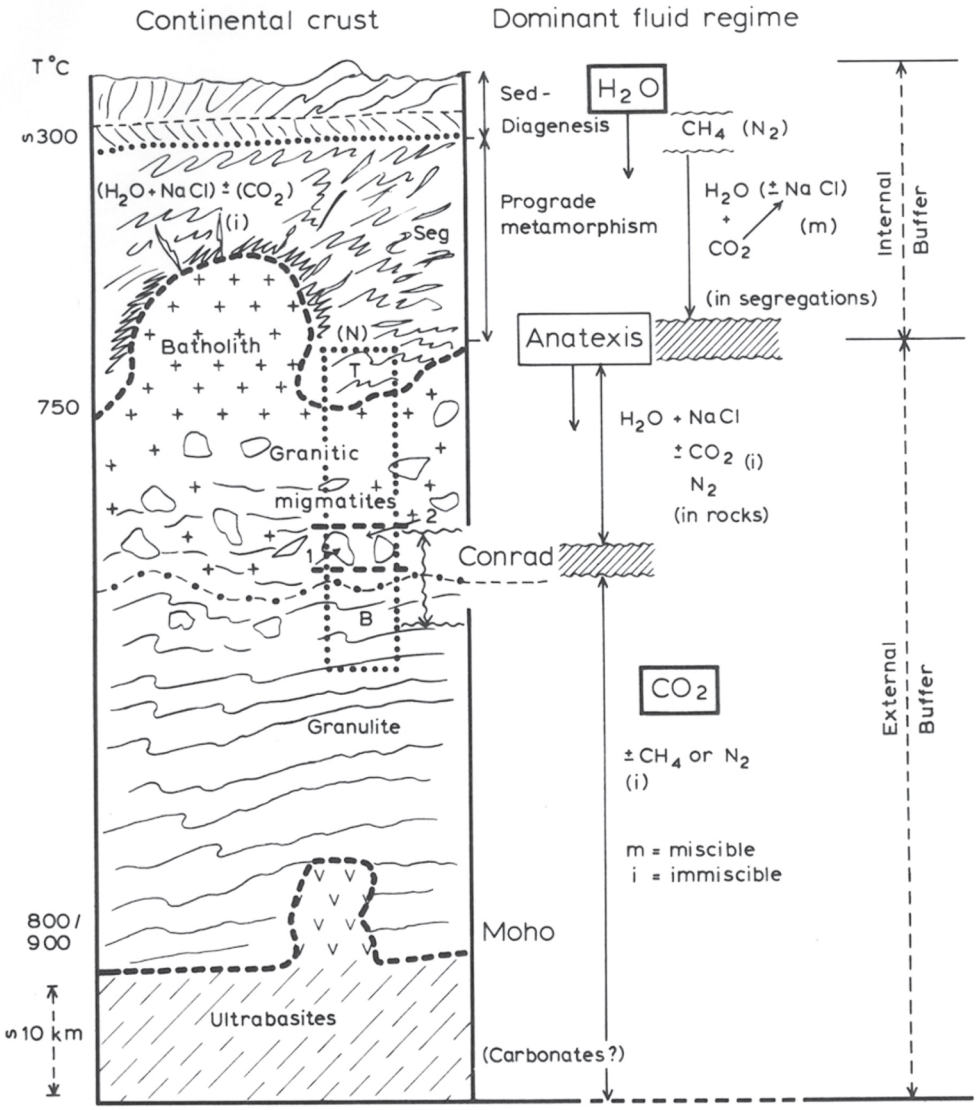

Fig. 9.1: From Touret & Dietvorst (1983), model of fluid distribution in the continental lithosphere.

CO_2 tends to be present in deep rock, especially in marbles, whereas H_2O is present in more shallow environments. CH_4 is mainly present in sedimentary rock that has suffered some diagenesis. N_2 is not restricted to a specific environment. CH_4 and H_2S can be both products of the reduction and fermentation of organic matter in shallow sediments (Fig. 9.2). The absence of CH_4 in Bayramic may have resulted from higher metamorphic condition of the marbles.

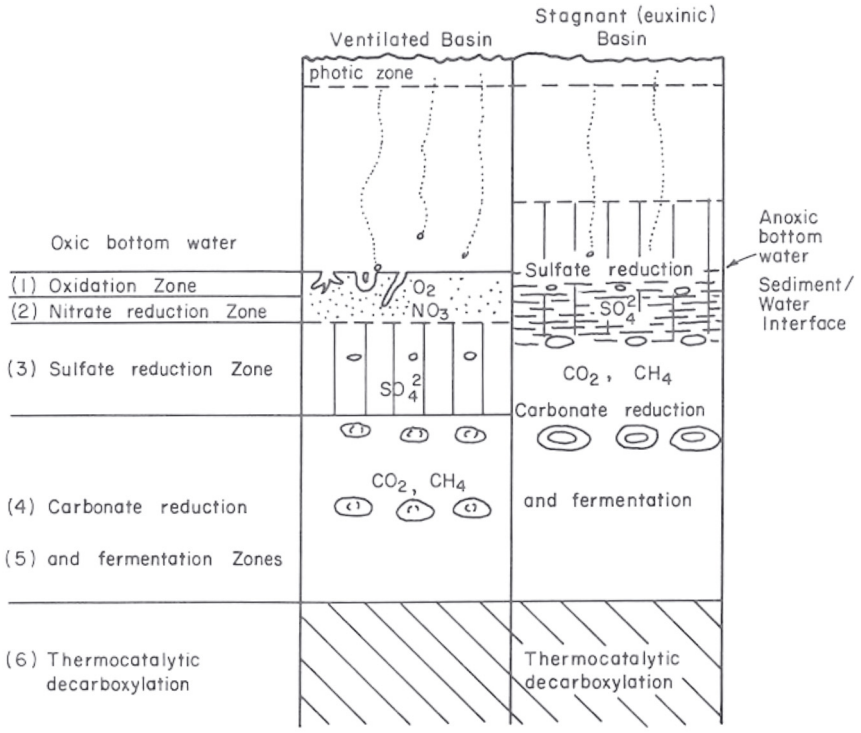

Fig. 9.2: From Hesse (1986), stages of organic matter oxidation in anoxic sediments.

The water-rich inclusions have been investigated by microthermometry and crush/leach. Those inclusions were probably trapped in the marble after the gas-rich inclusions. The water-rich inclusions from Bayramic illustrate higher trapping condition than the other sample localities, which may reflect the higher metamorphic conditions as inferred from the absence of CH_4.The trace element composition of the marbles, as obtained from ICP-MS, indicate that the rock was in equilibrium with seawater. This water is most probably conserved as water-rich fluid inclusions in the calcite. The influence of intrusive rock, i.e. diorite (Bay 10) and granite (Orh 37), is restricted to changing the trace element composition of the marbles, but no fluid inclusions related to those rocks have been observed.

Comparison with other studies of fluid inclusions in marbles is extremely difficult because the literature hardly reveals any data about a similar system. Fluid inclusions in calcite in marbles are believed to be unreliable for the interpretation of metamorphic conditions, because of the high probability of post-entrapment modifications. In general, quartz veins that occur in association with marbles are preferable objects for fluid inclusion studies. This study illustrates that marbles can preserve fluids, mainly gases, that were produced by diagenesis and metamorphism.

9.3. Removal of gases from marble

A procedure to remove gas-rich fluids out of the marbles is by decrepitation (explosion of inclusion by overheating). This procedure is favoured because mechanical milling of the marbles cannot remove inclusions that are smaller than approximately 1 µm in diameter (i.e. related to the finest milling size). The amount of heat that is needed for decrepitation depends on the size and composition of the inclusion and the type of host mineral. Strong minerals, such as quartz need higher temperatures than weak minerals, such as calcite. For example the amount of overheating required to initiate stretching of inclusions in sphalerite range from <8°C for an inclusion of several hundred micrometers in diameter to >75°C for a 10-µm-diam inclusion (Bodnar & Bethke, 1984).

Heating of fluid inclusions after homogenization causes a fast increase of internal pressure (Fig. 9.3). At certain internal overpressures, the mineral around the inclusion will develop micro cracks along which the fluid can escape.

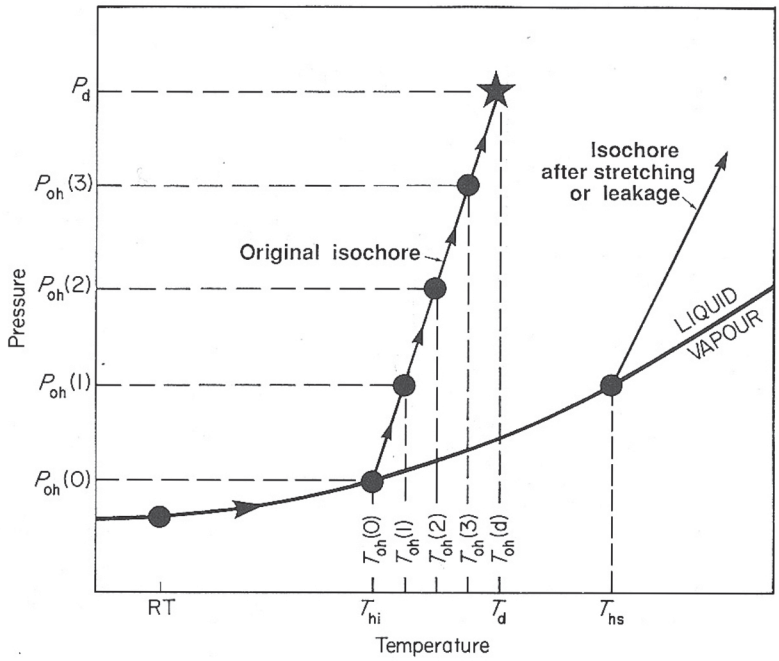

Fig. 9.3: From Bodnar et al. (1989), schematic representation of the *P-T* path followed by a fluid inclusion during heating from room temperature to the temperature at which decrepitation occurs.

10. References

BAKKER R. J., DIAMOND L. W., (2006): Estimation of volume fractions of liquid and vapour phases in fluid inclusions, and definition of inclusion shapes.-American Mineralogist, Vol. 91, p. 635-657

BAKKER R. J., PIRIBAUER C. J., STRAUSS V., (2005): Development of a high quality Raman spectral library for minerals and fluids.- Mitt.Österr.Miner.Ges. 151 (2005)

BAKKER R. J., (2004): Raman spectra of fluid and crystal mixture in the system H_2O, H_2O-NaCl and H_2O-$MgCl_2$ at low temperatures: Application to fluid-inclusion research.- The Canadian Mineralogist, Vol. 42, p. 1283-1314

BODNAR, R. J., BINNS, P. R., HALL, D. L. (1989): Synthetic fluid inclusions – VI. Quantitative evaluation of the decrepitation behaviour of fluid inclusions in quartz at one atmosphere confining pressure.- J. metamorphic Geol, 7, p. 229-242

BODNAR, R. J., BETHKE, P. M. (1984): Systematics of Stretching of Fluid Inclusions I: Fluorite and Sphalerite at 1 Atmosphere Confining Pressure.- Economic Geology, Vol. 79, p. 141-161

BURKE, E. A. J., (2001): Raman mircospectrometry of fluid inclusions.-Lithos 55, p. 139-159

CULLITY, B. D., (1978): Elements of x-ray diffraction, Second edition.-Addison-Wesley Publishing Company, Inc.

DIPPEL, B., (2002): (www.raman.de/english/html/basics.htm)

FORSCHUNGSZENTRUM JÜLICHONLINE (2002): (http://www.fz-juelich.de/zch/index.php?path=exrd&index=157&print=1)

GÖNCÜOGLU, C. M., DIRIK, K., KOZLU, H. (1997): Pre-Alpine and Alpine Terranes in Turkey: Explanatory Notes to the Terrane Map of Turkey.-IGCP Project No. 276, Vol. Annales geologiqes Des Pays Helleniques, p. 515-536

HESSE, R., (1986): Diagenesis; Early diagenetic pore water/sediment interaction; modern offshore basins.- Geoscience Canada, Vol.13, no.3, p.165-197

HOPE G.A., WOODS R., & MUNCE C.G., (2001): Raman microprobe mineral identification.- Minerals Engineering, Vol. 14, No. 12, p. 1565-1577

LIFSHIN, E., (1999): X-ray Characterization of Minerals.-Wiley-VCH Verlag GmbH, Weinheim, p. 261

NOTHDURFT L. D., WEBB G. E., KAMBER B. S., (2003): Rare earth element geochemisty of Late Devonian reefal carbonates, Canning Basin, Western Australia: Confirmation of a seawater REE proxy ancient limestones.- Geochimica et Cosmochimica Acta, Vol. 68, No. 2, pp. 263-283

RAMAN, C. V., (1928): A new radiation.- Indien J. Phys.,Vol.2, 387)

PIRIBAUER, C., J., (2007): Die Genese des Amethystganges von Maissau, Niederösterreich.- Diplomarbeit, Montanuniversität Leoben, Lehrstuhl für Mineralogie und Petrologie

POTTS, P.J., (1987): A handbook of silicate rock analysis, 1. Title.- Blackie & Son Ltd, London, p. 622

SAMSON I., ANDERSON A., & MARSHALL D., (2003):Fluid Inclusions: Analysis and Interpretation, Volume 32.- Mineralogical Association of Canada, Canada, p. 374

TEGETHOFF, W. F., (2001):Calciumcarbonat Von der Kreidezeit ins 21. Jahrhundert.- Birkhäuser Verlag, Berlin, p. 342

TOURET, J. L. R., DIETVORST, P. (1983): Fluid inclusions in high-grade anatectic metamorphites.-J. Geol. Soc. London, Vol. 140, p. 635-649

WHITTINGHAM, S. M., (1989-1997): (http://materials.binghamton.edu/labs/xray/xray.html)

WITTKE, J. H., (1997-2003): (www.4.nau.edu/microanalysis/Microprobe/ProbeIntro-XRF.html)

11. Table of figures and tables

Figures

Tables

13. Appendix

13.1. Raman dates

Bay 1

Number of measurements	1. CO_2-Peak Area	2. CO_2-Peak Area	H_2S - Peak Area	Mole fraction of CO_2 [%]	Mole fraction of H_2S [%]
1	49,853.00	94,613.00	15,900.90	**95.96**	**4.04**
2	14,812.25	25,754.75	14,121.50	**97.90**	**2.10**
3	20,490.00	36,948.00	14,834.35	**93.63**	**6.37**
4	30,105.00	57,528.00	11,582.30	**95.20**	**4.80**
5	20,734.50	40,741.00	13,340.85	**97.48**	**2.52**
6	7,691.75	12,330.00	4,395.70	**95.93**	**4.07**
7	26,446.50	53,258.25	12,380.85	**95.89**	**4.11**
8	25,093.50	53,495.00	12,222.10	**97.06**	**2.94**
9	35,630.25	71,809.00	19,301.00	**97.05**	**2.95**
10	17,292.00	34,435.75	8,320.35	**96.61**	**3.39**
11	38,791.25	76,704.25	19,838.00	**96.95**	**3.05**
12	34,746.50	70,478.00	19,791.15	**96.75**	**3.25**
13	25,873.75	50,074.25	14,078.85	**96.46**	**3.54**
14	12,431.00	22,628.75	5,622.10	**96.51**	**3.49**
15	12,476.75	26,213.25	11,848.75	**96.96**	**3.04**
16	20,473.25	44,835.50	14,072.75	**94.36**	**5.64**

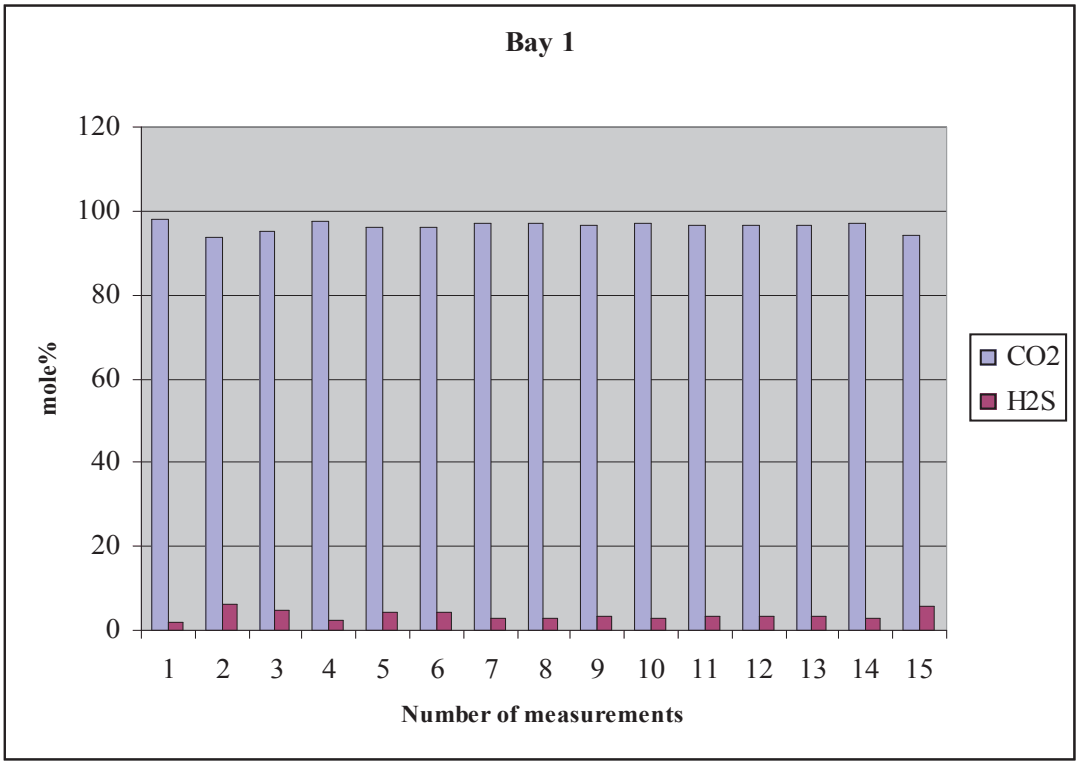

Bay 7

Number of measurements	1. CO_2-Peak Area	2. CO_2-Peak Area	H_2S - Peak Area	Mole fraction of CO_2 [%]	Mole fraction of H_2S [%]
1	4,079.00	9,242.00	5,903.20	**92.03**	**7.97**
2	929.50	1,544.00	493.00	**96.25**	**3.75**
3	2,138.50	3,742.00	1,407.20	**95.53**	**4.47**
4	9,504.00	20,928.00	14,391.50	**91.54**	**8.46**
5	2,170.00	3,427.00	1,574.00	**94.79**	**5.21**
6	2,371.00	4,050.50	2,441.80	**93.09**	**6.91**
7	5,772.50	11,650.00	4,262.60	**95.44**	**4.56**
8	4,456.00	8,625.00	261.20	**99.61**	**0.39**
9	2,584.00	4,072.00	1,812.80	**94.95**	**5.05**
10	2,350.00	4,132.00	1,183.90	**96.56**	**3.44**
11	3,336.50	6,267.50	2,341.00	**95.46**	**4.54**
12	1,737.50	2,932.00	700.50	**97.15**	**2.85**
13	3,871.50	8,719.00	2,151.10	**96.77**	**3.23**
14	5,952.00	13,015.50	3,052.00	**96.95**	**3.05**
15	4,652.00	9,595.00	2,546.80	**96.63**	**3.37**
16	4,397.50	8,208.00	2,683.00	**96.01**	**3.99**
17	6,146.00	12,517.00	3,752.50	**96.22**	**3.78**
18	5,107.00	10,627.00	355.20	**99.56**	**0.44**
19	2,474.00	4,838.00	1,606.90	**95.88**	**4.12**
20	4,517.00	9,700.50	3,575.20	**95.32**	**4.68**

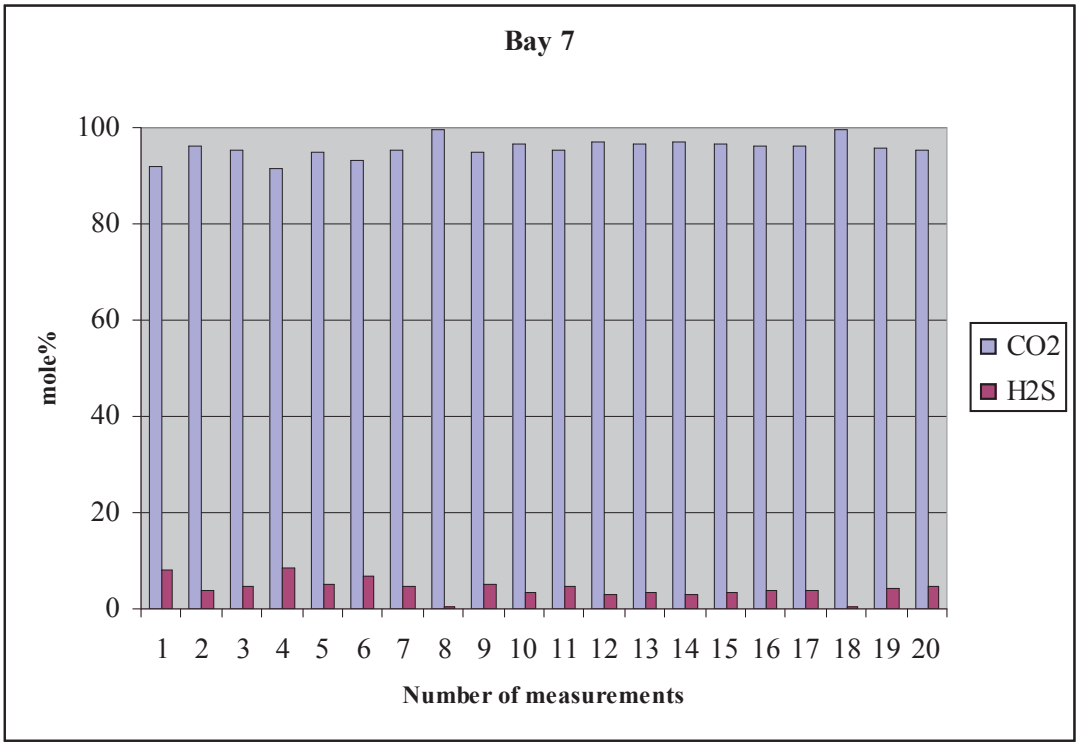

Orh 1							
Number of measurements	**1. CO_2-Peak Area**	**2. CO_2-Peak Area**	**H_2S - Peak Area**	**CH_4 - Peak Area**	**Mole fraction of CO_2 [%]**	**Mole fraction of H_2S [%]**	**Mole fraction of CH_4 [%]**
1	19,419.00	41,336.00	15095.8	12468.5	**92.36**	**4.48**	**3.16**
2	21,486.00	47,086.50	25805.1	22626.2	**88.61**	**6.51**	**4.87**
3	21,024.00	46,881.00	19250.5	21721.5	**90.20**	**4.99**	**4.81**
4	14,545.75	32,387.50	17255.6	17206.8	**88.27**	**6.34**	**5.39**
5	22,262.00	49,465.50	23648.5	19550	**90.10**	**5.80**	**4.09**
6	25,339.50	55,343.50	28443	24535.8	**89.32**	**6.15**	**4.53**
7	4,379.75	9,512.00	7231.75	6123.8	**85.10**	**8.65**	**6.25**
8	4,818.50	10,270.25	4607.3	2969.1	**91.54**	**5.46**	**3.00**
9	2,550.75	5,327.00	1998.5	1083.2	**93.24**	**4.62**	**2.14**
10	2,504.00	5,659.25	2434.1	1836.6	**91.26**	**5.31**	**3.42**
11	1,854.25	4,007.00	2385.5	1511.7	**89.09**	**7.08**	**3.83**
12	11,125.00	24,371.50	16246.35	6767.6	**89.19**	**7.97**	**2.83**
13	10,081.75	22,186.25	14214.6	6400.5	**89.36**	**7.69**	**2.95**
14	2,767.50	5,742.75	3207.95	1497.2	**90.67**	**6.68**	**2.66**
15	*0*	*0*	*339.6*	*153.8*	**0.00**	**72.13**	**27.87**
16	4,327.50	9,238.00	6660	4141.2	**87.20**	**8.36**	**4.44**
17	2,694.00	5,485.50	4415.3	2448.45	**86.56**	**9.13**	**4.32**
18	2,805.25	6,116.50	2970.7	1231.75	**91.91**	**5.98**	**2.11**
19	1,440.00	3,631.75	2904.4	930.85	**87.53**	**9.79**	**2.68**

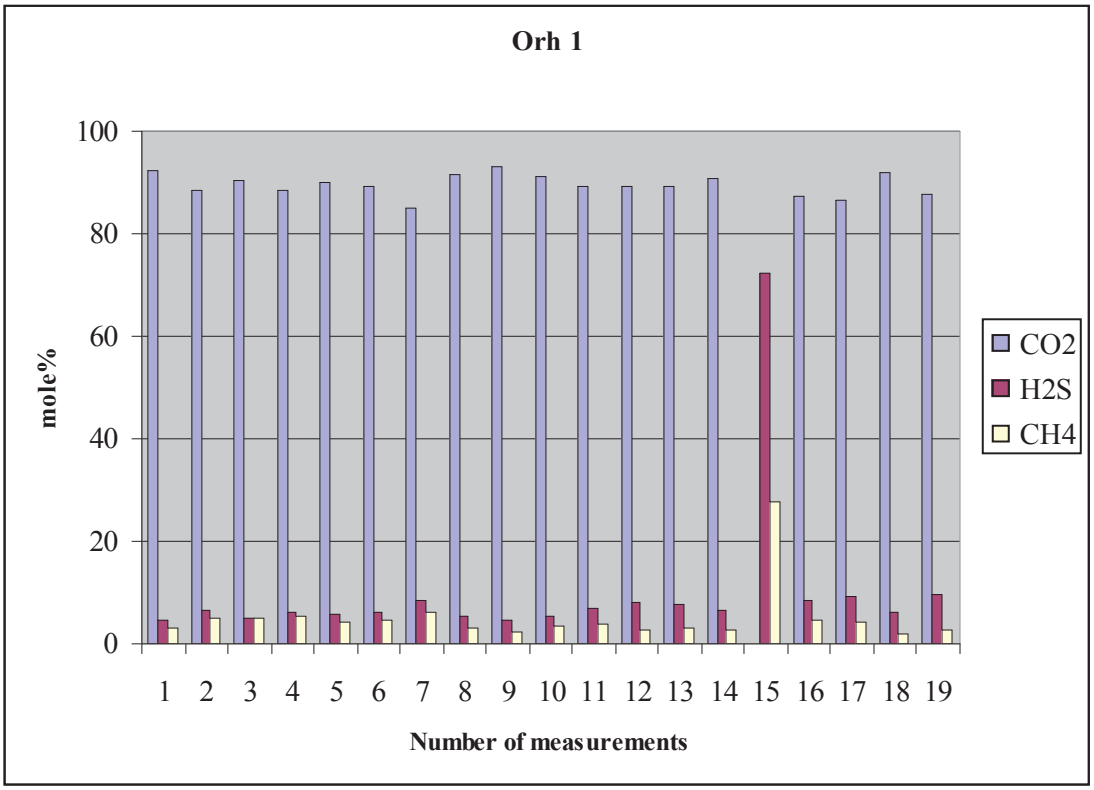

Orh 2							
Number of measurements	**1. CO_2-Peak Area**	**2. CO_2-Peak Area**	**H_2S - Peak Area**	**CH_4 - Peak Area**	**Mole fraction of CO_2 [%]**	**Mole fraction of H_2S [%]**	**Mole fraction of CH_4 [%]**
1	2,640.25	30,955.75	2,338.85	1,544.40	**97.92**	**1.33**	**0.75**
2	2,241.25	19,293.50	1,776.00	807.65	**97.81**	**1.58**	**0.61**
3	2,549.00	9,345.25	2,564.80	1,464.65	**94.11**	**3.96**	**1.93**
4	4,500.75	8,806.50	3,248.90	1,990.90	**93.23**	**4.45**	**2.32**
5	3,610.75	7,448.50	2,532.20	3,264.80	**91.41**	**4.09**	**4.50**
6	3,307.00	7,018.00	5,000.45	1,880.50	**88.89**	**8.41**	**2.70**
7	3,787.00	8,292.50	3,281.90	1,473.80	**93.16**	**4.94**	**1.89**
8	815.00	1,697.00	2,212.80	310.80	**83.85**	**14.43**	**1.73**
9	266.50	913.00	864.90	158.00	**85.80**	**12.29**	**1.92**
10	288.00	575.00	501.50	102.25	**88.24**	**10.02**	**1.74**
11	1,479.00	3,024.50	1,836.40	957.80	**89.68**	**7.14**	**3.18**
12	2,455.50	5,068.00	3,085.70	1,661.80	**89.53**	**7.17**	**3.30**
13	2,032.00	4,607.50	2,561.30	969.00	**90.94**	**6.85**	**2.21**
14	434.20	1,462.00	249.50	146.40	**96.29**	**2.47**	**1.24**
15	2,035.00	3,794.50	2,139.30	2,099.90	**88.36**	**6.33**	**5.30**
16	2,015.50	4,209.00	2,542.85	2,370.00	**87.47**	**6.98**	**5.55**
17	3,861.50	7,788.00	4,801.30	3,400.20	**88.56**	**7.13**	**4.31**
18	4,736.00	9,728.00	5,719.45	5,493.80	**87.68**	**6.77**	**5.55**
19	1,538.50	3,258.00	1,613.80	1,404.40	**89.73**	**5.90**	**4.38**

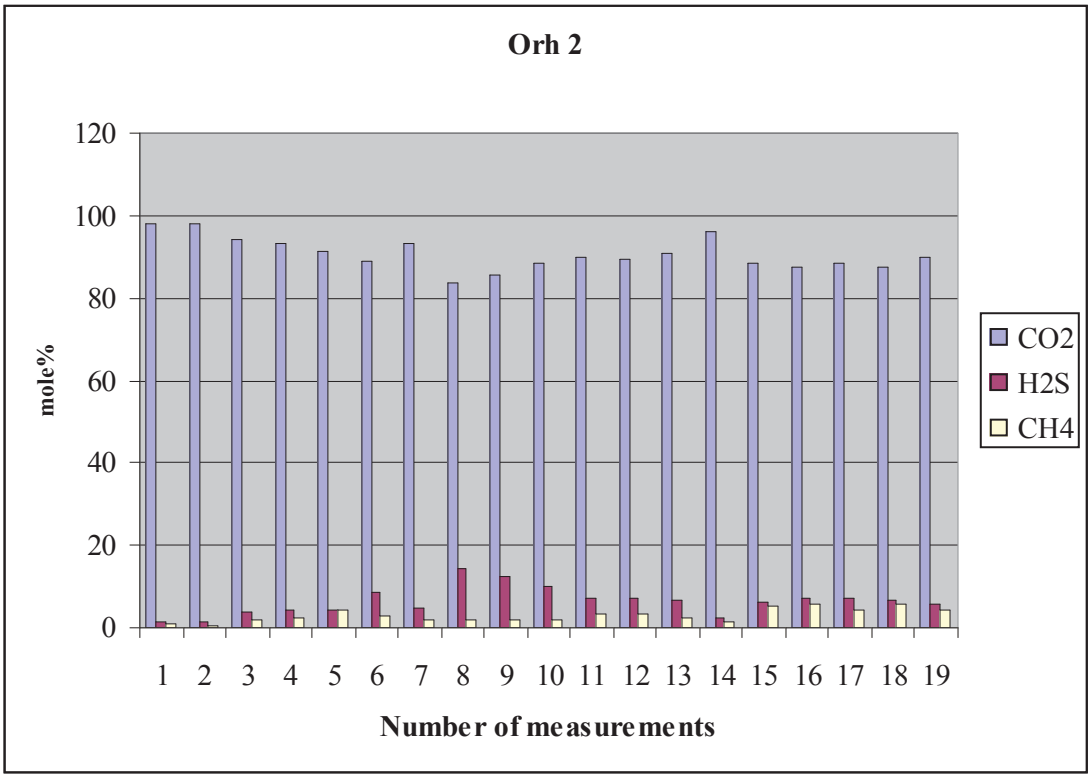

Orh 14							
Number of measurements	1. CO_2-Peak Area	2. CO_2-Peak Area	H_2S - Peak Area	CH_4 - Peak Area	Mole fraction of CO_2 [%]	Mole fraction of H_2S [%]	Mole fraction of CH_4 [%]
1	1,106.00	2,750.50	2,613.00	147.80	**79.68**	**20.32**	**0.00**
2	1,837.00	4,215.00	8,074.00	409.80	**77.29**	**21.72**	**0.99**
3	1,582.50	4,127.00	5,909.05	439.00	**87.82**	**11.62**	**0.56**
4	1,511.00	3,331.00	6,295.30	223.00	**78.63**	**20.49**	**0.89**
5	3,072.50	6,669.50	9,874.55	539.80	**82.31**	**16.64**	**1.05**
6	3,098.75	6,913.50	13,295.60	802.10	**79.26**	**20.13**	**0.61**
7	5,161.00	11,729.00	24,167.95	1,386.80	**82.84**	**16.40**	**0.76**
8	3,451.50	7,539.00	11,901.35	948.60	**78.57**	**20.38**	**1.05**
9	3,730.00	6,164.50	2,329.00	793.60	**77.33**	**21.61**	**1.06**
10	5,721.00	12,989.00	12,865.85	2,574.10	**81.57**	**17.25**	**1.17**
11	6,559.50	14,472.00	15,248.20	3,149.30	**94.40**	**4.34**	**1.26**
12	2,517.50	6,328.00	6,350.90	1,769.75	**86.41**	**11.61**	**1.98**
13	2,529.50	5,606.50	1,726.80	702.60	**85.72**	**12.14**	**2.14**
14	1,249.50	2,349.00	1,097.65	211.80	**85.21**	**11.95**	**2.84**
15	1,268.00	2,614.00	1,347.50	437.00	**94.71**	**3.93**	**1.36**
16	3,053.00	7,357.50	6,724.30	1,454.20	**93.51**	**5.57**	**0.92**
17	2,205.50	5,311.50	4,175.40	2,602.20	**92.03**	**6.24**	**1.73**
18	2,765.00	6,133.25	8,154.00	3,512.60	**87.00**	**10.98**	**2.03**
19	1,776.50	3,873.00	7,375.90	0.00	**85.75**	**9.30**	**4.95**
20	2,916.00	7,055.00	14,345.40	767.20	**80.34**	**14.38**	**5.29**

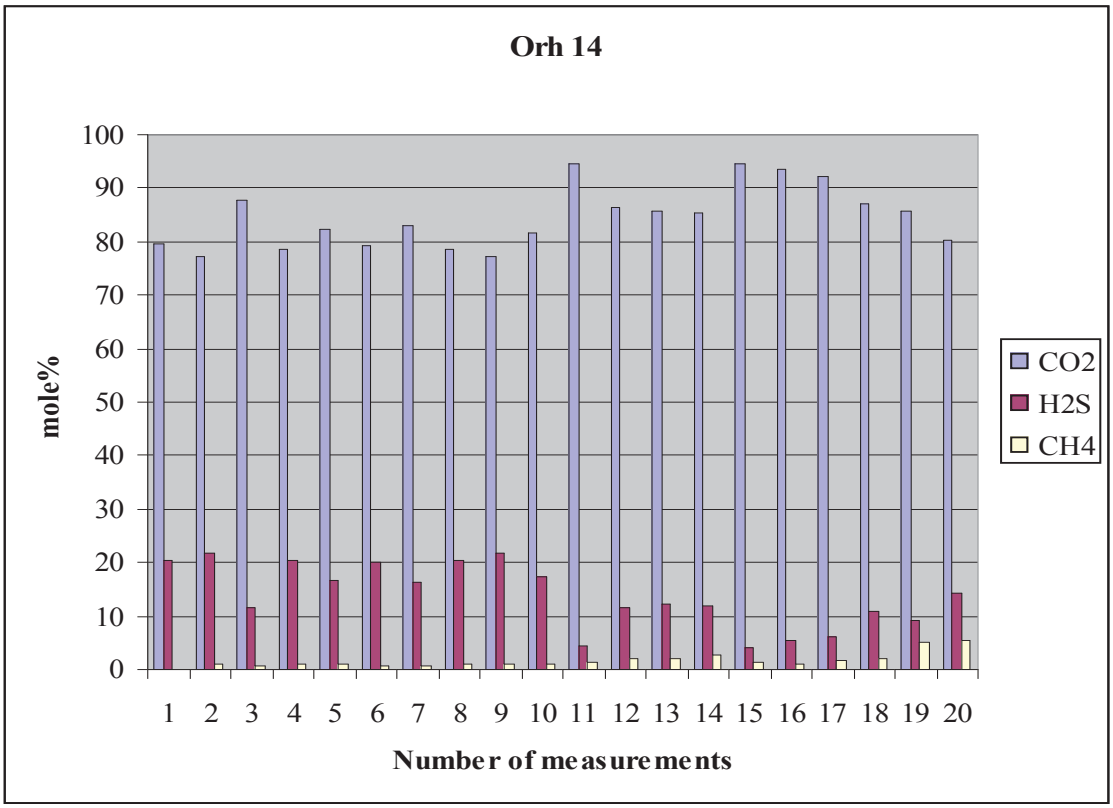

Mer-blau

Number of measurem.	1. CO_2-Peak Area	2. CO_2-Peak Area	H_2S - Peak Area	CH_4 - Peak Area	N_2 - Peak Area	Mole fraction of CO_2 [%]	Mole fraction of H_2S [%]	Mole fraction of CH_4 [%]	Mole Fraction of N_2 [%]
1	361.50	731.50	964.80	300.20	0.00	**82.09**	**14.15**	**3.76**	**0.00**
2	1,827.00	4,578.00	6,486.50	4,289.60	628.20	**69.83**	**13.81**	**7.79**	**8.56**
3	2,212.00	5,301.00	6,102.50	4,748.80	357.80	**75.56**	**11.99**	**7.96**	**4.50**
4	509.00	1,059.00	2,280.10	548.20	0.00	**74.50**	**21.16**	**4.34**	**0.00**
5	1,205.00	2,845.00	5,063.10	1,861.40	87.00	**74.20**	**18.20**	**5.68**	**1.99**
6	440.50	866.50	1,695.20	381.50	0.00	**76.81**	**19.46**	**3.74**	**0.00**
7	420.00	630.00	2,061.20	1,505.80	509.00	**44.88**	**17.21**	**10.73**	**27.19**
8	3,145.00	7,737.50	6,994.50	3,340.20	602.60	**80.26**	**10.08**	**4.11**	**5.56**
9	461.00	1,487.50	1,565.60	724.50	400.80	**67.75**	**10.63**	**4.20**	**17.42**
10	2,012.00	5,063.50	5,283.00	2,619.20	347.50	**78.81**	**11.49**	**4.86**	**4.84**
11	2,804.00	7,719.00	10,515.50	5,384.20	1,293.80	**69.73**	**4.35**	**2.54**	**17.66**
12	518.50	1,083.50	472.50	324.00	300.00	**75.45**	**4.35**	**2.54**	**17.66**
13	433.50	1,359.00	1,475.10	676.00	883.50	**54.36**	**8.74**	**3.42**	**33.49**
14	3,587.00	8,374.00	12,350.20	5,480.10	865.10	**73.08**	**14.74**	**5.58**	**6.61**
15	406.00	1,175.00	870.50	385.80	0.00	**87.09**	**9.37**	**3.54**	**0.00**

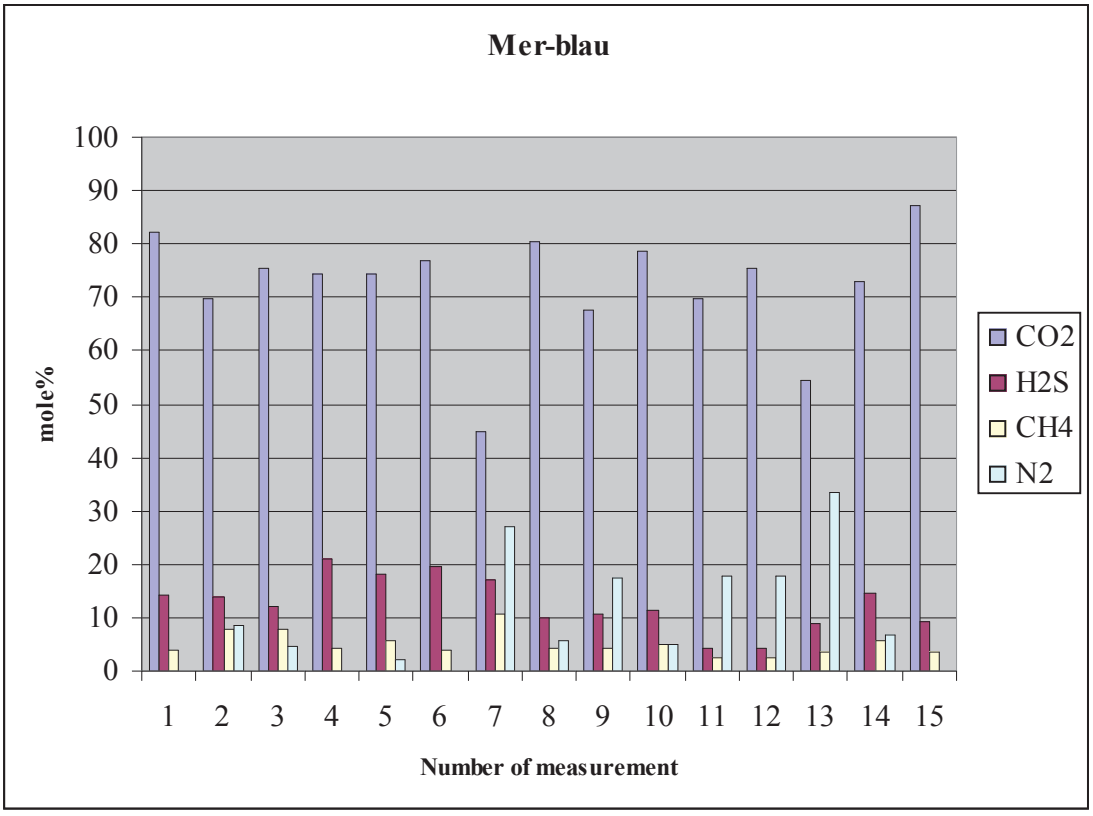

Mer-grau

Number of measurem.	1. CO_2-Peak Area	2. CO_2-Peak Area	H_2S - Peak Area	CH_4 - Peak Area	N_2 - Peak Area	Mole fraction of CO_2 [%]	Mole fraction of H_2S [%]	Mole fraction of CH_4 [%]	Mole Fraction of N_2 [%]
1	4,101.00	9,551.00	7,564.15	9,183.60	672.90	**78.01**	**8.44**	**8.75**	**4.81**
2	1,870.50	4,317.00	7,988.80	3,358.00	168.20	**72.64**	**18.32**	**6.57**	**2.47**
3	1,846.50	4,475.00	7,414.50	3,074.20	174.00	**74.37**	**17.04**	**6.03**	**2.56**
4	485.00	999.00	1,338.00	903.00	0.00	**78.28**	**13.78**	**7.94**	**0.00**
5	710.00	1,396.00	2,621.20	984.20	0.00	**75.70**	**18.40**	**5.90**	**0.00**
6	1,759.00	3,855.50	6,431.00	3,457.00	212.80	**72.80**	**16.29**	**7.47**	**3.45**
7	1,721.00	3,746.50	6,881.80	4,228.80	0.00	**72.74**	**17.88**	**9.38**	**0.00**
8	1,474.00	3,405.00	6,404.80	3,769.80	202.80	**69.58**	**17.84**	**8.96**	**3.62**
9	2,937.00	6,716.00	12,527.20	5,228.20	486.00	**71.09**	**18.02**	**6.42**	**4.47**
10	2,519.00	5,508.00	8,659.40	4,726.50	412.20	**72.83**	**15.35**	**7.15**	**4.68**
11	2,302.50	4,880.00	7,130.00	3,885.20	213.50	**75.69**	**14.67**	**6.82**	**2.81**
12	3,104.00	6,193.00	4,848.40	3,023.60	65.50	**85.85**	**8.74**	**4.65**	**0.76**
13	2,678.50	5,469.00	4,839.60	2,480.80	155.50	**83.99**	**9.74**	**4.26**	**2.00**
14	1,349.00	2,741.00	2,364.80	713.00	2.00	**87.52**	**9.88**	**2.54**	**0.05**
15	1,864.00	3,715.00	2,302.10	1,284.10	29.40	**88.85**	**7.16**	**3.41**	**0.59**
16	1,972.00	4,138.00	2,884.10	1,625.50	93.80	**86.53**	**7.98**	**3.84**	**1.66**
17	2,846.00	6,020.00	4,617.20	2,290.20	54.00	**86.78**	**8.83**	**3.74**	**0.66**
18	874.00	1,805.50	5,983.40	945.50	64.60	**65.57**	**28.60**	**3.86**	**1.98**
19	1,454.00	3,240.00	9,000.20	2,020.90	302.20	**65.50**	**24.53**	**4.70**	**5.27**
20	942.00	2,142.00	3,432.80	1,149.00	418.50	**69.01**	**15.00**	**4.28**	**11.71**
21	1,082.00	2,390.00	2,413.20	827.00	97.80	**82.60**	**11.21**	**3.28**	**2.91**
22	1,101.50	2,582.00	3,142.60	683.20	90.50	**81.42**	**13.57**	**2.52**	**2.50**

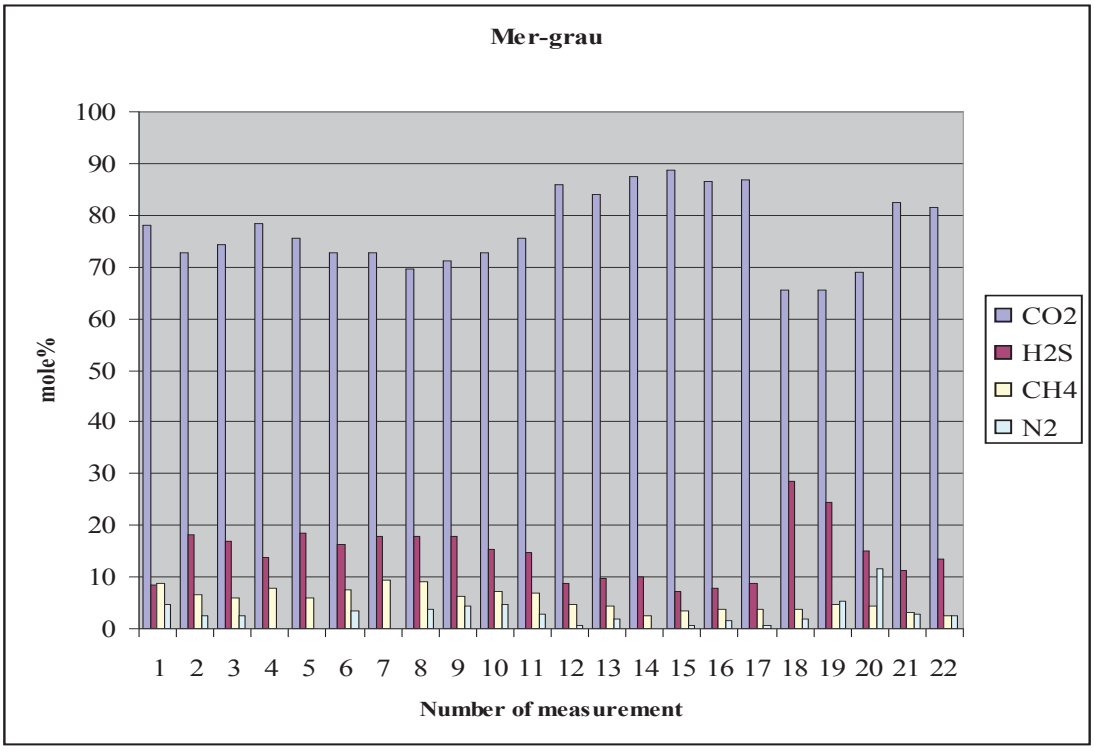

13.2. Crush and Leach dates

No.	Sample	Li	Na	K	Mg	Ca	F	Cl	Br	J	PO4	SO4
2595	Bay 1	0.3	2273	805	3227	18744	16	4613	20	174.0		743
2596	Bay 4	0.5	1004	295	2605	13831	5	2379	6	48.0		347
2597	Bay 10	81.0	2118	388	6168	28104	1217	2758	6	0.7		39416
2598	Bay 23	6.4	976	417	1140	12282	220	3350	3	6.6		6142
2599	Bay 24	3.0	1453	364	2411	17315	19	3019	11	94.4		788
2600	Orh 1a	0.1	756	206	561	7578	10	1309	4	3.0		190
2601	Orh 1b	0.3	1548	381	5045	14770	14	2548	6	19.4		2981
2602	Orh 2a	0.2	905	227	1353	11876	15	1522	5	10.9		833
2603	Orh 2c	0.4	1253	428	3791	21508	30	2093	11	21.2		3754
2604	Orh 14a	0.1	887	197	1335	8766	5	1568	6	6.8		317
2605	Orh 14b	0.1	1062	230	3054	14720	25	1354	7	15.1		2812
2606	Orh 26	0.1	725	156	2101	10658	22	1300	4	7.1		1019
2607	Orh 37a	0.2	536	144	1182	8101	11	1145	3	0.8		341
2608	Orh 37b	0.3	643	183	1194	8104	17	1211	3	0.5		508
2632	Calcit	n.a.	537	142	171	8108	17	1083	6	0.0	n.a.	92
2633	Merl-hellblau	7.6	3829	404	4721	23746	11	7977	61	59.5	n.a.	902
2634	Merl-blau	15.9	11739	815	7611	22839	18	21513	163	354.1	n.a.	13940
2635	Merl-grau	25.8	14166	1190	9393	26354	68	26831	169	203.2	n.a.	14072

13.3. RFA dates

Sample	Bay 1	Bay 10	Bay 23	Bay 24	Bay 4	Orh 14a	Orh 14b	Orh 1a	Orh 1b	Orh 26	Orh 26-2	Orh 2a	Orh 2c	Orh 37a	Orh 37b
LOI ()	43.70	44.42	43.56	43.44	43.94	43.36	43.42	43.32	43.96	40.13	40.13	43.01	43.74	44.22	41.00
SiO2 (%)	<0.02	<0.02	0.05	<0.02	<0.02	<0.02	<0.02	<0.02	<0.02	<0.02	<0.02	0.35	0.05	0.15	0.29
Al2O3 (%)	0.01	0.01	0.13	0.02	0.03	0.01	0.06	0.01	0.05	0.01	0.02	0.30	0.11	0.04	0.09
Fe2O3 (%)	0.04	0.03	0.51	0.04	0.07	0.03	0.04	0.03	0.04	0.04	0.04	0.10	0.05	0.08	0.09
MnO (%)	0.009	0.014	0.043	0.006	0.020	0.005	0.005	0.005	0.005	0.006	0.005	0.005	0.005	0.011	0.011
MgO (%)	0.94	5.13	0.53	0.80	2.27	0.56	1.62	0.28	3.67	0.97	0.98	0.28	3.36	0.80	0.49
CaO (%)	55.00	50.00	54.60	55.17	53.22	55.17	54.09	55.80	51.65	55.08	55.11	55.15	51.88	54.77	55.20
Na2O (%)	0.04	0.05	0.07	0.07	0.03	0.06	0.07	0.06	0.05	0.07	0.14	0.05	0.06	0.07	0.07
K2O (%)	<0.01	<0.01	0.01	<0.01	<0.01	<0.01	<0.01	<0.01	0.01	<0.01	0.01	0.07	0.03	<0.01	0.01
TiO2 (%)	<0.01	<0.01	0.01	<0.01	0.01	0.01	0.01	<0.01	0.01	<0.01	0.01	0.03	0.02	0.01	0.01
P2O5 (%)	<0.01	<0.01	<0.01	<0.01	<0.01	<0.01	0.01	<0.01	<0.01	<0.01	<0.01	<0.01	<0.01	0.02	0.03
Sum (%)	**99.93**	**99.70**	**99.57**	**99.57**	**99.70**	**99.22**	**99.36**	**99.52**	**99.54**	**96.33**	**96.68**	**99.47**	**99.42**	**100.31**	**97.40**
Ba (PPM)	<30	<30	<30	<30	<30	<30	<30	<30	<30	<30	<30	<30	<30	<30	<30
Ce (PPM)	<30	<30	<30	<30	<30	<30	<30	<30	<30	<30	<30	<30	<30	<30	<30
Cd (PPM)	<30	<30	<30	<30	<30	<30	<30	<30	<30	<30	<30	<30	<30	<30	<30
Co (PPM)	<20	<20	<20	<20	<20	<20	<20	<20	<20	<20	<20	<20	<20	<20	<20
Cr (PPM)	*22*	*16*	*18*	*17*	*17*	*21*	*27*	*25*	*25*	*28*	*27*	*35*	*21*	*19*	*23*
Cu (PPM)	<20	<20	<20	<20	<20	<20	<20	<20	<20	<20	<20	<20	<20	<20	<20
Ga (PPM)	<20	<20	<20	<20	<20	<20	<20	<20	<20	<20	<20	<20	<20	<20	<20
Hf (PPM)	<20	<20	<20	<20	<20	<20	<20	<20	<20	<20	<20	<20	<20	<20	<20
La (PPM)	23	24	3	28	32	43	31	21	32	12	39	36	0	29	12
Mo (PPM)	<30	<30	<30	<30	<30	<30	<30	<30	<30	<30	<30	<30	<30	<30	<30
Nb (PPM)	<20	<20	<20	<20	<20	<20	<20	<20	<20	<20	<20	<20	<20	<20	<20
Ni (PPM) <20	*15*	*14*	*15*	*14*	*15*	*16*	*12*	*12*	*16*	*15*	*11*	*12*	*16*	*14*	*17*
Pb (PPM)	<20	<20	<20	<20	<20	<20	<20	<20	<20	<20	<20	<20	<20	<20	<20
Rb (PPM) <15	*6*	*4*	*4*	*4*	*5*	*6*	*5*	*5*	*5*	*5*	*4*	*7*	*5*	*5*	*5*
Sc (PPM)	<20	<20	<20	<20	<20	<20	<20	<20	<20	<20	<20	<20	<20	<20	<20
Sr (PPM)	200	200	515	173	173	117	126	103	103	149	151	94	144	144	163
Th (PPM)	<20	<20	<20	<20	<20	<20	<20	<20	<20	<20	<20	<20	<20	<20	<20
U (PPM)	<20	<20	<20	<20	<20	<20	<20	<20	<20	<20	<20	<20	<20	<20	<20
V (PPM)	<20	<20	<20	<20	<20	<20	<20	<20	<20	<20	<20	21	<20	<20	<20
Y (PPM)	<20	<20	<20	<20	<20	<20	<20	<20	<20	<20	<20	<20	<20	<20	<20
Zn (PPM) <20	*15*	*23*	*25*	*11*	*17*	*8*	*8*	*7*	*8*	*9*	*10*	*8*	*9*	*14*	*19*
Zr (PPM)	<20	<20	<20	<20	<20	<20	<20	<20	<20	<20	<20	<20	<20	<20	<20

13.4. XRD dates

Bay 1

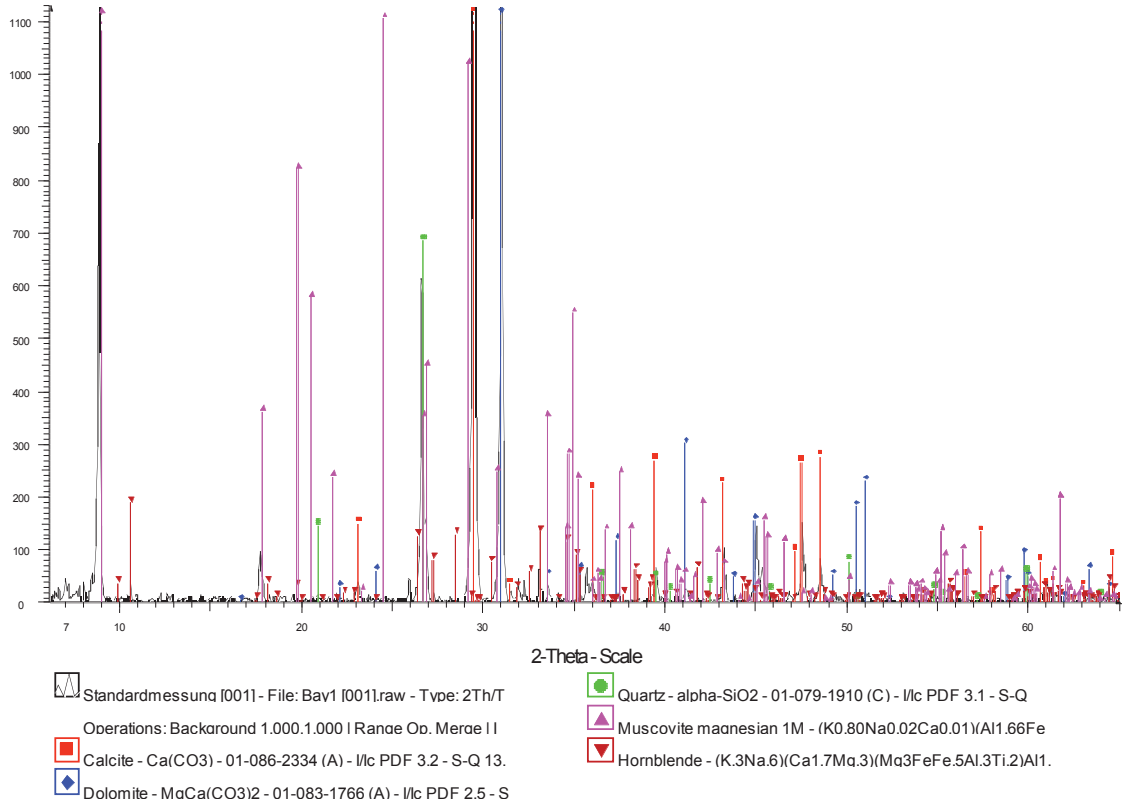

Bay 4

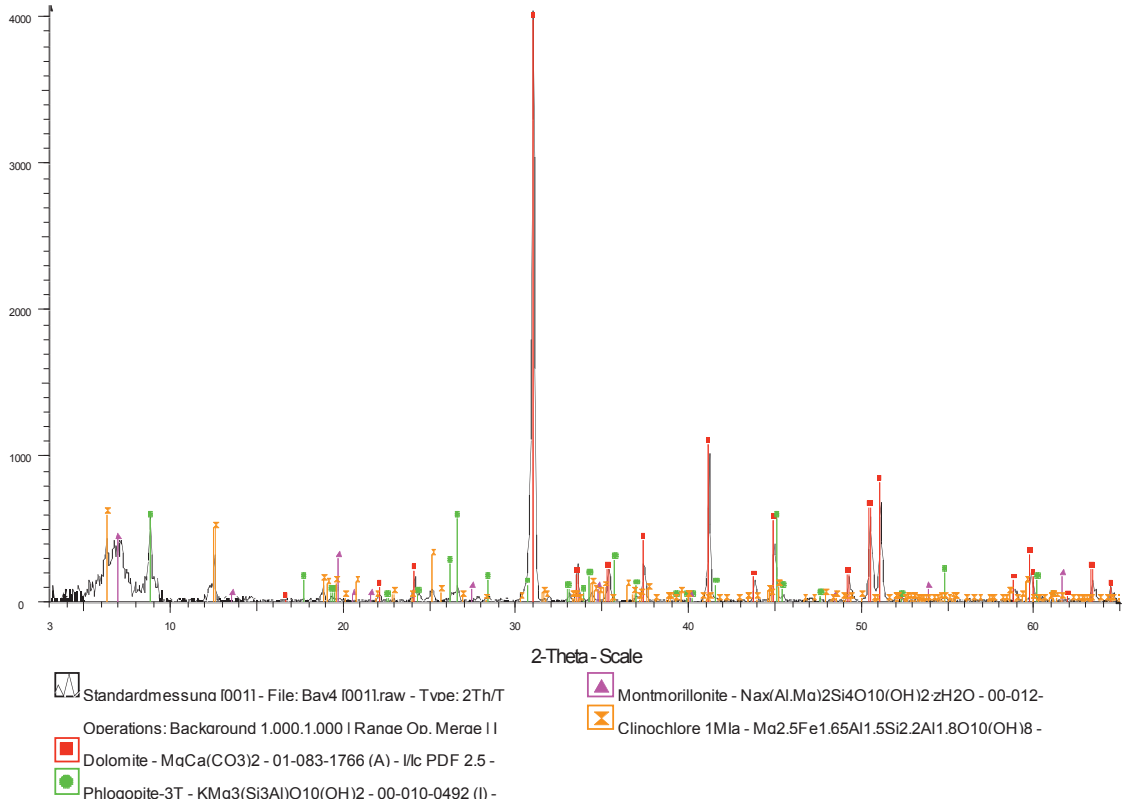

Bay 10

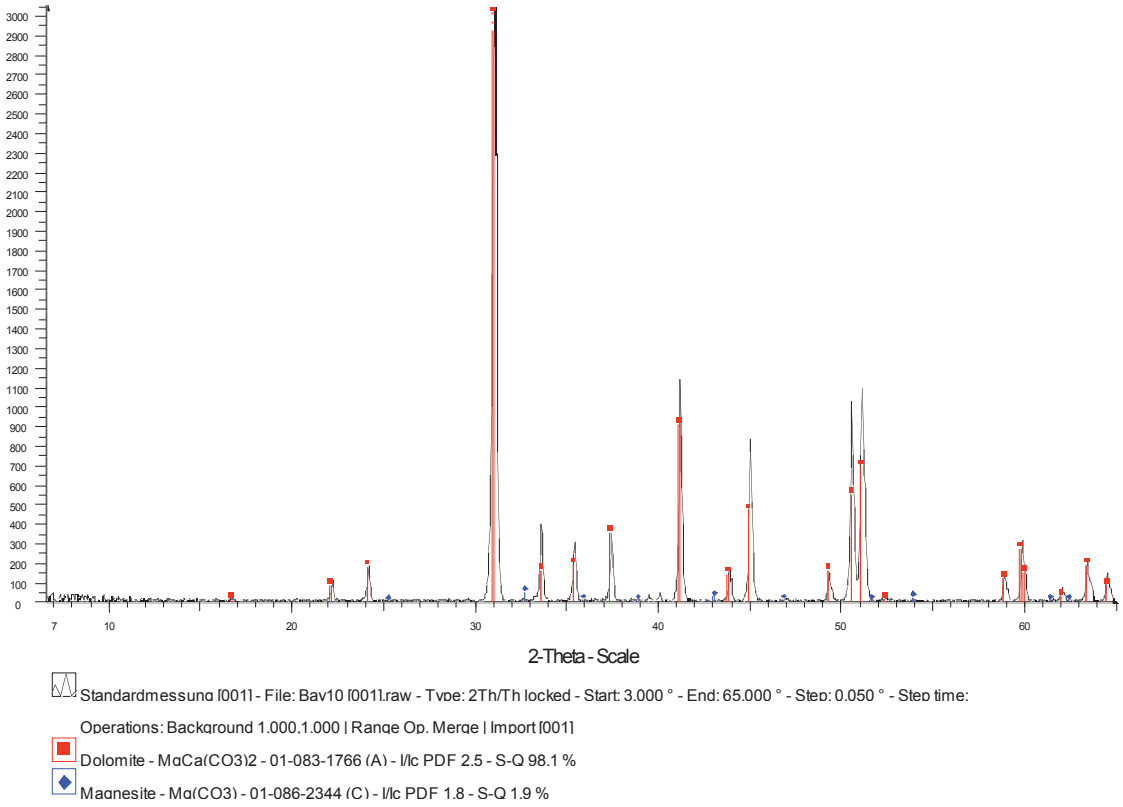
2-Theta - Scale
Standardmessung [001] - File: Bay10 [001].raw - Type: 2Th/Th locked - Start: 3.000 ° - End: 65.000 ° - Step: 0.050 ° - Step time:
Operations: Background 1.000,1.000 | Range Op. Merge | Import [001]
Dolomite - MgCa(CO3)2 - 01-083-1766 (A) - I/Ic PDF 2.5 - S-Q 98.1 %
Magnesite - Mg(CO3) - 01-086-2344 (C) - I/Ic PDF 1.8 - S-Q 1.9 %

Bay 23

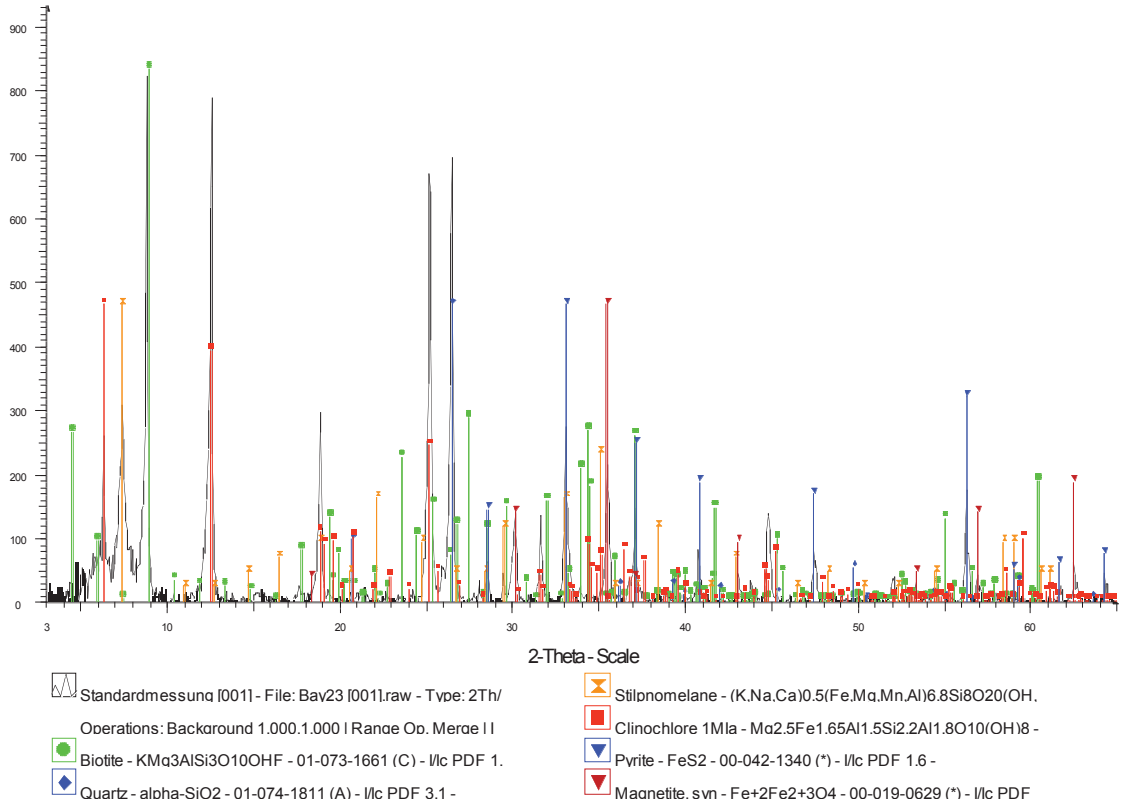
2-Theta - Scale
Standardmessung [001] - File: Bay23 [001].raw - Type: 2Th/
Operations: Background 1.000,1.000 | Range Op. Merge | I
Biotite - KMg3AlSi3O10OHF - 01-073-1661 (C) - I/Ic PDF 1.
Quartz - alpha-SiO2 - 01-074-1811 (A) - I/Ic PDF 3.1 -
Stilpnomelane - (K,Na,Ca)0.5(Fe,Mg,Mn,Al)6.8Si8O20(OH,
Clinochlore 1Mla - Mg2.5Fe1.65Al1.5Si2.2Al1.8O10(OH)8 -
Pyrite - FeS2 - 00-042-1340 (*) - I/Ic PDF 1.6 -
Magnetite, syn - Fe+2Fe2+3O4 - 00-019-0629 (*) - I/Ic PDF

Bay 24

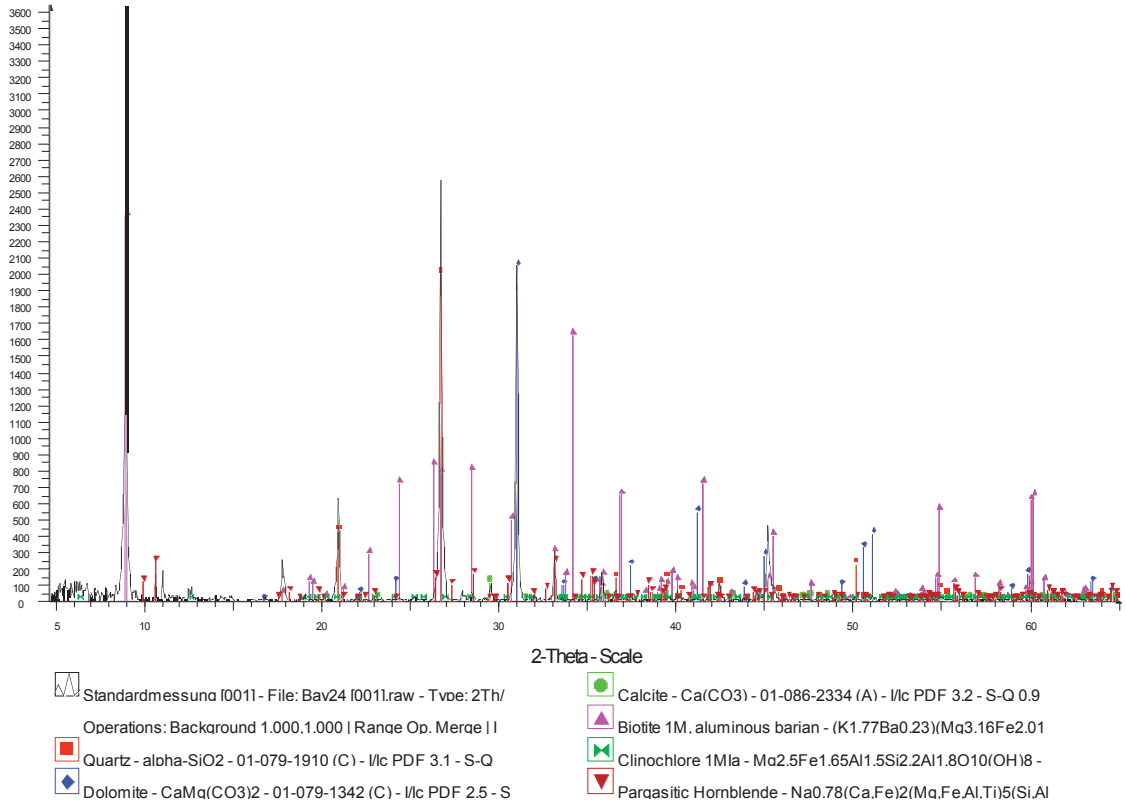
2-Theta - Scale
Standardmessung [001] - File: Bay24 [001].raw - Type: 2Th/
Operations: Background 1.000,1.000 | Range Op. Merge | I
Quartz - alpha-SiO2 - 01-079-1910 (C) - I/Ic PDF 3.1 - S-Q
Dolomite - CaMg(CO3)2 - 01-079-1342 (C) - I/Ic PDF 2.5 - S
Calcite - Ca(CO3) - 01-086-2334 (A) - I/Ic PDF 3.2 - S-Q 0.9
Biotite 1M, aluminous barian - (K1.77Ba0.23)(Mg3.16Fe2.01
Clinochlore 1Mla - Mg2.5Fe1.65Al1.5Si2.2Al1.8O10(OH)8 -
Pargasitic Hornblende - Na0.78(Ca,Fe)2(Mg,Fe,Al,Ti)5(Si,Al

Orh 1

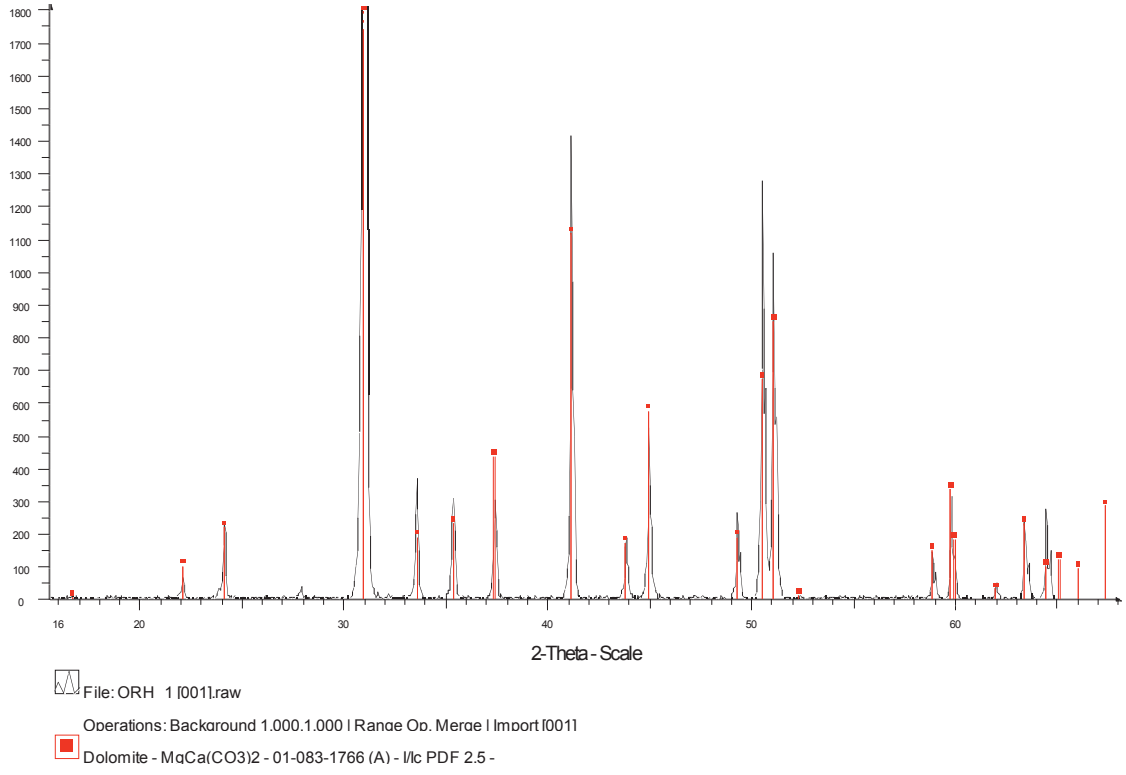
2-Theta - Scale
File: ORH 1 [001].raw
Operations: Background 1.000,1.000 | Range Op. Merge | Import [001]
Dolomite - MgCa(CO3)2 - 01-083-1766 (A) - I/Ic PDF 2.5 -

Orh 2

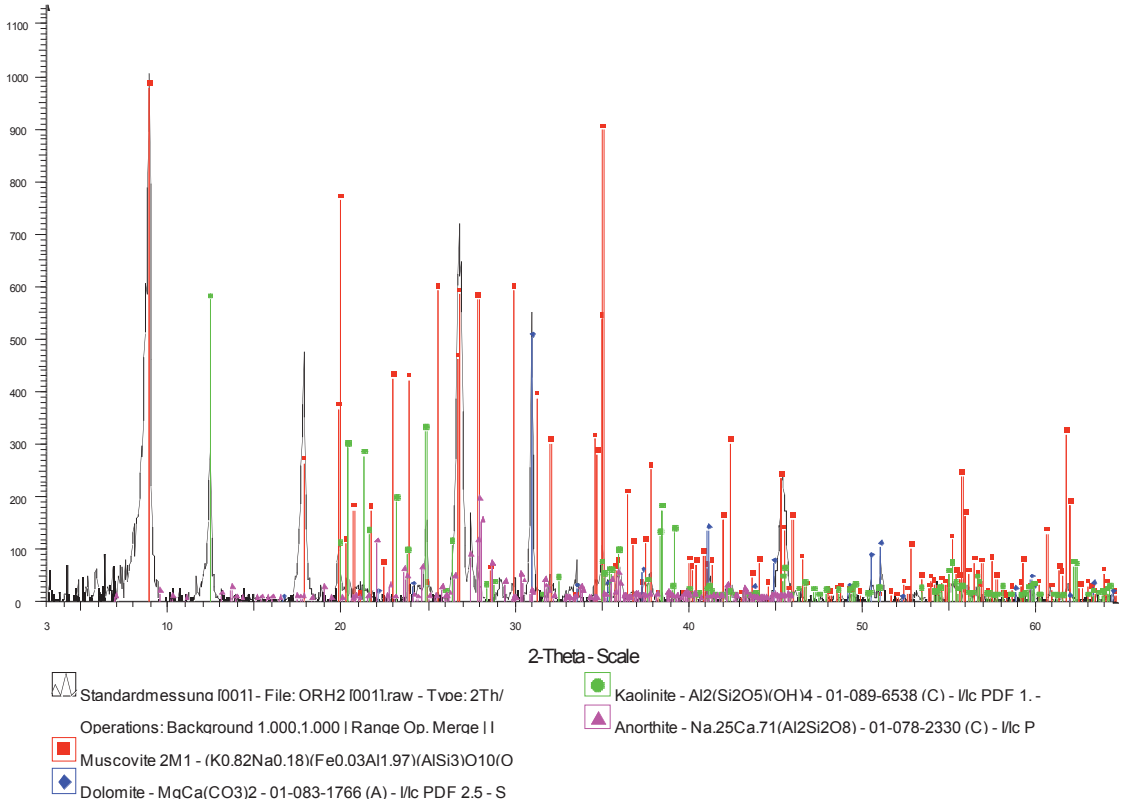
2-Theta - Scale
Standardmessung [001] - File: ORH2 [001].raw - Type: 2Th/
Operations: Background 1.000,1.000 | Range Op. Merge | I
Muscovite 2M1 - (K0.82Na0.18)(Fe0.03Al1.97)(AlSi3)O10(O
Dolomite - MgCa(CO3)2 - 01-083-1766 (A) - I/Ic PDF 2.5 - S
Kaolinite - Al2(Si2O5)(OH)4 - 01-089-6538 (C) - I/Ic PDF 1. -
Anorthite - Na.25Ca.71(Al2Si2O8) - 01-078-2330 (C) - I/Ic P

Orh 14 a

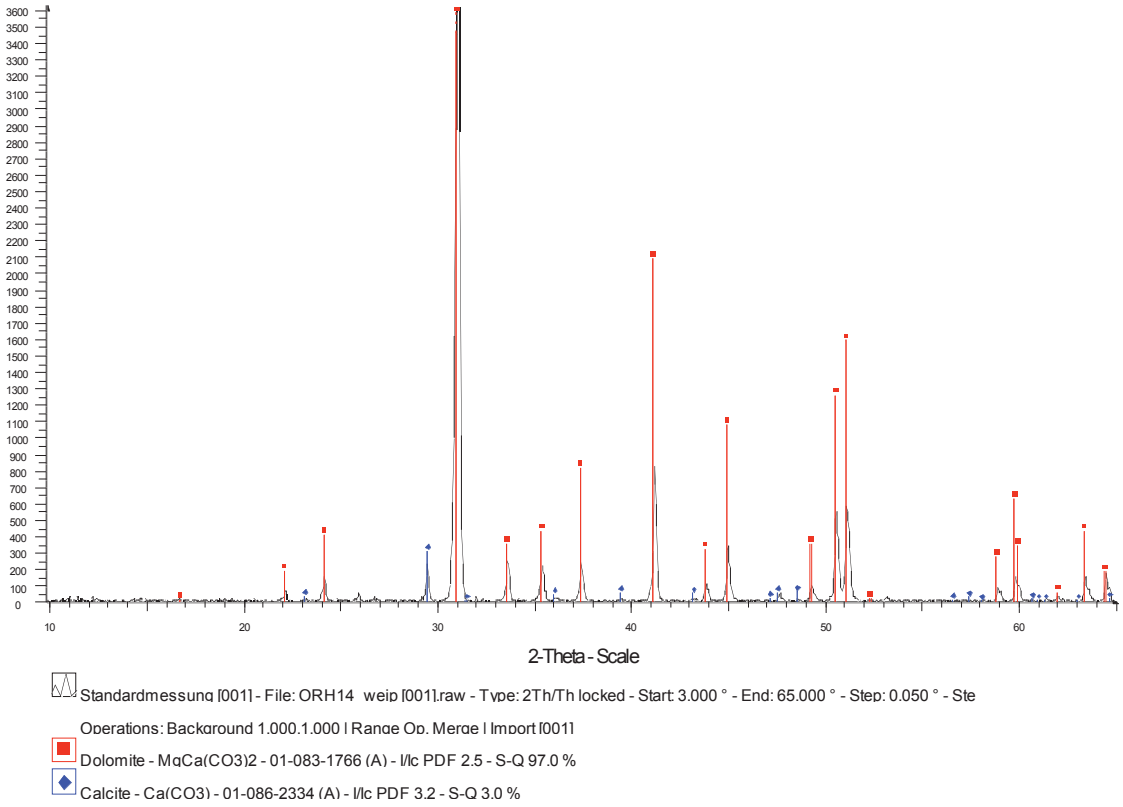
2-Theta - Scale
Standardmessung [001] - File: ORH14_weip [001].raw - Type: 2Th/Th locked - Start: 3.000 ° - End: 65.000 ° - Step: 0.050 ° - Ste
Operations: Background 1.000,1.000 | Range Op. Merge | Import [001]
Dolomite - MgCa(CO3)2 - 01-083-1766 (A) - I/Ic PDF 2.5 - S-Q 97.0 %
Calcite - Ca(CO3) - 01-086-2334 (A) - I/Ic PDF 3.2 - S-Q 3.0 %

Orh 14 b

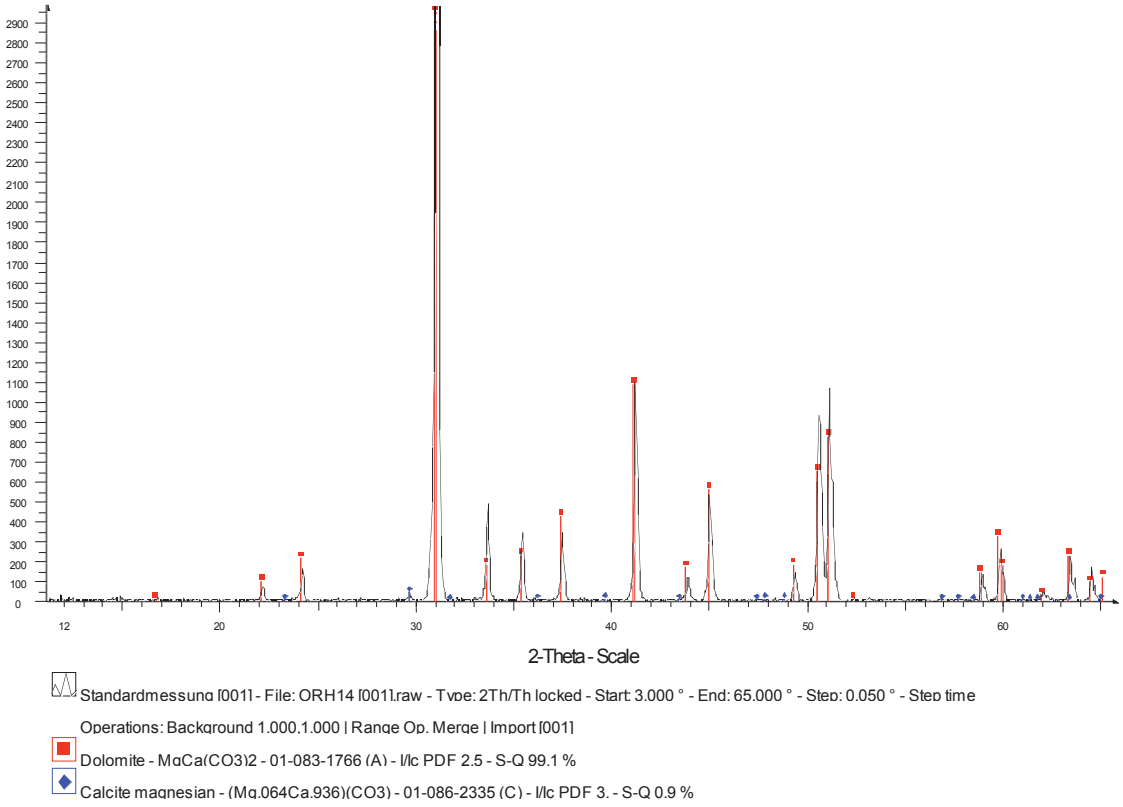

Orh 15

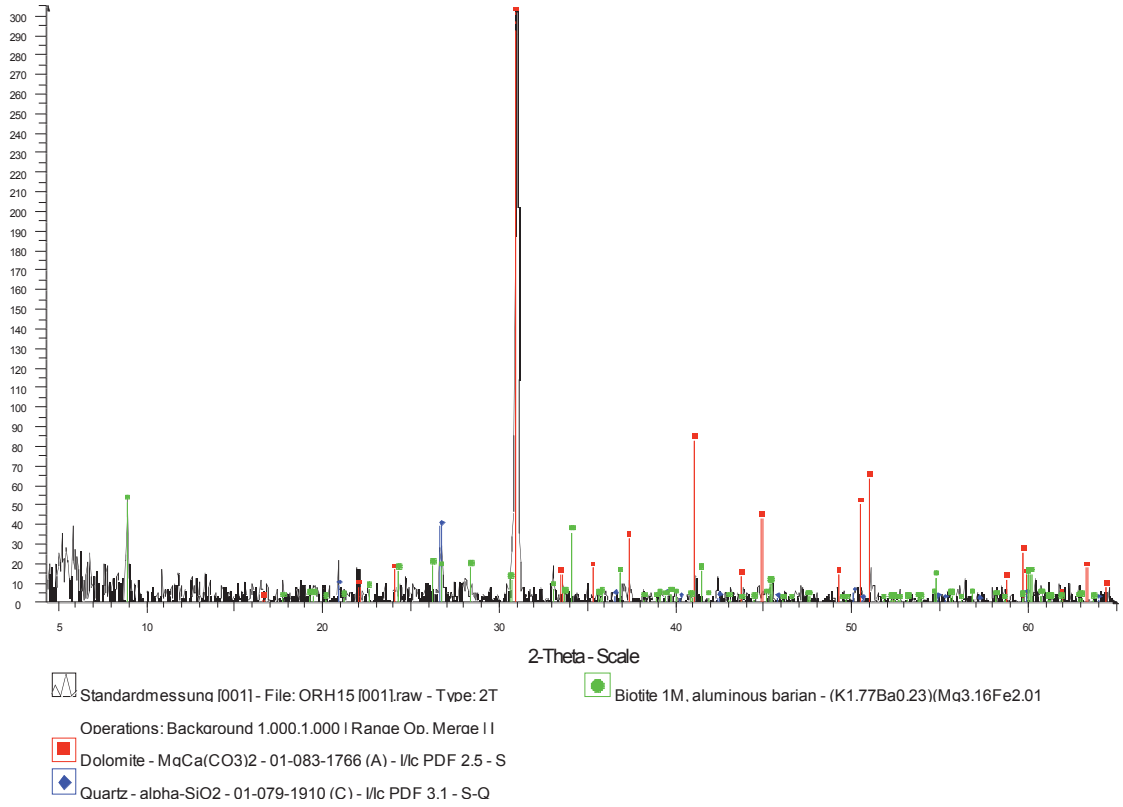

Orh 26

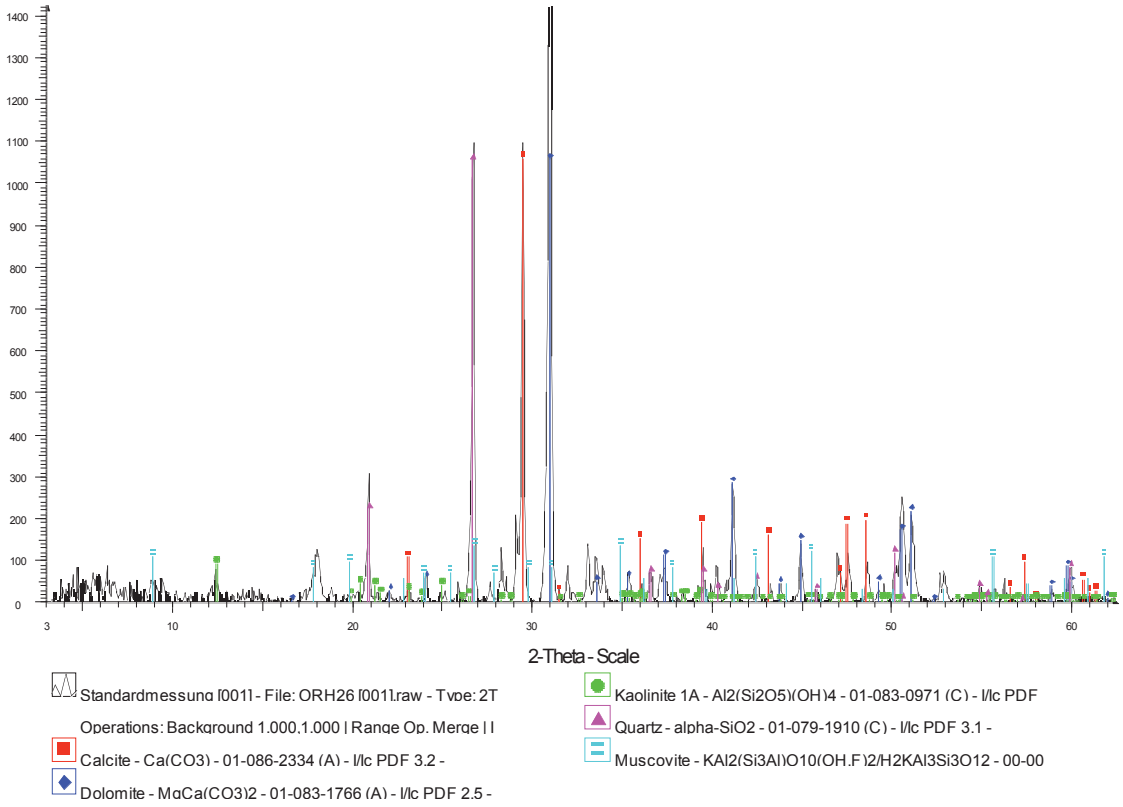
2-Theta - Scale
Standardmessung [001] - File: ORH26 [001].raw - Type: 2T
Operations: Background 1.000,1.000 | Range Op. Merge | I
Calcite - Ca(CO3) - 01-086-2334 (A) - I/Ic PDF 3.2 -
Dolomite - MgCa(CO3)2 - 01-083-1766 (A) - I/Ic PDF 2.5 -
Kaolinite 1A - Al2(Si2O5)(OH)4 - 01-083-0971 (C) - I/Ic PDF
Quartz - alpha-SiO2 - 01-079-1910 (C) - I/Ic PDF 3.1 -
Muscovite - KAl2(Si3Al)O10(OH,F)2/H2KAl3Si3O12 - 00-00

Orh 37

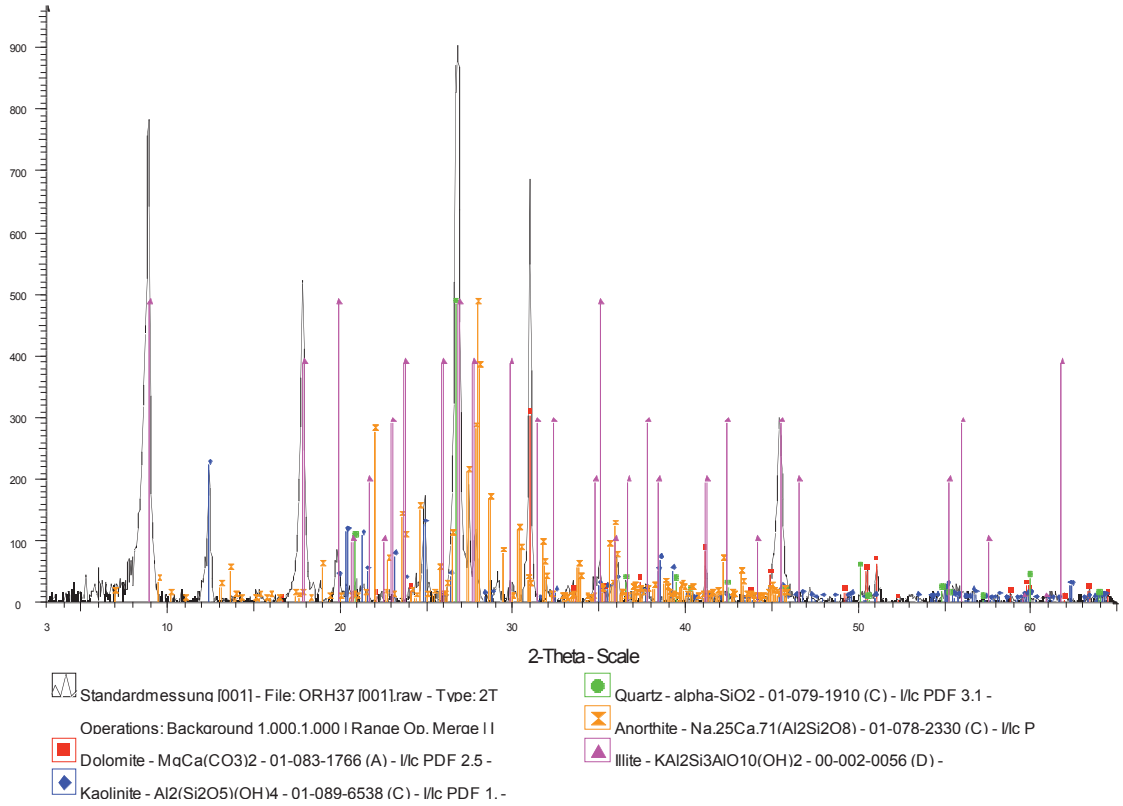
2-Theta - Scale
Standardmessung [001] - File: ORH37 [001].raw - Type: 2T
Operations: Background 1.000,1.000 | Range Op. Merge | I
Dolomite - MgCa(CO3)2 - 01-083-1766 (A) - I/Ic PDF 2.5 -
Kaolinite - Al2(Si2O5)(OH)4 - 01-089-6538 (C) - I/Ic PDF 1. -
Quartz - alpha-SiO2 - 01-079-1910 (C) - I/Ic PDF 3.1 -
Anorthite - Na,25Ca,71(Al2Si2O8) - 01-078-2330 (C) - I/Ic P
Illite - KAl2Si3AlO10(OH)2 - 00-002-0056 (D) -

Merluzzi hellblau

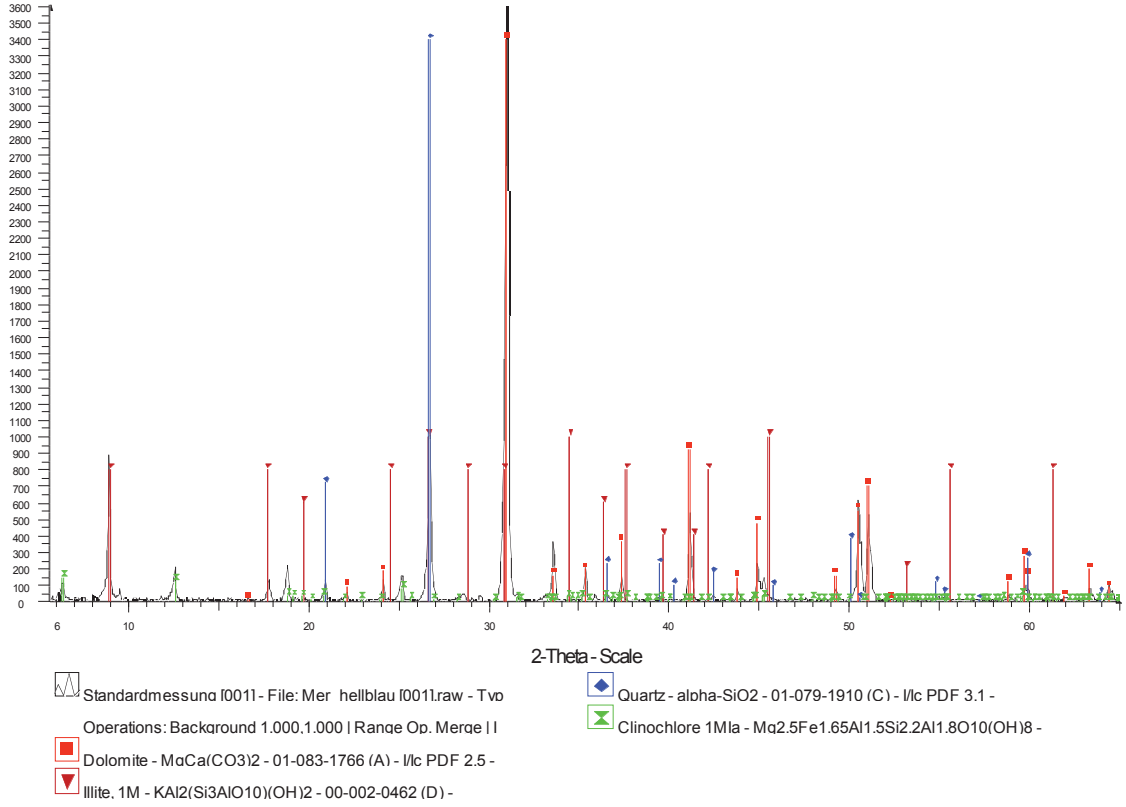

Merluzzi Grau

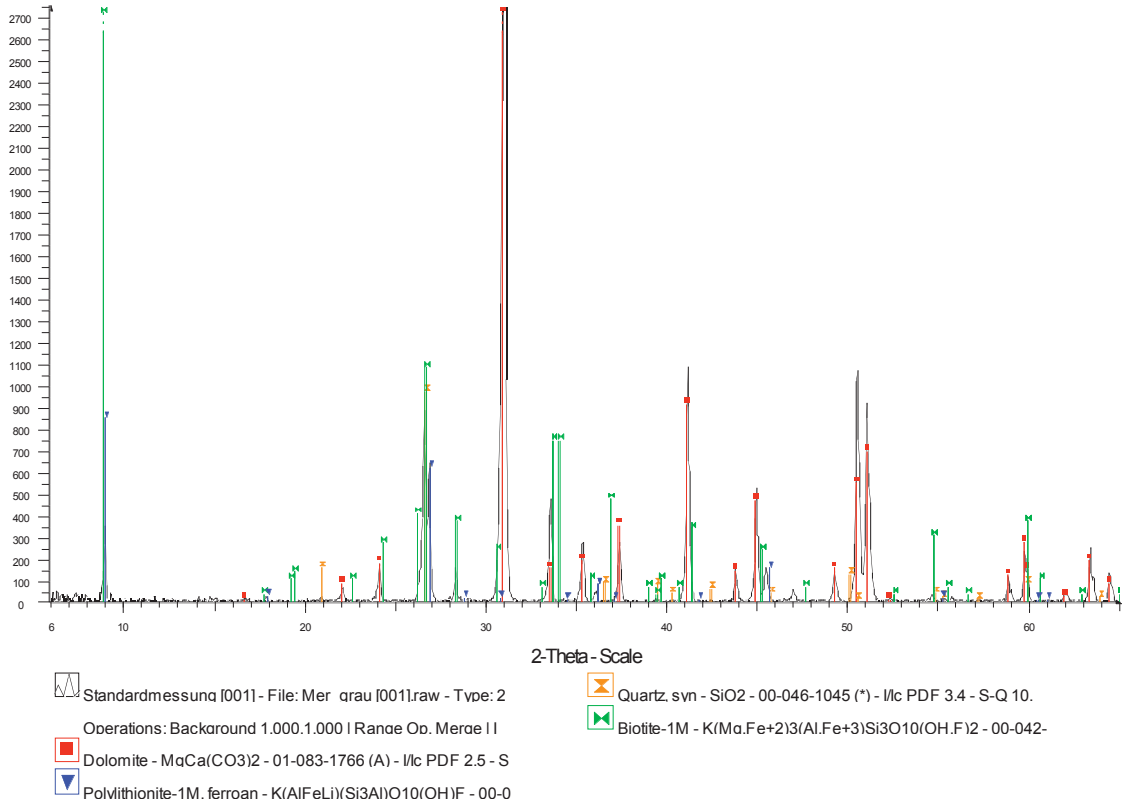

Merluzzi Blau